
OPTIMIZING SPECTRAL UTILIZATION OF LPWANS



Jathun Gamage Isuru Amalinda

School of Computer Science & Engineering

A thesis submitted to the Nanyang Technological University
in partial fulfillment of the requirements for the degree of
Doctor of Philosophy

2023

Statement of Originality

I hereby certify that the work embodied in this thesis is the result of original research, is free of plagiarised materials, and has not been submitted for a higher degree to any other University or Institution.

4th August 2023

.....
Date

.....
ITU NTU NTU NTU NTU NTU NTU NTI
NTU NTU NTU NTU NTU NTU NTU NTI
NTU NTU NTU NTU NTU NTU NTU NTI
NTU NTU NTU NTU NTU NTU NTU NTI

Jathun Gamage Isuru Amalinda

Supervisor Declaration Statement

I have reviewed the content and presentation style of this thesis and declare it is free of plagiarism and of sufficient grammatical clarity to be examined. To the best of my knowledge, the research and writing are those of the candidate except as acknowledged in the Author Attribution Statement. I confirm that the investigations were conducted in accord with the ethics policies and integrity standards of Nanyang Technological University and that the research data are presented honestly and without prejudice.

4th August 2023

.....

Date

NTU NTU NTU NTU NTU NTU NTU NTI
NTU NTU NTU NTU NTU NTU NTU NTI
NTU NTU NTU NTU NTU NTU NTU NTI
NTU NTU NTU NTU NTU NTU NTU NTI



Prof. Mo Li

Authorship Attribution Statement

This thesis contains material from a peer-reviewed conference paper and a journal where I was the first author, a LoRaWAN Technical Recommendation (TR) based on said work and one on-going work.

Chapter 3 is published as [A. Gamage, J.C Liando, C. Gu, R. Tan and M. Li, "LMAC: Efficient Carrier-Sense Multiple Access for LoRa"](#) in proceedings of the [26th Annual International Conference on Mobile Computing and Networking \(MobiCom'20\)](#), April 2020, Article Number 43, DOI: [10.1145/3372224.3419200](https://doi.org/10.1145/3372224.3419200).

The contributions of the co-authors are as follows:

- Prof M. Li helped plan the milestones of the project as a whole and iteratively guided the project towards a complete research paper. Prof M. Li improved the writing quality and presentation style of the paper.
- I engineered the method, conducted indoor/outdoor experiments and prepared the manuscript as a whole. I handled all revisions, rebuttals until publication for both conference article and the journal article.
- Prof. R. Tan made significant improvements to the writing and presentation of the paper. He also provided regular input during discussions throughout the project.
- J.C Liando aided in conducting large scale LoRaWAN simulations and writing the drafts.
- Prof. C. Gu aided in performing the literature survey, outdoor experiments and creating figures.

Chapter 4 contains results from a journal publication and a technical recommendation.

One published as [A. Gamage, J.C Liando, C. Gu, R. Tan, M. Li and O. Seller, "LMAC: Efficient Carrier-Sense Multiple Access for LoRa"](#) in proceedings of [ACM Transactions on Sensor Networks \(TOSN'23\)](#), Volume 19, Issue 2, February 2023, DOI: [10.1145/3564530](https://doi.org/10.1145/3564530).

One published as [A. Gamage, G. de Guillebon, M. Luis, M. Li, O. Seller, "Technical Recommendations for Enabling CSMA for LoRaWAN, TR13 – 1.0.0"](#) by the LoRa Alliance.

- I was responsible formulating the TR as a whole. I conducted various experiments to evaluate various aspects of LMAC on LoRAWAN.
- Prof. M. Li proposed initial the idea of extending LMAC as a TR. Prof. M. Li aided in writing of the technical recommendation, provided guidance throughout the process until the acceptance of the TR.

- O. Seller provided insights from a regulatory and interoperability perspective which formed the essential enhancements in the extended journal publication. O. Seller also contributed to improving the writing of the TR. He conducted and presented simulation results during CSMA Task Force (CSMA-TF) meetups. He also helped solve technical challenges needed to comply with worldwide regulations and the LoRaWAN standard.
- G. de Guillebon, served as the chairperson of the CSMA-TF. He also made contributions to the writing of the TR.
- M. Luis provided guidance throughout the CSMA-TF meetings and aided in improving the content of the TR.

Chapter 5 contains results from an on-going work. The paper will be titled "Borderless: Efficient Spectral Utilization for LoRa" and would be authored by A. Gamage, M. Li and A. Kuster.

- I proposed the initial idea to Prof. M. Li. I conducted experiments, developed the DSP algorithm to prove the feasibility of Borderless.
- Prof. M. Li provided guidance throughout the project. He helped plan the milestones of the project. He also aided in formulating the initial DSP processing steps.
- A. Kuster aided in discussions.

4th August 2023

.....

ITU NTU NTU NTU NTU NTU NTU NTI
NTU NTU NTU NTU NTU NTU NTU NTI
ITU NTU NTU NTU NTU NTU NTU NTI
NTU NTU NTU NTU NTU NTU NTU NTI



.....

Date

Jathun Gamage Isuru Amalinda

Acknowledgements

I extend sincere gratitude to my mentor, Prof. Mo Li. I count myself immensely fortunate to be part of the Wireless And Networked Distributed Sensing (WANDS) group under your guidance. Your style of teaching to understand the quality-driven approach to scientific research is something I truly appreciate. Your time, trust, and thoughtful guidance invested in my development will forever be cherished. Above all, your kindness deeply resonates with me.

Heartfelt gratitude goes to my parents. Your unwavering support and countless sacrifices throughout my life have been the force propelling my accomplishments both as an academic and a swimmer. From childhood until now, your selfless dedications have formed the pillars of my strength.

My deepest and heartfelt gratitude goes to my beloved wife. Your unwavering trust and support have been the backbone of my journey. Despite the geographical distance, your words of wisdom have often been my guiding light during the toughest of times. Your innate ability to help me unravel solutions to complex problems has been nothing short of miracles. Your faith in me has not only made this journey possible but also filled it with a sense of purpose and determination. You are the joy in my heart. Thank you for being you.

I extend my deepest appreciation to the world's best brother, Samiru, for your irreplaceable companionship throughout my journey.

My deepest appreciation also goes to my WANDS family, and to all those in my personal and professional circles. Each contribution, no matter the scale, has significantly shaped my journey, helping me arrive where I am today.

From the bottom of my heart, thank you, one and all.

“There is no devil in the details, there is nothing but beauty.”

—Gamage, Amalinda

To all who passionately craft the future of wireless.

Abstract

The emergence of the Internet of Things (IoT) has been pivotal in advancing urban and industrial efficiency, largely enabled by the growth of long-range low-power wide-area networks (LPWANs). These networks have facilitated IoT integration into diverse applications, including environmental monitoring, traffic control, and smart metering. In the LPWAN domain, LoRa modulation stands out for its long-range communication capabilities, addressing challenges posed by the rapid expansion of IoT devices. Despite being relatively new, LoRa has rapidly expanded to nearly 150 countries, redefining LPWAN standards. However, there is significant potential for further optimization. This thesis focuses on enhancing LoRa networks. First we identify a fundamental limitation in current LoRa networks: their reliance on the basic ALOHA mechanism for media access control, a result of LoRa's lack of carrier sense capability. Our research reveals that the recently introduced channel activity detection feature in LoRa, initially aimed at energy-efficient preamble chirp detection, can also reliably detect payload chirps. This discovery leads to the development of an efficient carrier-sense multiple access protocol, named LMAC, tailored for LoRa networks.

We present three progressive versions of LMAC, each building upon the last. These versions implement carrier-sense multiple access and optimize communication load distribution among channels defined by frequencies and spreading factors. This optimization is based on local information from end nodes and, additionally, global information from gateways. Our empirical studies, including a 50-node lab testbed and a 16-node university deployment, demonstrate that LMAC significantly outperforms the traditional ALOHA mechanism. The results show up to 2.2 times higher goodput and a 2.4 times reduction in radio energy per successfully delivered frame, indicating that replacing LoRaWAN's ALOHA with LMAC could yield considerable network performance enhancements.

In addition to the initial focus on LMAC, this thesis then tackles the implementation and optimization of this protocol within the industrial requirements of LoRaWAN. We explore the complexities of aligning LMAC with global regulatory compliance and ensuring its interoperability with existing network deployments. This involves a thorough analysis of LMAC's performance under a variety of network conditions and scenarios. The research presents a significant step towards integrating LMAC into the LoRaWAN standard, highlighting its potential in enhancing the overall efficiency and effectiveness of LoRaWAN networks.

Furthermore, the thesis addresses the increasing demand for spectral resources in the rapidly expanding IoT ecosystem. The surge in IoT nodes places significant strain on the limited and crowded spectrum. To address this, we propose a strategy for more efficient spectrum utilization: the concept of unchannelized or 'borderless' spectrum utilization for LoRa, allowing nodes to transmit frames at any selected central frequency, thereby enhancing spectral efficiency. This borderless approach poses challenges, such as detecting the central frequency of arbitrarily placed frames prior to demodulation. We provide solutions to these challenges, ensuring effective implementation of this novel spectrum utilization method.

Contents

Acknowledgements	ix
Abstract	xiii
List of Figures	xvii
List of Tables	xxi
Symbols and Acronyms	xxiii
1 Introduction	1
2 Primer on LoRa and Related Works	9
2.1 Primer on LoRa and LoRaWAN	9
2.2 Primer on LoRa demodulation	11
2.3 LoRa Performance Measurements	13
2.4 LoRa MACs	14
2.5 LoRa PHY	15
2.6 LoRa Collision Resolving	16
2.7 Spectral Optimization	18
3 Efficient Carrier-Sense Multiple Access (CSMA)	21
3.1 Enabling LoRa Carrier Sense	21
3.2 LoRa Testbed Design	25
3.3 Design of LMAC	27
3.3.1 LMAC-1	28
3.3.2 LMAC-2	30
3.3.3 LMAC-3	32
3.4 Evaluation	34
3.4.1 Indoor Experiments	34
3.4.2 Outdoor Experiments	38
3.4.3 Energy Overhead	40
3.5 LoRaWAN Implications	42
3.5.1 Data Rates of LMAC-based LoRaWANs	42

3.5.2	Network Capacity	43
4	Technical Recommendations for Enabling CSMA for LoRaWAN	45
4.1	Aligning LMAC with Industrial Desires	47
4.1.1	Enhancing Weak Nodes	47
4.1.2	Hidden Terminals, Exposed Terminals and Interoperability .	49
4.2	Enabling Regulatory Compliance	53
4.2.1	Modifications for Equal Spectral Utilization	54
4.2.2	Modifications for Regions with LBT	55
4.3	LMAC Based CSMA Protocol for LoRaWAN	57
4.3.1	The Rationale of the Proposed Protocol	57
4.3.2	State Transitions	60
4.3.3	Recommended CSMA Parameters	63
4.3.4	Recommended CAD Configuration	64
4.3.5	CAD Energy Overhead	66
5	Efficient Spectral Utilization for LoRa	69
5.1	Motivation	69
5.1.1	LoRa Channel Plans	70
5.1.2	Guard Band Efficacy vs. Interferences	71
5.2	Methodology	75
5.2.1	Frame Tagger	75
5.2.2	Collision Avoidance.	81
5.3	Evaluation	82
5.3.1	Performance Under Concurrent Frames	82
5.3.2	Performance Under Overlapping Frames.	84
5.4	Discussion	87
6	Conclusion and Future Work	89
6.1	Discussion	89
6.2	Future Directions	90
List of Author's Awards, Patents, and Publications		93
Bibliography		95

List of Figures

1.1	LoRaWAN Medium Access	5
2.1	The LoRaWAN network architecture comprises of nodes (end-devices), LoRa gateways, network servers and application servers.	11
2.2	Standard LoRa demodulation pipeline. Fig. 2.2a represents a data chirp. Fig. 2.2b represents a base downchirp. Fig. 2.2c represents the multiplicative result of the received data chirp and the base downchirp. Fig. 2.2d represents the FFT of the multiplicative result. Fig. 2.2e presents a partial LoRa frame at 868.1MHz with the first data chirp.	12
3.1	CAD results in SF12 and SF11 when there is an ongoing frame in SF12. Spectrogram shows the frame chirps.	22
3.2	Indoor 0-7 & outdoor 8-31 locations where CADs are performed.	22
3.3	CAD on various types of CSS signals. Top row shows the CSS signals; middle row shows the generated up chirps; bottom row shows the cross-correlation results. (a) CAD on a preamble chirp; (b) CAD on parts of two consecutive preamble chirps; (c) CAD on a data chirp; (d) CAD on parts of two consecutive data chirps; (e) CAD on chirps in a different SF.	23
3.4	CAD efficiency and SNR at various locations.	24
3.5	Current draw of SX1276 when it is idle, performing CAD, and transmitting in SF7.	25
3.6	(a) Testbed architecture. (b) Indoor testbed devices. (c) Outdoor gateway.	26
3.7	PRR vs. demand under ALOHA. Error bar shows the max, min, and mean PRR among 50 nodes.	27
3.8	Following LMAC-1, node-B detects a collision when node-A is transmitting in the same CH/SF.	28
3.9	Numbers of frames transmitted by all the nodes (TX) and received by the gateway (RX) under LMAC-1. More utilized channels with higher bars suffer from more frame losses, i.e., larger differences between TX and RX bars.	29
3.10	In LMAC-2, upon detecting that the selected CH/SF is unavailable, the node will search for the next CH/SF and perform DIFS on the new CH/SF.	31

3.11	Channel occupancy matrices (Γ) maintained by node 24, node 17, node 12, and gateway in a single experiment. A hatched pattern represents a null value due to no CADs performed in the corresponding CH/SF from the start of the experiment.	31
3.12	Overview of LMAC-3 protocol.	32
3.13	Network performance comparison among ALOHA, LMAC-1, LMAC-2, and LMAC-3. LMACs maintain about 90% network PRRs, achieve higher goodputs, and reduce energy consumption per frame reception.	34
3.14	CDFs of the per-node network performance under ALOHA, and LMAC-1/2/3 when the network demand is 2,600 B/s. Most LMAC nodes outperform ALOHA nodes except for a small set of ALOHA nodes. The steeper CDFs of LMACs suggest that the performance metrics are fairer among the nodes.	35
3.15	Under LMAC-2/3, both PRR and frequency channel load have limited variations. LMAC-1 may have lower PRRs. Under ALOHA, the frequency channel loads are scattered and the PRRs are low.	37
3.16	Average CADs performed per frame by each node under LMAC-2 and LMAC-3 when the demand is 500 frames a minute.	38
3.17	Performance of nodes in an outdoor environment from the perspective of average SNR of a node.	39
3.18	Cumulative effective traffic as SNR increases.	40
3.19	Percentage energy overhead of LMACs versus demand.	41
3.20	LoRaWAN performance.	42
3.21	Number of successfully received frames in one minute vs. various parameters (a) varying payload size with SF7 and CR4/8; (b) varying SF with 16-byte payload and CR4/8; (c) varying CR with 16-bytes payload and SF7.	44
4.1	SNR variation of a weak LoRa frames while nodes perform LMAC-2 under schemes (a) LMAC and (b)ALOHA. PRR variation of weak frames for varying demands under LMAC-2 and ALOHA in (c)	48
4.2	Interference to an SF-12 frame under two scenarios are showcased. (a) under LMAC-2, CH-1 experiences less instantaneous interference to the SF-12 frame as nearby SF-7 transmissions are less likely to collide with each other. (b) CH-2 shows a scenario under ALOHA where the absence of carrier sensing has caused two nearby SF-7 frames to collide resulting in higher instantaneous interference to the SF-12 frame.	49
4.3	Throughput and PRR variations of LMAC-2 under varying hidden terminal loads. In this scenario, hidden terminals are ALOHA nodes. Therefore, the experiment also predicts the extent of interoperability of LMAC with ALOHA for varying combinations.	50
4.4	Conditions for the occurrence of an exposed terminal.	51
4.5	Approximating an exposed terminal	52

4.6	Histogram showing the distribution of exposed terminal scenarios in a simulated LoRa network.	53
4.7	RSS variation under LoS and indoor environments.	56
4.8	LoRaWAN Medium Access State Transition Diagram	60
5.1	Organization of channels within a LoRaWAN/LoRa network. Each channel is composed of communication bandwidth and a guard band.	70
5.2	By adjusting the distance between CH-1 and CH-2 in the spectrum the % overlap between them can be adjusted.	72
5.3	Spectrograms of frames overlapped at 0%, 23%, 40% overlaps on CH-1 and CH-2.	72
5.4	PRR vs % Overlap for different SF and dB values	73
5.5	A partially colliding chirp segment from CH-2 falls in-band with CH-1. After standard demodulation process, the overlapping segment of the chirp translates to a weak amplitude peak during demodulation of CH-1.	74
5.6	System overview of Borderless design	75
5.7	Fig. 5.7A-E highlights the pre-processing steps in Borderless. (A) Shows initial samples from the SDR at Borderless BW <i>happens to</i> contain a LoRa frame. (B) The Borderless BW buffer is upsampled 2X. (C) The upsampled buffer is given a positive frequency translation of half the value of Borderless BW, e.g., 500khz. (D) A series of downchirps, locally synthesized to match the exact length of Borderless buffer. (E) The spectrogram of the product of frequency translated signal in (C) with the series of downchirps in (D).	77
5.8	FFT of Fig. 5.7E. The detected peak-pairs are marked. Pair-1 is a result of the LoRa frame preamble in Fig. 5.7A. Additional peak pairs are normal and a result of dechirped data chirps and the scalloping loss after the standard FFT.	79
5.9	Illustration of the central frequency estimation process: a demonstration of the interplay between received preamble chirps, locally generated downchirps and the generated signature.	80
5.10	Seven LoRa frames occupying the Borderless BW.	83
5.11	Spectrograms of overlapped LoRa frames at different overlap percentages	85
5.12	Signatures and peak pairs of LoRa frames at 80% overlap. It can be clearly seen that even at 80% overlap, there exist two clear signatures for both frames overlapped at 80%. Similarly, two peak-pairs are observed detected peak pairs.	86
6.1	Illustration of the Downlink-Uplink Communication Conflict in LoRaWAN Networks: This figure demonstrates the issue where uplink communications are failed due to ongoing downlink transmissions from the gateway, highlighting the challenge of non-full duplex operation in LoRa gateways.	91

List of Tables

4.1	Minimum SNR requirements of LoRa SFs for successful reception at the gateway [1, 2]. A negative SNR implies that LoRa frames can traverse under the noise floor.	48
4.2	Table of Parameters	63
4.3	CAD Settings for different Spreading Factors	65
4.4	SX1262 CAD energy consumption (optimized for best detection) . .	66
4.5	Transmission characteristics of SX1262 under (868/915 MHz) band .	66
4.6	CSMA overhead for three different transmission power levels.	67
5.1	Comparison of Ground Truth and Estimated Frequencies Through Borderless Approach	83
5.2	Comparison of Ground Truth and Estimated Frequencies by Borderless Approach under Various Overlapping Scenarios Per Each Frame.	86

Symbols and Acronyms

Symbols

α	the learning rate
Ψ	the global channel occupancy matrix
Γ	the local occupancy matrix

Acronyms

LMAC	LoRa MAC
LPWAN	Low Power Wide Area Networks
IoT	Internet of Things
SF	Spreading Factor
CH	Channel
BO	Back-Off
CAD	Carrier Activity Detection
CSMA	Carrier Sense Multiple Access
MAC	Media Access Control
DCF	Distributed Coordination Function
DIFS	DCF Interframe Space
LBT	Listen Before Talk
NBO	Number of Back-off Slots
RSSI	Received Signal Strength Indicator
LOS	Line-Of-Sight
NLOS	Non Line-Of-Sight
PHY	Physical Layer
FMCW	Frequency-Modulated Continuous-Wave

FFT	Fast Fourier Transform
LPF	Low Pass Filter
HPF	High Pass Filter
BPF	Band Pass Filter
SNR	Signal-to-noise Ratio
STFT	Short Time Fourier Transformation
COTS	Commercial Off-The-Shelf
PRR	Packet Reception Ratio
QoS	Quality of Service
DSSS	Direct Sequence Spread Spectrum
I/Q	In-phase and Quadrature
SFD	Start Frame Delimiter
COTS	Commercial off-the-shelf

Chapter 1

Introduction

Long-range communication capabilities of LPWANs will increase the degree of connectivity of IoT and enable deep penetration of networked intelligence into urban territories (e.g., wide areas, buildings, and underground structures) that have challenged the existing low-power short-range wireless technologies. As such LPWANs form an important class of wireless networks for geographically distributed Internet-of-Things (IoT). Among various LPWAN technologies (including NB-IoT and SigFox), LoRaWAN [3], an open data link layer specification based on the LoRa physical layer, offers the advantage of using license-free Industrial, Scientific and Medical (ISM) bands,(e.g., EU 868 MHz and US 915 MHz), low-cost end devices, and the independence from managed cellular infrastructures. LoRa, developed by Semtech [4, 5], serves as a physical layer modulation technology for the LoRaWAN stack. After its introduction, LoRa quickly gained significant interest from both the scientific community as well as from the industry, leading to collaborative efforts from both communities to solve common challenges. The popularity of LoRa is due to a set of key features that are uniquely suited to address the challenges posed by the advent of IoT [6–13]. Recent advancements related to LoRa are aimed at addressing challenges related to battery life, coexistence, fairness and the communication range of LoRa nodes.

LoRa’s unique modulation provides long communication distances and extended battery life for nodes. The modulation method used for LoRa is a variant of Chirp Spread Spectrum (CSS) technology, which Semtech claims is resilient to high levels of interference, multi-path, and Doppler effects—making it a strong

candidate for use on the ISM spectrum[14–19]. LoRa modulation also supports high channel capacity, thereby offering high network scalability. This means that a single channel can handle simultaneous transmissions from multiple devices, a significant improvement over traditional LPWAN technologies. Although LoRa’s physical layer is a proprietary technology of Semtech, many of its aspects are publicly accessible [20–22].

LoRa operates on the unlicensed ISM bands. Therefore, the efficient use of the finite, free to use, bands is key to ensuring a scalable and a reliable LPWAN technology for the future. The scarcity of spectral resources compels the innovation of novel approaches to ensure its optimal use. The urgency is further exacerbated by the proliferation of IoT devices, which are projected to reach an astounding number by year 2050.

Multiple access for LoRa. A fundamental expectation of LPWANs is reliable transmission. The importance of avoiding unnecessary re-transmissions is twofold: preserving the battery life of LPWAN nodes, which are expected to last several years on a small cell battery, and minimizing the wastage of scarce spectral resources. Currently, the LoRa networks, including those organized in an *ad hoc* manner or by following the LoRaWAN specification, adopt the ALOHA media access control (MAC) mechanism for each logic communication channel defined by radio frequency and the spreading factor (SF) of the chirp spread spectrum (CCS) modulation. The primitive ALOHA, though enabling simple network implementation, is not competent for scaling with the communication demand. As such, even though each end device conforms to the channel access time requirement (e.g., 0.1% or 1% duty cycle in Europe [23]), the ALOHA-based LoRa networks will have degraded network performance due to massive collisions when the numbers of end devices grow sharply in this era of IoT [24–33].

The absence of carrier sense capability on off-the-shelf LoRa end devices impeded studies and implementations of the more advanced carrier-sense multiple access (CSMA) schemes. However, a recently introduced feature called Channel Activity Detection (CAD) sheds light on CSMA for LoRa networks. The CAD, which is available on all of the latest LoRa radios (e.g., SX126x and SX127x), is designed for energy-efficient preamble detection. Although it is not for full-fledged carrier sense, our extensive measurement study shows that CAD can also detect the payload chirps with satisfactory performance. Specifically, it achieves more than 95%

accuracy in detecting the occupancy of a logic channel due to an ongoing frame transmission.

Most existing CSMA designs from other wireless technologies are based on energy detection on the spectrum. For instance, they adopt received signal strength (RSS) as an indicator of the presence of an on-going transmission[34, 35]. Simply porting them to LoRa networks may yield inefficiency. To achieve efficient CSMA for LoRa networks, the unique features and constraints of LoRa radios need to be considered. For instance, LoRa frame can traverse below the noise floor; Concurrent transmissions with different SFs are encouraged in the same frequency channel. These features render the traditional energy detection based CSMA designs ineffective. Thus, a clean-slate CSMA redesign based on LoRa’s physical layer characteristics is needed. To this end, we follow the *progressive systems development* methodology to design an efficient CSMA-based LoRa MAC (LMAC). The advancing versions of LMAC integrate various new designs and features based on the precedent code base to address additional and realistic networking problems. Their details are as follows.

LMAC-1: LMAC-1 implements the basic functionality of CSMA, i.e., to avoid collisions by refraining from transmission when the channel is busy. We implement the Distributed Inter-Frame Space (DIFS) mechanism that performs a fixed number of CADs and a random back-off (BO) mechanism. LMAC-1 shall outperform ALOHA in terms of packet reception ratio (PRR) and network goodput when the communication demand increases.

LMAC-2: LMAC-1 falls short of balancing the communication loads. As a result, the busier logic channels have higher frame loss rates. LMAC-2 aims to balance the loads among the logic channels by allowing LoRa end nodes to select the less crowded logic channels based on their local information. We devise an *indirect channel probing* approach for each end node to update its knowledge regarding the channels’ crowdedness based on the CAD results during DIFS and BO processes. Thus, LMAC-2 remains as a fully distributed MAC that aligns well with the LoRaWAN Class A specification. In addition, it does not introduce extra CAD overhead compared with LMAC-1. LMAC-2’s channel selection shall equalize the channel utilization and bring forth a performance improvement.

LMAC-3: In LMAC-2, the LoRa end nodes may develop biased local views regarding the channel loads. In LMAC-3, the gateway broadcasts global views of channel loads using periodic beacons. The beaconing renders LMAC-3 consistent with the LoRaWAN Class B specification. Upon receiving the global view, the LoRa end nodes update their local views to guide the channel selection before transmission. With the gateway’s assistance, LMAC-3 shall further improve network performance with respect to LMAC-2.

To support system design and evaluation, we construct a testbed consisting of 50 LoRa end nodes and a LoRa gateway in a lab environment. We conduct extensive, comparative evaluation experiments with goodput, PRR, and radio energy consumption per successfully delivered frame as main performance metrics. The results show that, compared with ALOHA which yields sub-50% PRR, all LMAC versions maintain sub-90% PRR when the communication demand increases. With respect to ALOHA, LMAC-1, LMAC-2, and LMAC-3 respectively bring $1.5\times$, $1.9\times$, and $2.2\times$ goodput improvements, and $2.08\times$, $2.37\times$, $2.38\times$ reductions in radio energy per successfully delivered frame. In addition, LMAC-3 achieves the most balanced channel loads. The experiments on a deployment of 16 LoRa end nodes in a university also shows significant performance improvements brought by LMAC in comparison to ALOHA.

In Chapter 3, we leverage CAD for carrier sense on LoRa end devices and design LMAC to improve the goodput and PRR of LoRaWAN networks. LMAC requires no modifications to the LoRa PHY layer and the LoRaWAN specification. To the best of our knowledge, this work presents the first systematic research and implementation of CSMA for LoRa networks. To this end, chapter-3 makes the following contributions. (1) We study LoRa CAD and show its full-fledged channel-selective carrier sense capability. (2) We design advancing versions of LMAC to address LoRa’s unique features and various realistic networking problems. The fully distributed LMAC-2 and the gateway-assisted LMAC-3 are the final yields of this work that align well with the LoRaWAN Class A and Class B specifications respectively. (3) Our testbed experiments show that, compared with ALOHA, LMAC brings doubled goodput and halved radio energy consumption under saturated communication demands. (4) We make available an LMAC integrated LoRaWAN codebase in [36].

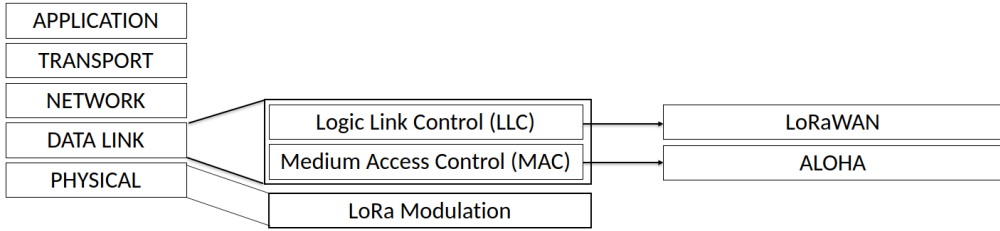


FIGURE 1.1: LoRaWAN Medium Access

Standardization of LMAC as the LoRaWAN MAC. LoRaWAN is a data link layer specification based on LoRa. It defines three classes, namely, Class A(ll end devices), Class B(eacon), and Class C(ontinuous listening). While the three classes have distinct characteristics in response times and energy expenditures, they are all based on the primitive ALOHA MAC as shown in Fig. 1.1. Although the requirement on the channel access time (e.g., 0.1% and 1% in Europe) mitigates channel contention, the ALOHA-based LoRaWAN cannot sustain the growth of end devices. Besides MAC, LoRaWAN also includes other link layer functions such as adaptive data rate and payload encryption [3]. Recognizing that CSMA could significantly enhance LoRaWAN, we embarked on the journey of standardizing LMAC as a part of the global LoRaWAN standard. This required a multi-faceted approach, encompassing industry-academic collaborations, technical adaptation of LMAC to industrial requirements, and compliance with global regulatory standards. These efforts paved way for further research to refine LMAC to seamlessly integrate with the LoRaWAN ecosystem.

The LoRa Alliance [37] is a non-profit association dedicated to maintaining and advancing the global LoRaWAN standard. This global association brings together numerous prominent tech companies and universities, all collaborating to drive the innovation and future trajectory of the LoRaWAN protocol [38]. Holding the authority to make crucial decisions about the LoRaWAN protocol, the LoRa Alliance has seen substantial growth since its inception. A significant branch of the Alliance is the Technical Committee (TC), responsible for standardizations, certifications, and addressing all technical aspects associated with LoRaWAN. The TC comprises industry pioneers and academics who actively participate in discussions. Members of the TC can submit proposals to enhance the LoRaWAN specification. These proposals undergo evaluation by other TC members, and if accepted, a specialized "Task Force" is formed to actualize the objectives. The key to a proposal's acceptance lies in its promised enhancements to all LoRaWAN stakeholders. Staffed by

industry veterans, the Task Force ensures steady progress through regular meetings until the objectives are met, often a process spanning over a year. Upon completion, the Task Force chair presents the results to the TC chair for mandatory review and feedback by the Certifications Committee, Security Committee, and a selected group of TC members. The approved deliverables are then shared with all TC members a week prior to a meeting, where a quorum must be achieved for final approval. Assuming no objections, the deliverables undergo an Intellectual Property Rights (IPR) review before being incorporated into the LoRaWAN standard. This rigorous process guarantees that approved Technical Recommendations (TRs) are thoroughly vetted, ensuring their relevance LoRaWAN.

Chapter 4 delves into the process of aligning LMAC-2 with the demands of the industrial LoRaWAN protocol. LMAC-2 which was initially proposed in [39] and subsequently refined in [40] undergoes further modifications to ensure global industrial adoption. The chapter showcases further investigations on LMAC-2’s performance under low-SNR frames and interoperability with existing deployments. The chapter also discusses the challenges faced during this process, particularly in ensuring global regulatory compliance across different regions. We also delve into details state transitions of a modified LMAC-2 based CSMA protocol for LoRaWAN. Finally, we provide recommendations for configuring the CAD engine of the commonly used SX126X radios. The chapter as a whole represents a significant step towards LMAC’s widespread adoption within the LoRaWAN ecosystem.

Spectrum-wide multiple access for LoRa. So far, we have discussed traditional spectrum management methods that rely on channelized transmissions. This strategy divides the spectrum into distinct, non-overlapping frequency bands—channels with the primary goal of minimizing *inter-channel interference* to ensure less interference to the transmitted intelligence. However, channelization comes with the downside of significant underutilization of the spectrum due to the creation of guard bands. In the case of LoRaWAN, these unused segments account to 37% of the spectrum, a significant portion that could have been otherwise utilized for communication, thereby compounding to the challenges associated with limited spectral resources. Given the escalating demands, the growing instances of intra-channel interferences, and the rising prominence of private LoRa networks, it may be beneficial to revisit the long-standing practice of channelized spectrum access.

These factors, combined with the potential for interference from non-LoRa modulations which do not adhere to LoRa channel plans are potential limitations in the current approach. While the channelized strategy has served us well thus far, the changing landscape of wireless communication invites us to contemplate whether this approach remains the most effective method for spectrum management.

To this end, we next investigate an unchannelized approach to LoRa multiple access, which allows a node to transmit a frame at any central frequency within the spectrum. The chosen frequency is not bound by a pre-defined list of channels but is arbitrarily selected from a vast pool of possibilities. This unconventional approach deviates from the restrictive, predefined channel plans characteristic of traditional channelized networks. The result is a more versatile and expansive utilization of the available spectrum.

In the context of a channelized LoRa network, the most damaging form of interference occurs when collisions take place across the same SF on the same channel. Given the predefined channel plans of these networks, such collisions are entirely overlapping and, therefore, significantly disruptive. However, the unchannelized approach presents an intriguing alternative. By allowing for a higher range of central frequencies for transmission, it introduces an element of randomness, making such 100% overlapping collisions far less likely. This characteristic could lead to improved resilience to intra-channel interference, offering a new way to tackle the challenges of spectrum efficiency within the burgeoning IoT ecosystem.

Chapter 5 presents the concept of truly *borderless* spectrum utilization as a potential solution to these challenges. In that, we examine if the protections sought through guard bands and channel plans can be achieved differently, specifically by eliminating the concept of guard bands and employing a contiguous spectrum which enables a wider bandwidth for communication. The borderless approach aims to provide improved spectral efficiency but also introduces unique challenges. At the absence of channelization, LoRa nodes could place frames anywhere in-band, leading to a scenario where the gateway needs detect an infinite number of central frequency (F_c) possibilities that a node might choose to transmit on. Furthermore, the arbitrary placement of frames could lead to a unique class of collisions occurring across both time and frequency which have not been studied prior. While our work focuses on LoRa communication as an example, the core concept of a channel-free approach could be extended to other protocols. Our research thus aims to explore

the viability of the borderless approach to spectrum utilization, provide a comprehensive overview of its potential, and examine its implications for the future of wireless networks and the IoT ecosystem. We seek to guide future research and contribute to the ongoing conversation around spectrum efficiency and utilization. Our exploration is, therefore, not only for the betterment of LoRa networks but a step towards a broader understanding of borderless spectrum utilization.

In this thesis, Chapter 2 establishes a foundation by reviewing existing literature in LPWAN technologies, pinpointing key areas for enhancement. This review directly informs the developments in Chapter 3, where the LMAC protocol is introduced. LMAC addresses the inherent limitations in LoRa's media access control, marking a important advancement in LoRa spectral utilization. The subsequent Chapter 4 extends beyond this theoretical development, delving into the practical aspects of LMAC. This includes its standardization and integration of LMAC to the global LoRaWAN standard. The narrative continues in Chapter 5, which proposes the 'Borderless' spectrum utilization method. This approach represents a significant departure from traditional channelized spectrum management, further enhancing the efficiency and capacity of LoRa networks. It also encourages broader discussions on spectrum management, aligning with the growing needs of the IoT ecosystem.

Outline of Thesis. This thesis contains six chapters. The literature review is presented in Chapter 2. Chapter 3 presents a MAC protocol that enhances the LoRa communication. Chapter 4 describes standardization efforts, further evaluations and a modified version of LMAC-2 which has been accepted as the MAC of LoRaWAN under TR13-1.0.0 published by the LoRa Alliance. Chapter 5 Presents an on-going work named Borderless, a method that further optimizes the use of ISM band for LoRa operation. We conclude this thesis and plan the future work in Chapter 6.

Chapter 2

Primer on LoRa and Related Works

Building upon the significance of LoRa as an LPWAN technology, Chapter 2 delves into the specifics of LoRa. We review related works to contextualize LoRa’s unique features and limitations, setting the stage for the subsequent chapters which aim to address some of these limitations such that spectral utilization of LoRa is enhanced.

2.1 Primer on LoRa and LoRaWAN

LoRa. A typical LoRa network consists of a number of geographically distributed end devices that transmit/receive data to/from one or more gateways. The radio frequency (RF) spectrum allotted to LoRa is also shared with a number of other physical layer protocols. LoRa physical layer divides the spectrum into multiple frequency channels (CHs), where each CH supports both *uplink* and *downlink* communications. LoRa employs CSS modulation, in which each *chirp* linearly sweeps a mandatory predefined bandwidth BW from the minimum frequency f_{min} to the maximum frequency f_{max} of the CH. CSS represents data by the initial frequency of a chirp.

A LoRa frame has three parts: a preamble of eight up chirps, a Start Frame Delimiter (SFD) of $2\frac{1}{4}$ down chirps, and a payload of multiple data chirps. Each data chirp lasts exactly a duration of T_{sym} milliseconds (ms). A data chirp starting

from an arbitrary frequency f_x represents an RF symbol out of 2^{SF-1} total symbols where SF is the spreading factor. The chirp starting from f_x linearly increases in frequency over time, reaches f_{max} , wraps around, and resumes its journey from f_{min} back to f_x . As such, each data chirp sweeps the entire bandwidth BW . Demodulation is performed at the gateway by relating the FFT bins of the multiplication of the payload with a series of down chirps.

LoRa physical layer allows concurrent transmissions in the same CH by using the distinct slopes of the concurrent chirps, i.e., SFs. This feature enhances a LoRa end device's ability to co-exist among many end devices that use the same CH. LoRa supports six SFs, from SF7 to SF12. In the rest of this paper, we use the notation CH/SF to denote a *logic channel* in which the simultaneous transmissions collide.

LoRaWAN. LoRaWAN is a data link layer specification based on LoRa. LoRaWAN adopts a star-topology network architecture defined by its bidirectional communication protocol. A LoRaWAN network comprises of end devices, gateways, network servers and application servers. End devices, also known as nodes, clients, or points, carry a variety of sensors and serve as the primary sources of data. Gateways, sometimes referred to as base stations, act as intermediaries, bridging the communication between end devices and network servers.

A communication process begins when an end device transmits a frame of data. This transmission is picked up by one or more gateways within range, which then relay the frames to their respective network servers. These network servers, acting as the controllers of the LoRa network, are charged with managing devices and applications and play an instrumental role in routing the data to the appropriate application servers.

In scenarios where the application server needs to communicate back to the nodes, the process works in reverse. Feedback is sent from the application server to the network server, forwarded to the gateway, and finally relayed back to the originating end device. This comprehensive network arrangement supports efficient two-way communication, underpinning the versatility and robustness of LoRaWAN. This process is illustrated in Fig 2.1 at a high level.

The most energy-efficient, Class A, allows nodes to remain in sleep mode for the majority of the time, only awakening when there's a necessity to transmit data.

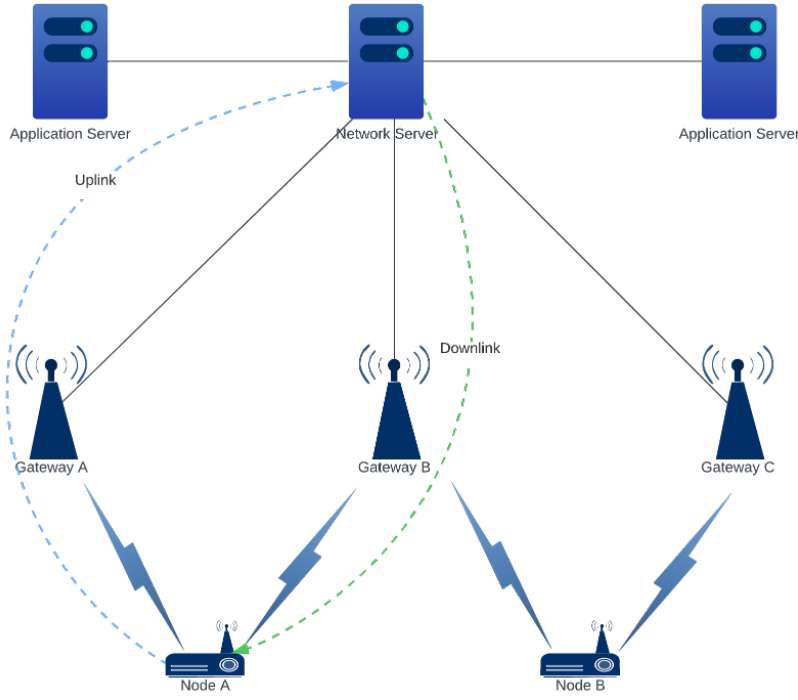


FIGURE 2.1: The LoRaWAN network architecture comprises of nodes (end-devices), LoRa gateways, network servers and application servers.

Following a Class A transmission, two reception windows are specifically opened by a node for possible downlink reception. In comparison, Class B employs the use of synchronized beacons to schedule multiple reception windows for downlink communication. While this ensures a quicker delivery of downlink messages compared to Class A, it also leads to higher energy consumption due to the periodic opening of reception windows. Class C nodes, on the other hand, have their reception windows permanently open, resulting in the maximum energy consumption among all classes. In a majority of scenarios, particularly those involving battery-powered devices and requirements for network scalability, Class A is the preferred mode. For instance, in a smart city setting, one gateway might be tasked with supporting hundreds or even thousands of nodes.

2.2 Primer on LoRa demodulation

This section offers a concise introduction to the standard demodulation process of LoRa. It also serves as a preamble to Chapter 5.

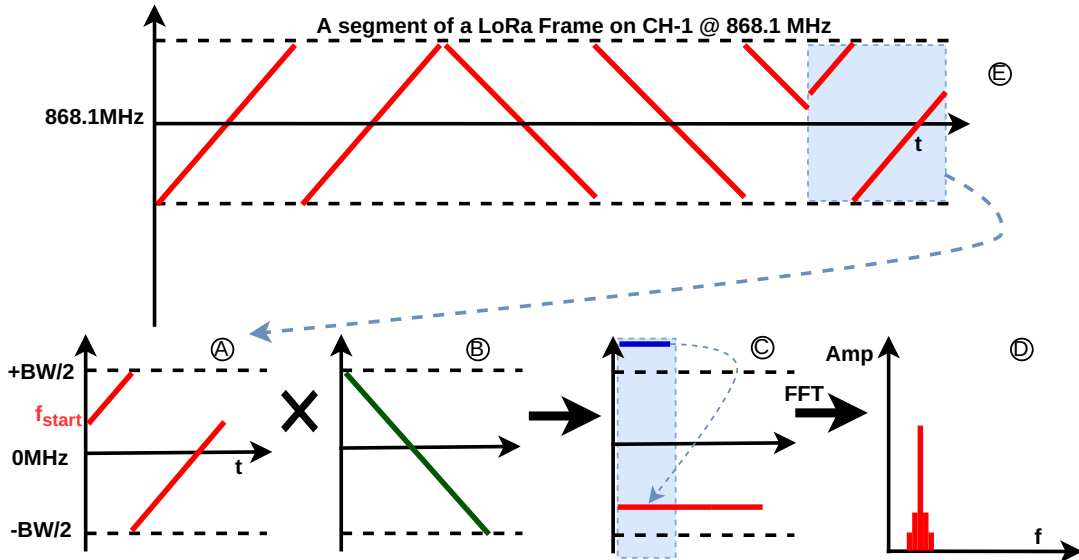


FIGURE 2.2: Standard LoRa demodulation pipeline. Fig. 2.2a represents a data chirp. Fig. 2.2b represents a base downchirp. Fig. 2.2c represents the multiplicative result of the received data chirp and the base downchirp. Fig. 2.2d represents the FFT of the multiplicative result. Fig. 2.2e presents a partial LoRa frame at 868.1MHz with the first data chirp.

Central to LoRa PHY communication is a chirp symbol. A single LoRa frame consists of three sections: preamble, Start Frame Delimiter (SFD), and a sequence of data symbols. The preamble of a LoRa frame is made up of base up-chirps. A LoRa data chirp is a single symbol with an initial frequency f_{start} that encapsulates encoded data. The receiver recovers this data through the standard demodulation process. This process is briefly explained next.

A LoRa gateway typically listens on a larger bandwidth, e.g., 1.6MHz of BW covering 8 X 200kHz channels [41]. To demodulate a LoRa frame, the receiver undertakes the following steps. First, the channel of interest, say CH-1 at 868.1MHz needs to be BPFed at LoRa BW. Second, I/Q data at CH-1 needs to be frequency translated to baseband—centered to 0Hz. Thirdly, the signal is resampled to LoRa BW, e.g., 125kHz. Next, it performs detection for possible LoRa frames and synchronizes with the first data chirp. Finally, it utilizes a local base down-chirp whose frequency linearly decreases from $\frac{BW}{2}$ to $-\frac{BW}{2}$. The FFT is performed on the product of each received data chirp and the locally generated down-chirp. The peak frequency bin from the FFT for each multiplicative result corresponds to the initially encoded data at the transmitter.

A key highlight from Fig. 2.2 is that most known literature¹ rely on resampling the received samples to 125kHz LoRa BW prior to performing dechirping to ensure that both the aliased component as well as the in-band component from the multiplicative result fall on to same FFT bin. To further illustrate this, the out of band component of the multiplicative result (indicated in blue) aliased to the 2nd Nyquist zone falling back in band is illustrated in Fig. 2.2c. The FFT of the multiplicative result produces a lightly noisy bin that uniquely relates to the originally encoded data as shown in Fig. 2.2d. The scalloping loss around the bin is expected and mostly attributes to the aperiodic nature of the samples processed through the FFT.

2.3 LoRa Performance Measurements

The emergence of LoRa/LoRaWAN has triggered a range of performance studies. These investigations focus on exploring the performance attributes of LoRa networks, including throughput, communication range, scalability, and energy efficiency. Several notable large scale studies have been conducted to estimate the performance of LoRa networks using real LoRa testbeds. They are briefly summarized below.

Liando, Jathun Gamage et al. [42] carried out a series of tests using a testbed of over 50 nodes and three gateways. Their findings suggested that while the communication range in a LOS scenario reaches up to 10 km, this decreases dramatically to approximately 2 km under NLOS conditions. They also estimated that the lifespan of a node under various configuration settings can range from 1.19 to 4.54 years. Their work indicated that a gateway could support up to 6,249 nodes with a PRR of 70%. Furthermore, their study offered insights into aspects like parameter optimization, early studies of LoRa medium access, concurrent reception, and physical layer. Tian et al. [43] released a comprehensive dataset covering network and link-level performance over a four-month period in a 21-node outdoor LoRa network. The dataset includes attributes like basic factors (time, SF, transmission power, etc.), connectivity and link quality (PRR, Received Signal Strength (RSS), Signal to Noise Ratio (SNR)), and environmental factors (node-measured temperature, weather condition, etc.) Xu et al. [44] explored the performance

¹Pyramid [22] resamples the received samples to 250kHz instead of 125kHz.

of LoRaWAN networks within multi-story buildings. They investigated a range of factors, including large-scale and temporal fading characteristics, coverage, and energy consumption. They concluded that various factors like building materials and layout significantly affect path loss. They also noted that the temporal fading adheres to a Rician distribution, with K-factors ranging between 12 and 18 dB. Such performance measurements pave way to understand capabilities and limitations of LoRa networks.

2.4 LoRa MACs

Slotted ALOHA and the scheduled time-division multiple access (TDMA) can reduce collisions compared to collision performance under ALOHA. Specifically, the end node will transmit in certain time slots to alleviate the collision issue caused by random access in ALOHA. Several studies [45–47] focus clock synchronization that is needed by slotted ALOHA and TDMA. However, due to LoRa’s limited communication and energy bandwidths [24], the communications required for clock synchronization present a burden for LoRaWAN networks. Thus, CSMA becomes a desirable alternative to avoid collisions in LoRaWAN as it does not require clock synchronization. Beltramelli et al. present a stochastic geometry-based model [48] to analytically show that CSMA outperforms ALOHA in terms of reliability and energy efficiency. However, full-fledged implementation of CSMA for LoRa is challenging due to the lack of hardware support for carrier sense. To achieve carrier sense, DeepSense [49] detects on-air transmission of LPWAN radios by storing spectrograms as an image, then performing signal identification on the image with artificial neural networks. However, an additional SDR device and machine learning accelerator are needed. To implement CSMA with off-the-shelf LoRa devices, a previous work [50] ports the 802.11 CSMA protocol to LoRa, in which the carrier sense is performed by a stand-alone node near the transmitter. This introduces additional monetary cost and system complexity.

Subbaraman et al. [51] introduced a novel method called Busy Signal Multiple Access (BSMA) for managing communication within LoRa networks. This technique aims to introduce CSMA to LoRa with additional functionality detect even hidden terminal problems frequently encountered in LoRa/LoRaWAN implementations. In the BSMA approach, whenever a LoRa node transmits a frame towards

the gateway, the gateway too transmits a 'busy' signal within the same channel. The presence of this signal prompts other IoT devices in the network to delay their data transmissions, thereby preventing data collisions and enhancing the overall network efficiency. A critical requirement for the successful implementation of BSMA is a full-duplex LoRa gateway that is capable of both receiving and transmitting data concurrently. In their work, the authors have developed and tested the first full-duplex LoRa gateway in the 915 MHz ISM band. They successfully managed several challenges, including a 9x increase in delay spread and the need for a 1000x increase in self-interference cancellation. The authors highlight that their gateway is compatible with commercial off-the-shelf (COTS) LoRa nodes. They also claim improved network capacity compared to the traditional CSMA, and network fairness for all IoT devices, irrespective of their proximity to the gateway. However, it's important to note that the performance of the BSMA might be significantly impaired due to two inherent aspects of LoRa technology—the inherent orthogonality [42] of LoRa modulation, and the duty cycle limitations enforced by radio frequency regulatory authorities [40, 52, 53] worldwide.

However, to be an effective candidate for LoRa CSMA, a research work must meet several key criteria. First and foremost, it should be compatible with existing hardware (both nodes and gateways) without requiring hardware modifications. Secondly, it must show global regulatory compliance to ensure its applicability worldwide. Moreover, it should not compromise the inherent performance of LoRa modulation, such as SF orthogonality, low-SNR capabilities. Finally, it should allow seamless integration with existing infrastructure.

2.5 LoRa PHY

While LoRaWAN is an open standard, the LoRa PHY remains a proprietary. Therefore, specialized hardware is required for transmission and reception of LoRa messages. Notable examples of such hardware include the SX127X/ SX126X transceiver series developed by Semtech [54]. These configurable transceivers expose a serial interface that is capable of making only high-level configuration to the LoRa modem to transmit and receive payloads via LoRa modulation. The entire PHY layer is embedded within the hardware, rendering it inaccessible for any modifications beyond what is granted. This proprietary nature of the LoRa PHY

layer imposes a significant barrier to a comprehensive understanding of LoRa's intricacies. Despite these challenges, research has been conducted to reverse engineer the LoRa PHY layer extensively. One of the earliest comprehensive reverse engineering efforts of LoRa PHY was brought forward by Knight [20], which was later enhanced by Peiter et al. [55]. These seminal studies paved the way for further reverse engineering efforts in the field, including a notable study [56], where the authors improved the SNR performance of the demodulation pipeline to detect low SNR frames.

2.6 LoRa Collision Resolving

Given the network structure and long-range capabilities of LoRa, a single gateway can connect to thousands of nodes. This can create intense congestion during periods of high demand, leading to numerous collisions [57]. Collisions cause LoRa frames to overlap at the gateway, inducing packet loss and lowering the network's throughput.

The principle behind resolving these collisions involves separating the superimposed chirps pertaining to a single frame using time domain, frequency domain and phase features through digital signal processing (DSP). Detailed insights on LoRa demodulation are provided in Chapter 5, but here we provide a quick summary to set the stage for discussing collision resolution methods. A LoRa receiver leverages the preamble and the Start Frame Delimiter (SFD) of a LoRa frame to accurately anticipate the frame's start time [56]. This facilitates appropriate separation of the I/Q samples of each chirp into individual windows. Subsequently, each chirp in the frame is dechirped, and the peak bin of the FFT from each dechirped window denotes the bits per symbol that were originally transmitted. When multiple frames collide, the FFT of the dechirped window reveals multiple peaks, creating ambiguity. Collision resolution strategies focus on accurately discerning the respective bin belonging to each chirp amidst multiple collided frames of the same SF.

Choir [58] is the first work of its kind to resolve collisions for LoRaWAN which exploits the distinct carrier offsets resulting through unique hardware imperfections of nodes to disentangle the collided frames. As Choir uses a new PHY algorithm,

the gateway of Choir requires the use of an SDR, such as a USRP, and employ software demodulation implementations. Netscatter [59] reduces LoRa modulation to on-off keying to simplify the operation on backscatter devices. It can scale for concurrent demodulation of backscatter LoRa signals. However, the unique design of Netscatter’s on-off keying modulation does not conform to standard LoRa modulation. To address the significant attenuation of the signals transmitted from end devices deeply located within buildings, Charm [60] jointly processes the signals received by multiple gateways to increase received SNR and the network coverage. Effectively, Charm allows multiple LoRaWAN gateways to pool their received signals in the cloud to reconstruct a more coherent signal. Charm carefully detects and sends only the relevant chunks of the received signal to the cloud, thereby saving uplink bandwidth. To address channel contention, Chime [61] analyzes a single frame from a node through multiple gateways. With the aid of synchronized gateways and optimal frequency estimation, once a frame is received, a Chime gateway advises the node on the most optimal channel for transmission. Chime requires an SDR based gateway to collect the I/Q data and strict synchronization across those gateways. Voigt et al. exploits the use of multiple LoRa gateways and directional antennae to aid in decoding interfered LoRa frames [62]. However, directional antennae impede a nodes’ ability to be heard by multiple gateways hence coverage of a node.

Xia et al. [26] discovered that edges of symbols of interfering transmissions in the STFT of the dechirped I/Q samples are not aligned in time. Based on this observation, they devised FTrack, a method that disentangles collisions and recovers frames by exploiting these misaligned edges and frequency continuity. In a subsequent work [63], Xia et al. expanded their approach to incorporate time,frequency features, and Phase-based Parallel Packet decoder, termed PCube. PCube relies on and exploits the reception diversity of MIMO reception. It first calibrates the frequency offset of the received signal, extracting the accurate frame timing of each packet based on the LoRa preamble and SFD. It then measures the phases of all concurrent symbols and mitigates the impact of hardware-induced phase variance. Lastly, PCube extracts the air-channel phase of each symbol and groups symbols into their respective packets.

Tong et al. [64] introduced CoLoRa, a collision decoding method based on chirp

peak ratios. Similarly, NScale, proposed by Tong et al. [65], leverages the non-stationary amplitude scaling down-chirp to translate packet time misalignment into frequency features. Xu et al. [22] introduced Pyramid, a low-overhead method for real-time collision decoding that separates packets by exploiting the “top” of a pyramid of FFT peak heights.

Interference cancellation algorithms have also been applied, such as mLoRa by Wang et al. [66], which iteratively decodes and then cancels collision-free symbols, and methods by Temim et al. [67] and Shahid et al. [68] which utilize various interference cancellation approaches.

In summary, existing collision resolving methods have greatly enhanced the concurrent transmission capability of LoRa gateways and reduced severe collisions. Many of these methods have offers increased throughput, and some [60, 64, 65] particularly focusing on weak frames.

2.7 Spectral Optimization

The rising demand from wireless devices leads to the overutilization of the shared ISM spectrum. As a result, unique methods such as overlapping channel plans have been explored in addition to well-understood techniques like CSMA and TDMA, particularly in mainstream wireless technologies like 802.11 WiFi [34].

Consequently, multiple WiFi access points sharing a common range employ overlapping channels. Mishra et al. [69] propose that the use of overlapping channels need not always be detrimental. Through a blend of theoretical analysis and practical measurements, the authors demonstrate that judicious use of some overlapping channels could enhance spectrum utilization and improve the performance of wireless applications. They suggest a model to boost the performance of two previously proposed channel assignment algorithms, revealing that employing overlapping channels can enhance end-to-end application throughput in specific scenarios. The experiments conducted under this study utilize the IEEE 802.11b direct sequence spread spectrum (DSSS) modulation standard operating in the 2.4GHz band.

In [70], Bahl et al. present the design and implementation of WhiteFi, the first Wi-Fi-like system constructed on top of UHF white spaces. Meanwhile, Remap [71] presents an innovative paradigm for managing collisions in OFDM networks with overlapping channels. Remap leverages partially concurrent transmissions, exploiting collision-free sub-carriers for decoding through multiple retransmissions. However, such works primarily aim to address high-speed wireless networks that employ unique higher power, higher bandwidth modulation schemes.

This concept of partially overlapping channels has also permeated LPWAN technologies. In [72], L. Wang et al. propose a method termed Intelligent Overlapping that enhances spectrum efficiency by leveraging coding redundancy to expand LoRaWAN spectral utilization. This approach allows for partially overlapping channels for concurrent spectrum access. The strategy uses deep reinforcement learning for spectrum management. The authors utilize deep-Q-learning to learn the extra coding redundancy from the data on the non-overlapping spectrum, which is then employed to recover data on the overlapping spectrum.

ART [73] and FAVOR [74] by Feng Li et al. present frameworks for addressing the coexistence of ZigBee and WiFi networks, aiming to enhance ZigBee network performance in WiFi-heavy environments. ART, including components like FAVOR and P-CSMA (Probabilistic CSMA), manages frequency and temporal dimensions to improve network coexistence. FAVOR specifically allocates continuous center frequencies to nodes or links, effectively even utilizing the "frequency white space" left unutilized by WiFi networks. Concurrently, P-CSMA adjusts CSMA to handle WiFi interference. Both frameworks have demonstrated their effectiveness in enhancing network throughput and transmission quality through extensive experimentation.

The core of ART involves a synchronization process between transmitters and receivers. This synchronization, driven by centralized frequency allocation and scheduling, is established and updated periodically based on the FAVOR algorithm. Such coordination ensures receivers are always tuned to the exact frequencies of their corresponding transmitters. However, maintaining this synchronization, especially in dynamic environments with fluctuating WiFi interference, presents significant challenges. Regular updates of frequency choices require recurrent communication, leading to communication overhead. Additionally, the reliance on a coordination mechanism can be problematic in large-scale or highly mobile networks,

impacting the efficiency and responsiveness of the ART framework in real-world applications.

To the best of my knowledge, no research efforts has been published on truly channelless operation for LoRa enabling arbitrary central frequency access to the spectrum.

Chapter 3

Efficient Carrier-Sense Multiple Access (CSMA)

Chapter 3 introduces the LMAC protocol as a response to address a gap in LoRa medium access control highlighted in Chapter 2, presenting a novel approach.

3.1 Enabling LoRa Carrier Sense

Carrier sense capability is desirable for advancing LoRa. Two factors, however, challenge effective LoRa carrier sense. First, LoRaWAN encourages concurrent transmissions in a single CH using different SFs. Second, most CSS-based modulation methods including LoRa allow signals to traverse below the noise floor. For instance, a LoRa receiver’s sensitivity is 10^5 times higher than that of Wi-Fi [75, 76]. The above two factors render the traditional RSS-based channel occupancy detection futile. In this section, we first highlight the limitations of traditional RSS-based carrier sensing for LoRa. We then extend the understanding of LoRa CAD beyond the technical documentation [55, 77] and evaluate the effectiveness of using CAD for the purpose of carrier sensing.

Channel Activity Detection (CAD). LoRa recently included CAD as a power-optimized mechanism to detect preamble chirps preceding full-fledged payload demodulation. This allows a LoRa node to energy-efficiently detect an incoming frame without resorting to power-hungry continuous RX mode. Some details of

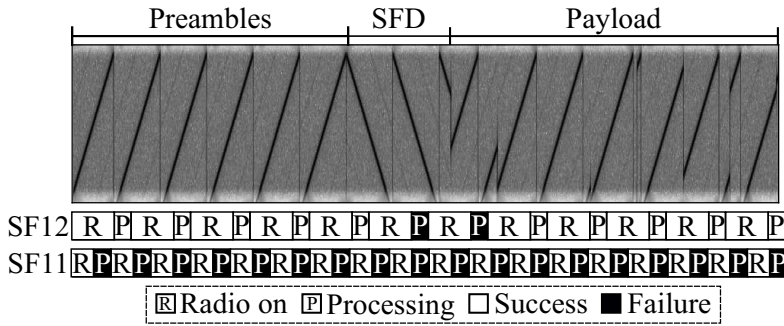


FIGURE 3.1: CAD results in SF12 and SF11 when there is an ongoing frame in SF12. Spectrogram shows the frame chirps.

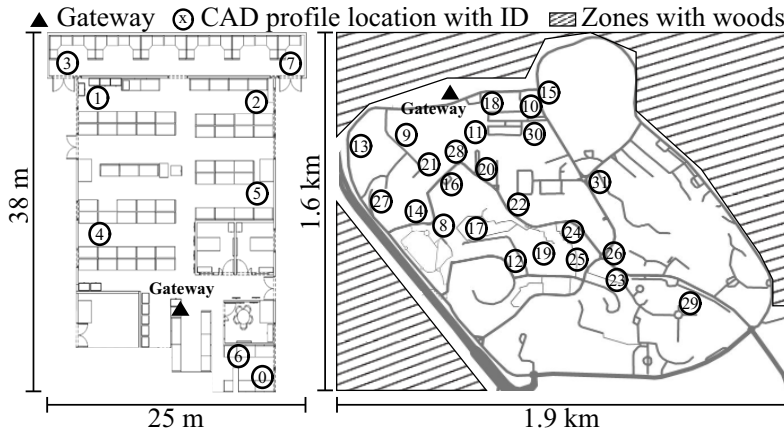


FIGURE 3.2: Indoor 0-7 & outdoor 8-31 locations where CADs are performed.

CAD are as follows. Prior to responding to a CAD request, the LoRa radio should be set on the desired CH/SF. A single CAD lasts $T_{sym} + \frac{32}{BW}$ ms, during which the radio takes the following steps. First, a lock in the phase-locked loop is achieved to tune the radio to the desired CH. The radio then switches to the receiving mode for T_{sym} ms. Second, the radio switches to processing mode to search for strong cross-correlation between the received I/Q samples and a locally generated up chirp of the same SF. The cross-correlation computation takes $\frac{32}{BW}$ ms. Lastly, a `CadDone` interrupt is generated. If the cross-correlation is high, a `CadDetected` interrupt is also generated.

To use CAD for carrier sense, we need to consider three factors: 1) How reliable is CAD? 2) Could CAD be performed on targeted SFs while the CH is also used by transmissions in others SFs? 3) How frequently can consecutive CADs be performed? To answer these questions, we conduct an experiment with three LoRa nodes and a software-defined radio (SDR) setup. In the experiment, a node transmits an SF12 frame on CH1 (868.1 MHz, 125 kHz BW). Two other nodes tune

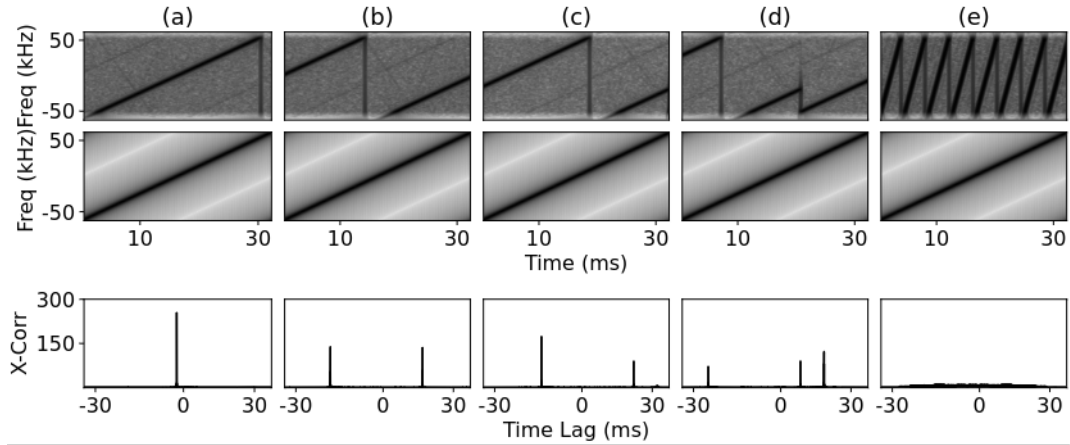


FIGURE 3.3: CAD on various types of CSS signals. Top row shows the CSS signals; middle row shows the generated up chirps; bottom row shows the cross-correlation results. (a) CAD on a preamble chirp; (b) CAD on parts of two consecutive preamble chirps; (c) CAD on a data chirp; (d) CAD on parts of two consecutive data chirps; (e) CAD on chirps in a different SF.

to CH1 and continuously perform CAD in SF11 and SF12, respectively. Fig. 3.1 shows a portion of the CH1 spectrogram recorded by the SDR and the two nodes' CAD results. We have the following two observations. First, CAD can detect data symbols. Second, CAD strictly adheres to the specified SF and does not generate false positives for other transmissions of different SFs in the same channel.

To develop a better understanding on the behavior of CAD, we conduct more experiments on the cross-correlation process of CAD. Cross-correlation computes the extent of similarity between a received chirp and the locally generated as a function of time lags applied to the locally generated chirp. Specifically, we compute the cross-correlation using two SF9 and SF12 frames recorded by the SDR. First, we test the case in which the incoming SF12 preamble chirp aligns ideally with the locally generated SF12 up chirp. The cross-correlation result shown in Fig. 3.3 indicates a clear spike signifying a detection. We then introduce a time offset of $\frac{T_{sym}}{2}$ ms, as shown in Fig. 3.3 on the incoming SF12 preamble chirps. As a result, the locally generated up chirp covers portions of two consecutive incoming chirps. Their cross-correlation produces two clear spikes corresponding to the portions of chirps. Next, we compute cross-correlation for an ideally aligned incoming data chirp which again results in two spikes corresponding to each segment of the data symbol as shown in Fig. 3.3. Afterwards, we compute cross-correlation for a data chirp with a time offset of $\frac{T_{sym}}{2}$ ms, and observe corresponding spikes as shown in Fig. 3.3. Note that the above simulated chirp offsets can be naturally incurred when

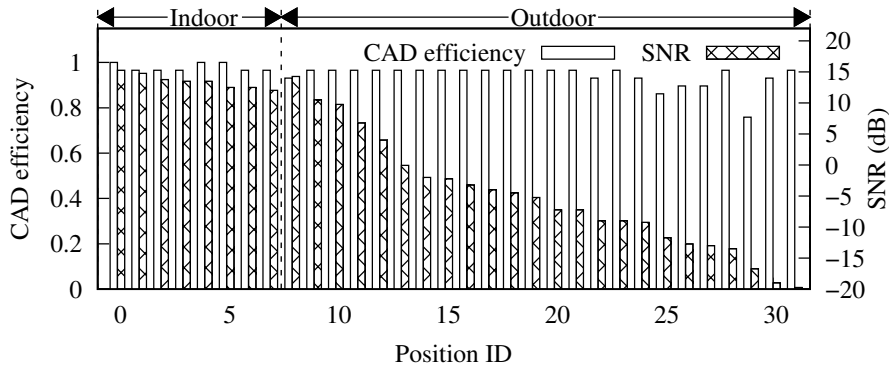


FIGURE 3.4: CAD efficiency and SNR at various locations.

the CAD process starts at an arbitrary point of the incoming frame. This can be observed from Fig. 3.1, i.e., a successful CAD does not necessarily need alignment with the incoming symbol. We then investigate how cross-correlation behaves for chirps in a different SF. In Fig. 3.3, CAD is performed between incoming SF9 chirps and locally generated SF12 chirps. It yields no peaks. Lastly, in order to predict the presence of a set SF, resulting peaks could be added and compared against a threshold.

Efficiency of CAD indoors and outdoors. LPWANs are typically deployed over large geographical areas. We also investigate the efficacy of CAD in an outdoor area. We deploy two LoRa gateways, one indoor and the other outdoor, and use a mobile LoRa node to perform CAD at multiple indoor and outdoor locations. At each location, we record the signal-to-noise ratio (SNR) reported by the LoRa node when successfully receiving a frame and the *CAD efficiency* that is the ratio of successful CADs among all CADs performed. Fig. 3.2 illustrates the experiment scenarios of (a) eight indoor locations across 800 m^2 of office spaces and (b) 23 outdoor locations scattered across a university area of 3.5 km^2 . Fig. 3.4 shows the SNR and CAD efficiency at all visited locations. The median CAD efficiency values are 98% and 94% indoors and outdoors respectively with SNR ranging from -15 dB to $+15 \text{ dB}$. Our results suggest that CAD maintains its functionality throughout LoRa's entire SNR range, effectively detecting even low SNR frames.

CAD energy footprint. Since CSMA introduces an additional energy overhead for each frame transmission, we profile the power consumption of CAD. To capture the power trace, we connect a power monitor [78] in series to the power supply pins of the SX1276 radio chip. Fig. 3.5 depicts the incurred current of a single CAD in comparison with those during the idle and transmission states. CAD draws 0.03 W,

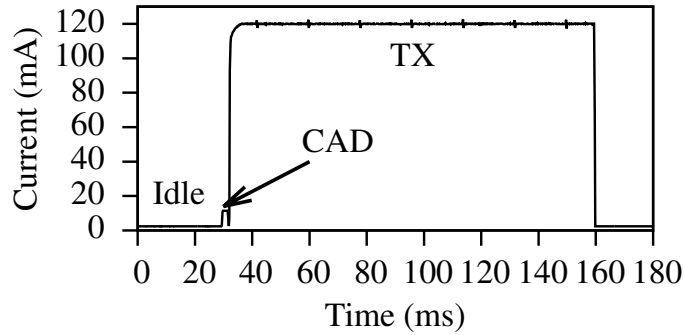


FIGURE 3.5: Current draw of SX1276 when it is idle, performing CAD, and transmitting in SF7.

which is $4.4 \times$ of the idle power and $11 \times$ less than the transmission power. A CAD in SF7 lasts for 1.2 ms only, consuming 0.029 mJ only. Under SF12, it lasts for 31.6 ms and consumes 1.1 mJ.

Summary. The above experiments give the following key observations. (1) CAD can be used as an effective and reliable carrier sense method; (2) CAD is SF-selective, i.e., it can detect transmissions in a specified SF while remaining insensitive to other transmissions in different SFs; (3) CAD is an energy-efficient operation compared with the energy consumption of data transmissions; (4) CAD works indoors and outdoors with high detection efficiency; (5) CAD can cater to unique physical layer properties of LoRa modulation to enable the missing carrier sense capability in LoRaWAN networks.

3.2 LoRa Testbed Design

To facilitate the design and evaluation of LMAC, we build a scalable LoRa testbed. This section presents the testbed design and experiment workflow which has been used for both indoor and outdoor experiments.

Testbed design. We aim to meet the following design requirements. First, the testbed should support a sparse deployment, i.e., across a university. Second, it should support convenient experiment configuration via a central controller. Third, it should provide a bidirectional backhaul link to disseminate configurations and receive experiment logs from the distributed LoRa nodes. Meeting these requirements imposes implementation challenges. For instance, it is non-trivial to synchronously control many LoRa nodes.

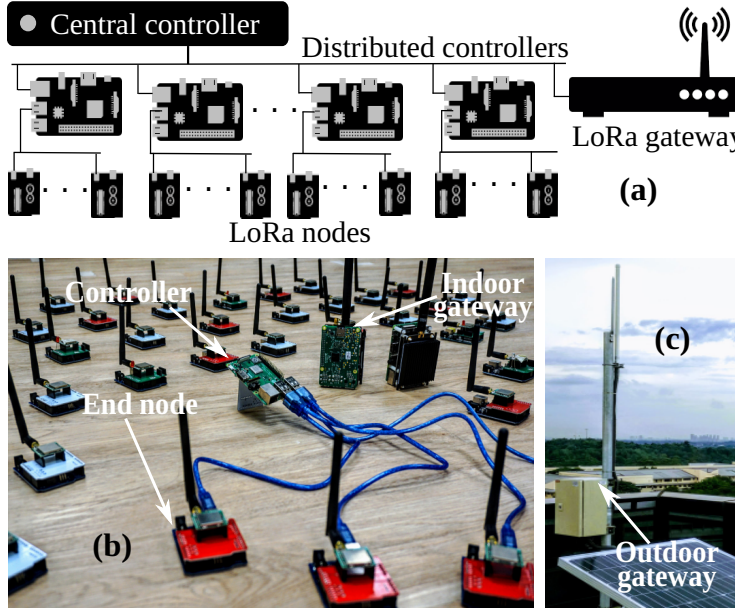


FIGURE 3.6: (a) Testbed architecture. (b) Indoor testbed devices. (c) Outdoor gateway.

Connecting each LoRa node to the *central controller* is not feasible as the LoRa nodes do not have wideband radios to support backhaul links. As such, we employ extensible units, each a cluster of LoRa nodes, and call them *distributed controllers*. The central controller and the distributed controllers are Raspberry Pi single-board computers that perform two coordinated roles. The distributed controllers execute and if necessary, relay control commands to LoRa nodes, thereby creating wideband out-of-band control links between the central controller and LoRa nodes.

Each testbed LoRa node is assembled in house by integrating an SX1276 LoRa transceiver with an Arduino Atmega328p MCU via a bridge board having a capacitor to support transient power requirements unsupported by USB power delivery [79]. Communications between LoRa nodes and a distributed controller (e.g., protocol firmware downloading and experiment log uploading) happens via an emulated serial interface. Fig. 3.6a illustrates the connectivity between each component of the testbed; Fig. 3.6b shows a shot of testbed hardware; Fig. 3.6c shows the outdoor gateway. To address the requirement of supporting geographically distributed nodes, testbed devices communicate through a network tunnel [80] from their local Ethernets.

Experiment workflow. An experiment includes the following steps: establishing connectivity among all components, loading a MAC protocol into LoRa nodes,

parsing experiment configurations, executing the experiments, and finally collating logs. In what follows, we provide some important details. At the beginning of an experiment, the central controller distributes a pre-compiled binary MCU program implementing a MAC protocol and two parameters (demand and experiment duration) to the distributed controller. The demand is the requested number of LoRa frames to be transmitted within the specified experiment duration. The extent that the requested demand is met reflects the network performance of the tested protocol. Varying the demand creates different levels of contention. After a mutual confirmation process to ensure that devices are ready, the central controller issues a start command to launch an experiment. Once the experiment duration expires, the distributed controllers report the following experiment logs back to the central controller: 1) LoRa node ID, 2) demand, 3) transmitted packets, 4) CADs performed on each CH/SF, and 5) the count of repeated experiments. In our experiments, all LoRa frames contain 16-byte payloads with the following fields to facilitate performance counting: 1) node ID, 2) packet counter, 3) demand, 4) the number of padding bits.

3.3 Design of LMAC

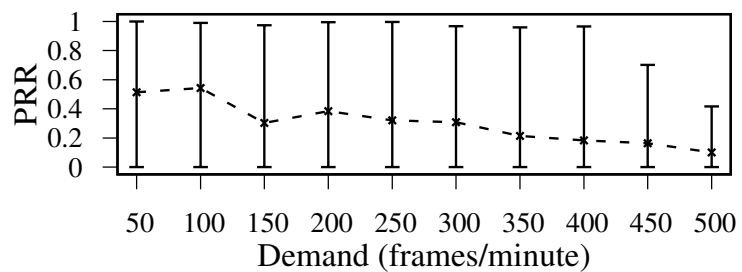


FIGURE 3.7: PRR vs. demand under ALOHA. Error bar shows the max, min, and mean PRR among 50 nodes.

This section presents the progressive design of LMAC to exploit CAD for CSMA-based MAC in LoRa networks. Under ALOHA, the end nodes access the medium abruptly regardless of the channel status, which results in excessive collisions when the communication demand is high. Fig. 3.7 shows an experiment result in which the average packet reception ratio (PRR) of ALOHA drops from 0.5 to 0.2, when the demand increases. The first version of LMAC, LMAC-1, uses CAD-based carrier sense to avoid the collisions.

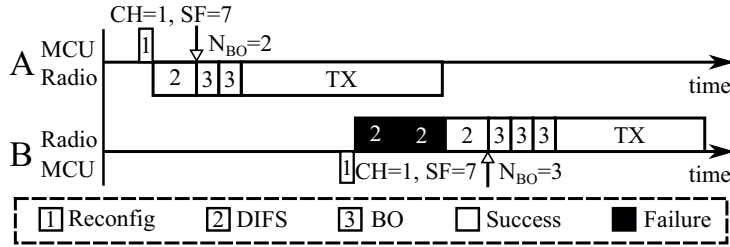


FIGURE 3.8: Following LMAC-1, node-B detects a collision when node-A is transmitting in the same CH/SF.

3.3.1 LMAC-1

LMAC-1 is largely based on the Distributed Coordination Function (DCF) that serves as one of the channel access methods of the IEEE 802.11. However, as LoRa differs significantly from 802.11 physical layer, changes are required to adapt DCF to LoRa. A key difference between 802.11 and LoRa is that LoRa does not have a feedback channel and thus cannot support the acknowledgment mechanism of DCF.

In LMAC-1, the CH/SF is chosen randomly for each transmission. An LMAC-1 node transmits a frame after the selected CH/SF is confirmed to be idle. To this end, LMAC-1 adopts the Distributed Inter-Frame Space (DIFS) mechanism from DCF with a fixed number of CADs per DIFS slot. When a DIFS slot completes with all CADs reporting idle channel, the MCU generates a random back-off (BO) value (N_{BO}) and enters the BO phase immediately. Then, the node decrements N_{BO} per each CAD reporting idle channel. The randomized initial value for N_{BO} reduces the possibility where two or more frames collide should the DIFS processes happen to start at the same time. Upon N_{BO} reaching zero, the node transmits the frame. Since a node continues checking the availability of the channel during the BO phase, an occupied channel will reset the node to the DIFS state. Should that occurs, the node needs to wait for an idle channel again and resumes counting down N_{BO} . Note that the initial N_{BO} value is not regenerated until the frame is transmitted. In the rest of this paper, we refer to CADs that report a busy channel as *failed* CADs and vice versa. A failed CAD operation within DIFS or BO will render a failed DIFS or BO slot respectively. Fig. 3.8 illustrates the process in which two nodes contend for the same CH/SF under LMAC-1. Node B detects an ongoing transmission during DIFS and continues performing DIFS until the channel is idle. Upon detecting an idle channel, node B enters the BO state

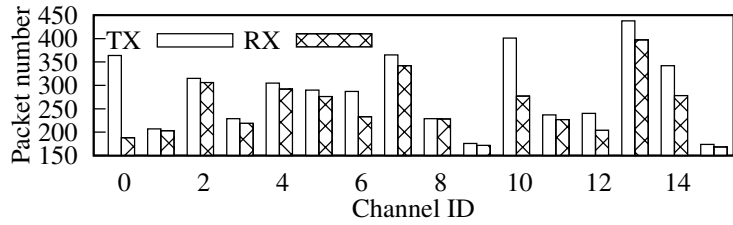


FIGURE 3.9: Numbers of frames transmitted by all the nodes (TX) and received by the gateway (RX) under LMAC-1. More utilized channels with higher bars suffer from more frame losses, i.e., larger differences between TX and RX bars.

with $N_{BO} = 3$ and starts decrementing N_{BO} with each successful CAD. Once N_{BO} reaches zero, node B transmits the frame. In the implementation of LMAC-1, we set the range for the initial value of N_{BO} to be [4, 64] and 12 CAD operations per DIFS slot.

LMAC-1 focuses on avoiding collisions. From the evaluation results that will be presented in §3.4, LMAC-1 improves the PRR significantly over ALOHA. In what follows, we present an experiment result that shows the imperfection of LMAC-1 and motivates LMAC-2. Fig. 3.9 presents the numbers of frames transmitted by all the end devices (labeled TX) and received by the gateway (labeled RX) in each CH/SF during an experiment. The difference between the TX and RX bars in a certain CH represents the number of lost frames. From the figure, an important observation is that, the busy channels (i.e., those with high bars) have more lost frames. The cause of the frame losses is explained as follows. The gateway radio chip SX1301 incorporates eight decoders that can be configured to demodulate incoming frames concurrently. Each decoder must be configured to a single CH but listens to all SFs. However, all decoders share an I/Q buffer. Should the decoders lag behind in decoding incoming I/Q data, a buffer overflow will occur, resulting in frame loss. This is because a decoder is tied to a specific frequency CH and a large number of frames arriving in that CH result in that a decoder lags behind compared to others. We refer interested reader to [42] for a thorough analysis of concurrent frame reception. The design of the SX1301 chip and the results shown in Fig. 3.9 imply that if the loads of the logic channels are equalized, the communication performance can be further improved.

To this end, the nodes can choose underutilized or idle channels instead of contending for a highly utilized channel. LMAC-2 aims to implement this feature.

3.3.2 LMAC-2

To select an underutilized channel, a node needs to track the utilization levels of all channels. Since continuous channel probing is time consuming, LMAC-2 leverages information from failed DIFS and BO operations to enable *indirect channel probing*. Thus, each LMAC-2 node maintains historical information regarding the crowdedness of past sensed CH/SF combinations. Later, the LMAC-2 node consults this information to shift to a better CH/SF when a channel is sensed busy during DIFS or BO. Doing so leads to more equalized channel loads and thus, better network performance. In addition, from the perspective of a node, the average number of CADs per transmission and the related time/energy expenditure can be reduced since busy channels are avoided. The key differences between LMAC-1 and LMAC-2 are as follows. In LMAC-1, a node fixates to a random CH/SF until a frame is transmitted. In contrast, an LMAC-2 node uses historical information to dynamically select the best CH/SF. The details of LMAC-2 are presented as follows.

Each LMAC-2 node maintains a *channel occupancy matrix* (Γ) of size $N_{CH} \times N_{SF}$, where N_{CH} and N_{SF} respectively represent the numbers of CHs and SFs. Each element in Γ , denoted by $\gamma_{CH,SF}$ represents the historical utilization rate for a given CH/SF. The $\gamma_{CH,SF}$ is updated for the $t + 1^{th}$ time whenever a node has a failed CAD during DIFS or BO. We adopt exponential averaging for the updating: $\gamma(t + 1) = \alpha \left(\frac{CAD_{busy}}{CAD_{total}} \right) + (1 - \alpha)\gamma(t)$, where α is the learning rate, CAD_{busy} and CAD_{total} are the number of CADs performed when the channel is busy and the total number of CADs performed respectively. The above exponential averaging is used for adapting to channel dynamics whilst maintaining historical information. As LoRa channels are highly dynamic, in our experiments, we set $\alpha = 0.8$ to ensure that higher importance is placed on the latest sensed channels.

We now describe how an LMAC-2 node uses Γ to select the next best CH/SF. A real-world LoRa deployment is subject to dynamic channel conditions. A channel that is seemingly busy may later become free. Therefore, simply choosing the least busy CH/SF according to the γ value may not always reap optimal network performance. As such, we randomize the choice. Specifically, we choose the best, the second best, and the third best CH/SF in terms of γ value with probabilities of 0.5, 0.3, and 0.2, respectively. This allows a forgiving approach for channels that were once crowded.

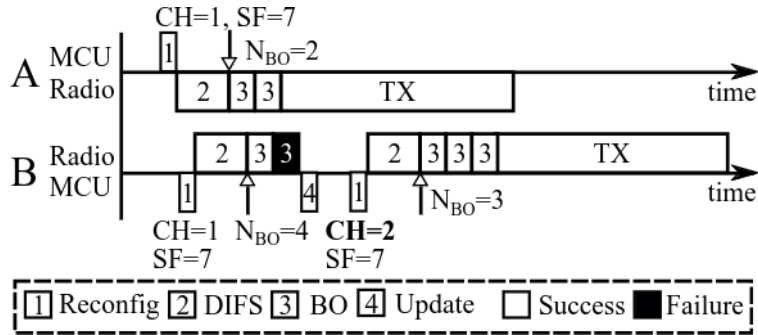


FIGURE 3.10: In LMAC-2, upon detecting that the selected CH/SF is unavailable, the node will search for the next CH/SF and perform DIFS on the new CH/SF.

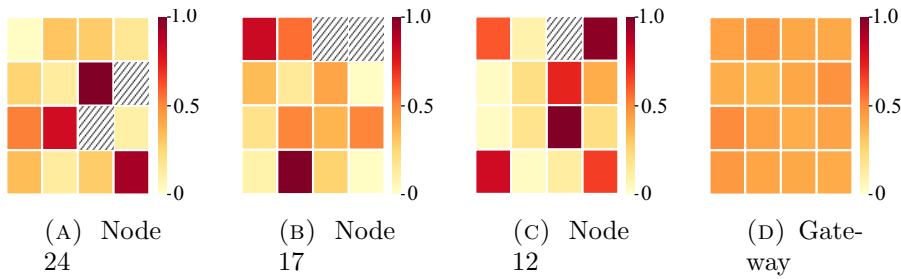


FIGURE 3.11: Channel occupancy matrices (Γ) maintained by node 24, node 17, node 12, and gateway in a single experiment. A hatched pattern represents a null value due to no CADs performed in the corresponding CH/SF from the start of the experiment.

The next SF selected is set higher or equal to that configured during deployment to ensure the frame robustness.

We use an example shown in Fig. 3.10 to illustrate the interaction between two LMAC-2 nodes that have selected the same CH/SF. Since node A completes BO earlier than node B, it proceeds with the transmission and node B reports a failed BO during node A's transmission. Thus, node B updates the occupancy matrix element corresponding to the current CH/SF, and re-configures the radio to the next CH/SF. Since the newly selected CH/SF is different from that used by node A, node B can complete DIFS and BO successfully and transmit the frame. If following LMAC-1, node B will wait till node A completes transmission.

As indirect channel probing is opportunistic, the channel occupancy matrices of LMAC-2 nodes are different. We illustrate this in Fig. 3.11. Specifically, Figs. 3.11a, 3.11b, and 3.11c visualize the Γ matrices maintained by node 24, node 17, and node 12 during an experiment. They are different. This difference leads to different channel selections of LMAC-2 nodes. LMAC-2 has the following two issues that

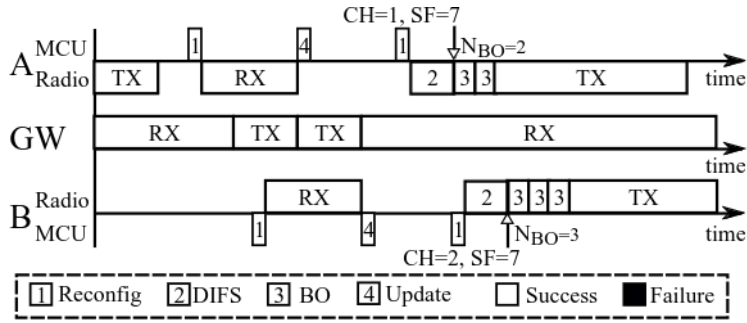


FIGURE 3.12: Overview of LMAC-3 protocol.

motivate LMAC-3. First, some elements in the Γ matrices remain null because no CADs have been performed on those corresponding CH/SF yet. Channels with null γ values may be busy. Without further information, avoiding these channels is wise but also losses opportunities in cases they are idle. Second, certain elements in Γ can be outdated due to lack of proactive channel probing. Addressing above two issues can advance LMAC to further reduce contention. To this end, we can exploit the global view of the gateway to complement the local views of LMAC-2 nodes. Fig. 3.11d shows the global channel occupancy matrix maintained by the gateway, which reflects the loads of all CH/SF combinations in real time. It does not suffer from null values and outdated issues. LMAC-3 is developed to use this global channel occupancy matrix.

3.3.3 LMAC-3

In LMAC-3, a gateway transmits a periodic beacon that contains the global channel occupancy matrix (Ψ) to the nodes in the network. Promptly, each receiving node follows a merging process to supplement its local occupancy matrix Γ with the gateway's global occupancy matrix Ψ . The Ψ is an $N_{CH} \times N_{SF}$ matrix where each element $\Psi_{CH,SF}$ represents the contention level in a given CH/SF.

Several challenges however need to be addressed for large-scale LoRa deployments to benefit from the global views of gateways. First, the process of disseminating a gateway's global view across the network should not be detrimental on the gateway's reception capability. Second, a LoRa node may receive overlapping coverage from two or more gateways. Due to network dynamics, a given CH/SF will face dissimilar contention across gateways.

Most commercial LoRa gateways only equip a single antenna and do not support duplex communications. As such, responding to each uplink frame with the Ψ matrix will reduce reception performance. Thus, to disseminate a gateway's global view, LMAC-3 employs time-distributed beacons via a predefined feedback channel similar to LoRaWAN Class B. Fig. 3.12 shows an example of this process where a gateway disseminates its Ψ to two nodes. Under LMAC-3, a LoRa gateway mostly stays in receiving mode and only switches to transmitting mode when it broadcasts beacons containing Ψ . Note that the nodes may miss a single beacon due to clock drifts. Thus, the beacon is transmitted twice on the feedback channel to increase the probability of reception. LMAC-3 does not require tight clock synchronization across nodes but coarse synchronization. Upon receiving Ψ , the nodes will perform the matrix merging that will be explained shortly and continue to transmit pending frames while awaiting the next beacon period. The Ψ matrix and the gateway ID is carried by a frame payload of 49 bytes where, an element $\Psi_{CH,SF}$ is represented by a 8-bit non-negative integer with 254 representing the highest load.

The $\Psi_{CH,SF}$ is formally defined as the ratio of the chirps that utilized the channel ($S_{CH,SF}^{RX}$) over the maximum possible during a beaconing period (T_{beacon}). The maximum number of chirps during a T_{beacon} is the multiplication of the chirp rate ($S_{CH,SF}$) and T_{beacon} . The chirp rate is defined as the reciprocal of the symbol duration in the considered SF. Following above, $\Psi_{CH,SF} = \frac{S_{CH,SF}^{RX}}{S_{CH,SF} \times T_{beacon}}$. To compute $S_{CH,SF}^{RX}$ for a given CH/SF, we count the number of chirps in the totally rx received frames in the CH/SF as follows: $S_{CH,SF}^{RX} = \sum_{i=0}^{rx} (n_i^{sfd} + n_i^{pre} + n_i^{pl})$, where n_i^{sfd} is the number of the SFD chirps in a frame, n_i^{pre} and n_i^{pl} are the numbers of preamble chirps and payload data chirps in the i^{th} received frame [81].

We now discuss how to merge Γ and Ψ . The simplistic approach of using Ψ solely to guide the channel selection is problematic, because the nodes will likely choose the same channel causing channel occupancy imbalance and contention. Our merging process adopts an element-wise weighted sum of Γ and Ψ , with a large weight for Γ and a small weight for Ψ . Thus, the merging result preserves the diversity of the nodes' observations while also capturing the global observations by the gateway.

To address the multiple gateway scenario, a gateway beacon integrates a single byte ID which aids in identifying different gateways. The $\Psi_{CH,SF}$ which has normalized channel contentions across gateways allows for simple merging of multiple Ψ matrices at node level. The above enables LMAC-3 to be scalable.

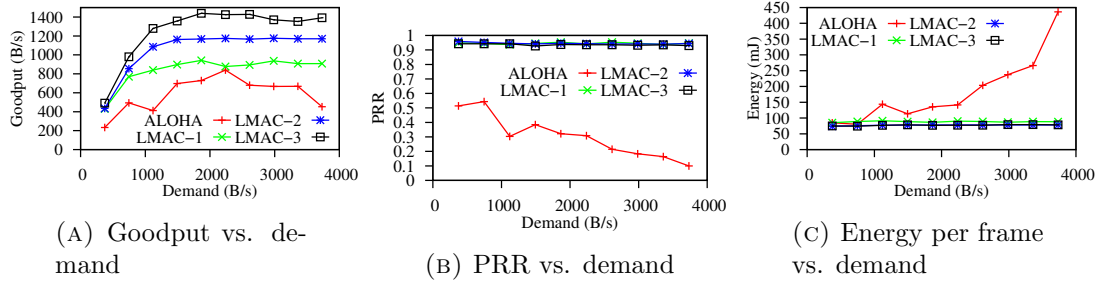


FIGURE 3.13: Network performance comparison among ALOHA, LMAC-1, LMAC-2, and LMAC-3. LMACs maintain about 90% network PRRs, achieve higher goodputs, and reduce energy consumption per frame reception.

Based on our empirical results under different environment conditions for varying contentions, we choose 0.8 and 0.4 respectively as weights for Γ and Ψ . The experiment results presented in §3.4 suggest that the determined weights provide high performance across various conditions and therefore can be used as is by new networks.

3.4 Evaluation

We conduct indoor and outdoor experiments using the testbed described in §3.2 to evaluate LMAC. We use PRR, goodput, and average energy consumption per successful reception as the performance metrics. We also consider protocol fairness in terms of the number of CADs performed by each node and distribution of channel loads.

3.4.1 Indoor Experiments

We conduct indoor experiments with co-located nodes in a lab environment, which allows us to better control the process and cover an extensive range of parameter settings. The experiments use 50 LoRa nodes. There are total of 16 CH/SF combinations used in the experiments (eight CHs and two SFs). In the experiments, we adopt the following default settings: 16-byte payload, 10-chirp preamble, and 2dB transmission power. Each experiment lasts one minute and is conducted in different times of the days over two months.

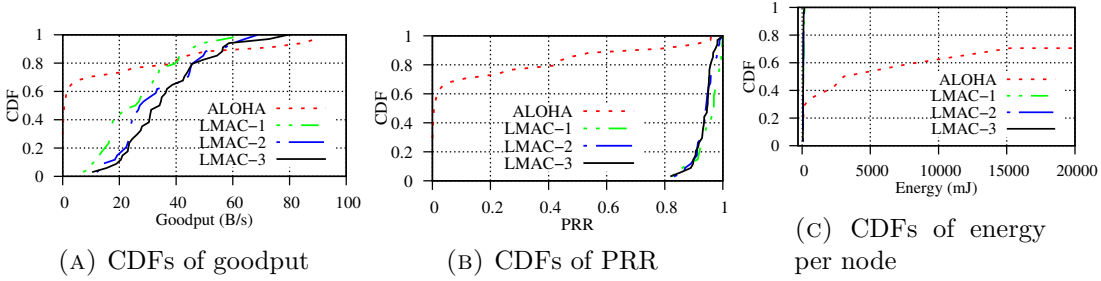


FIGURE 3.14: CDFs of the per-node network performance under ALOHA, and LMAC-1/2/3 when the network demand is 2,600 B/s. Most LMAC nodes outperform ALOHA nodes except for a small set of ALOHA nodes. The steeper CDFs of LMACs suggest that the performance metrics are fairer among the nodes.

Overall network performance. We evaluate the goodput, PRR, and node energy consumption when network demand varies under the four MAC protocols. Network goodput is the amount of meaningful data delivered per second. From Fig. 3.13a, we can see that compared with ALOHA, LMAC-1/2/3 improve the goodput by 1.52 \times , 1.87 \times , and 2.21 \times , respectively. Thus, LMACs can deliver data efficiently owing to the collision avoidance. Moreover, the performance increments of LMACs suggest the effectiveness of utilizing channel diversity and CH/SF selection. ALOHA goodput rises as the network demand increases but reduces once network demand is beyond 2500 B/s. This is consistent with the existing understanding of ALOHA performance. The goodputs of LMACs saturate and remain flat once the demand is beyond 2000 B/s. The saturation of LMACs goodput suggests the contention in channel utilization.

From Fig. 3.13b, the PRRs of LMACs are maintained above 90%, while that of ALOHA decreases with demand. The decline is due to increasing collisions. Differently, LMACs maintain high PRRs through avoiding collisions and busy CH/SF.

Fig. 3.13c shows the average energy consumed by a node per successfully delivered frame under the four MAC protocols. Compared with ALOHA, LMAC-1/2/3 reduce the energy by 2.08 \times , 2.37 \times , and 2.38 \times , respectively. Fig. 3.13c also shows that LMAC-2 and LMAC-3 consume similarly low energy, whereas LMAC-1 consumes slightly higher energy than LMAC-2/3. It is because LMAC-1 nodes continuously perform DIFS to contend for the channel. Differently, LMAC-2/3 perform less CADs due to wise CH/SF selection. In the experiment logs we find that LMAC-3 performs 1.92% less CADs than LMAC-2, whereas LMAC-2 performs 7.81% less CADs than LMAC-1. The goodput gain of LMAC-3 over LMAC-2 is

due to the time saved from less CADs performed. Specifically, LMAC-3 nodes can utilize the saved time for frame transmissions, while the PRRs of LMAC-2/3 are similar.

Overall, LMAC outperforms ALOHA through collision avoidance and achieves up to $2.21\times$ goodput improvement and $2.38\times$ reduction in nodes energy consumption, whilst maintaining above 90% PRR.

Per-node performance. A closer look at the results from a single experiment will provide more insights into the advantages of LMAC over ALOHA. Fig. 3.14 shows the cumulative distribution functions (CDFs) of the per-node network performance metrics. From Fig. 3.14a, majority of ALOHA nodes suffer low goodputs that are smaller than 5 B/s, while the remaining ALOHA nodes achieve goodputs scattered from 28 B/s to 74 B/s. The standard deviation of ALOHA’s per-node goodput is 26.79 B/s. In contrast, under LMACs, the CDFs do not exhibit undesirable long tails; the per-node goodputs are mostly within the range of 20 B/s to 60 B/s, with a standard deviation of 14.89 B/s. The above results suggest that, compared with ALOHA, LMACs achieve better balance among the nodes in utilizing the communication medium.

Fig. 3.14b shows the CDFs of the per-node PRRs. LMAC-2/3 achieve at least 80% PRR. The mean PRR values of all LMACs are above 90%. In contrast, about 40% ALOHA nodes suffer zero PRR, because the frames are lost due to collisions. The remaining nodes have scattered PRRs from 0 to 95%. Experiment logs suggest that ALOHA nodes with high PRRs dominate the CH/SF and hinder the reception of other nodes.

Fig. 3.14c shows the CDFs of the per-node energy consumption. Up to 30% ALOHA nodes cannot deliver a single packet. Thus, they are not accounted in the CDF. Another 40% ALOHA nodes consume excessive per-frame energy due to collisions. LMAC nodes are rarely affected by frame losses. The total energy consumed for channel probing trades for the exemption of futile energy consumption for transmitting lost frames. Overall, all LMAC nodes outperform 85% ALOHA nodes in terms of energy consumption.

In summary, a closer look into individual node performance reveals significant reduction in energy consumption per node which is hidden in the earlier results due to averaging. Moreover, under LMACs, the goodput and PRRs of each node

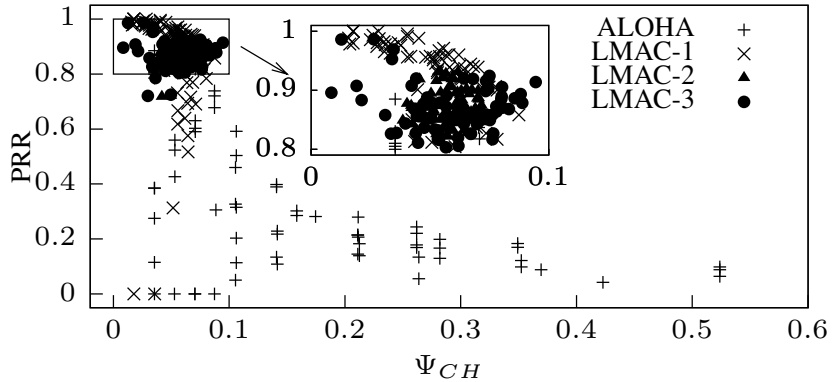


FIGURE 3.15: Under LMAC-2/3, both PRR and frequency channel load have limited variations. LMAC-1 may have lower PRRs. Under ALOHA, the frequency channel loads are scattered and the PRRs are low.

are more evenly distributed among nodes, while ALOHA nodes are clearly divided into the two extremes with a small number of exceptional nodes.

Balance and fairness. We evaluate the loads of all frequency channels under various MAC protocols. Since each channel supports multiple SFs, the frequency channel load (Ψ_{CH}) needs to be aggregated properly from the logic channels loads ($\Psi_{CH,SF}$) that are estimated by the gateway in the experiments. By averaging from SF7 to SF12 in each channel, the channel load for each frequency channel is obtained.

Fig. 3.15 shows the scatter plot of PRR versus channel load. The area of $\text{PRR} \in [0.8, 1]$, $\Psi_{CH} \in [0, 0.1]$ is zoomed in to present a detailed view of LMAC performances. PRR of ALOHA drops quickly with the frequency channel load. The result of ALOHA shown in Fig. 3.15 reinforces our understanding on the disadvantages of ALOHA’s completely uncoordinated transmissions. In contrast, the frequency channel loads of LMAC-1 are maintained within 0.1. This low load helps maintain satisfactory PRRs. It shows that LMAC-1 effectively avoids frequency channel saturation. More importantly, the channel selection mechanisms make LMAC-2 and LMAC-3 operating within the region with frequency channel load smaller than 0.1 and PRR within [80%, 100%]

Fig. 3.16 shows the sorted average numbers of CADs per frame performed by LMAC-2 and LMAC-3. LMAC-2 performs more CADs and yields a steeper slope which means higher variation. The additional channel information provided by the gateway helps LMAC-3 nodes to avoid known congested channels and perform less CADs. Many CADs are performed for every frame due to the DIFS design. Recall

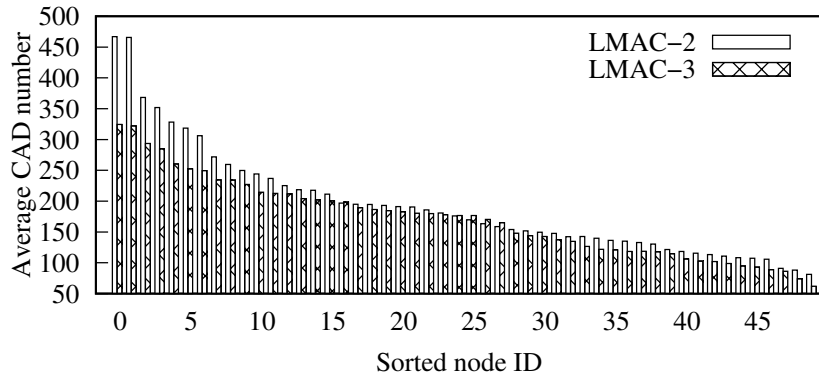


FIGURE 3.16: Average CADs performed per frame by each node under LMAC-2 and LMAC-3 when the demand is 500 frames a minute.

that each DIFS slot contains 12 CADs. Moreover, CADs are also performed during the decrement process of N_{BO} .

With the above experiments, LMACs yield a controlled and a fairer frequency channel utilization. This allows node performances to be more evenly distributed and ensure data delivery for each node. Moreover, the overhead of LMAC-2/3 is shown to be spread evenly among nodes where most nodes perform less than 250 CADs or 21 DIFS per transmission within a high contention network. The fewer CADs with high reception probability save radio energy for each successful frame delivery.

The latency introduced by LMAC is largely bound to network's contention levels. LMACs, under high contention levels, will incur higher latency due to the wait for free channels. ALOHA on the other hand is not subject to this latency but suffers from much higher frame loss rate due to collisions, which translates to much higher delay if retransmissions are used to ensure the same level of PRR.

3.4.2 Outdoor Experiments

To investigate the feasibility and performance of LMAC in an outdoor environment, a set of experiments were conducted in our university area. The experiment makes use of four distributed controllers and 16 end nodes. To exhibit the advantages of LMAC in a high-density network with low number of end nodes, the outdoor experiments use six CH/SF combinations. This set of experiments focus on LMAC-2 and LMAC-3 as the final yields of this paper. We collect 30 minutes of experiment

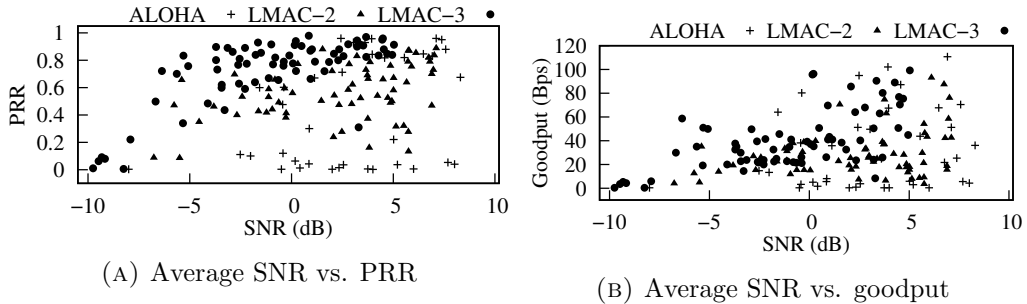


FIGURE 3.17: Performance of nodes in an outdoor environment from the perspective of average SNR of a node.

traces with 10 minutes for all protocols including ALOHA. Different from the indoor experiments, the outdoor experiments were conducted between 10AM to 10PM spanning across seven days.

The results of the experiments are presented in Fig. 3.17. Each point in the figure represents a node with the averaged SNR when the gateway received the frames. The standard deviation of SNR is between 0 to 3dB. The PRR (Fig. 3.17a) and goodput (Fig. 3.17b) of LMAC-2/3 spread across vertically and begin to concentrate downwards as SNR reduces. This shows the nodes with higher SNRs (i.e., well placed or nearby nodes) can deliver their frames more reliably. On the other hand, nodes with lower SNRs (i.e., poorly placed or obstructed nodes) most likely cannot reach the gateway and fail to deliver their frames. In contrast, ALOHA nodes are scattered in the plots with no clear pattern. Although there are nodes that achieve very high PRRs and goodputs, the majority of nodes have low PRRs and goodputs. The average PRR and goodput of ALOHA are 0.22 and 15.98 B/s respectively, while LMAC-2/3 reports 0.49 and 0.63 average PRRs with 25.17 B/s and 34.83 B/s average goodputs respectively. Notice that ALOHA has less points than LMAC-2/3. This is because more than 40% of ALOHA nodes' frames are lost at the gateway resulting in no SNR values registered for those nodes.

To understand the actual traffic of the network for each protocol, Fig. 3.18 presents each frame contribution to the effective traffic of the respective protocol. The results show that high SNR frames are more likely to be received by the gateway. Notice the effective traffic of ALOHA only starts to increase when SNR reaches 4dB while LMAC-2 and LMAC-3 effective traffic starts to increase at an earlier SNR. The late increase of ALOHA shows that frames with lower SNR are often drowned by higher SNR frames. Differently, LMAC-2/3 allow low-SNR nodes to transmit only when the channel is assessed to have low collision probability. Moreover, the

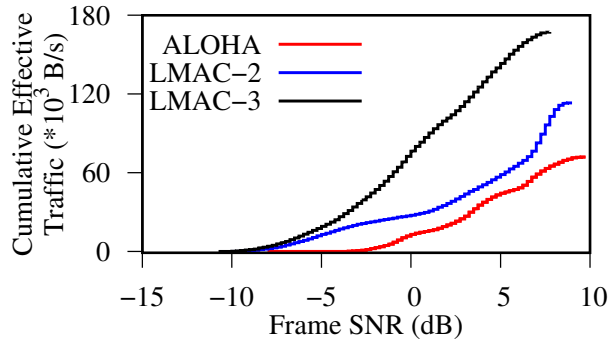


FIGURE 3.18: Cumulative effective traffic as SNR increases.

total effective traffic of ALOHA is lower than those of LMAC-2/3. This coincides with the earlier observation where more than 40% nodes are not accounted for due to no frame reception.

The above results suggest LMAC can be affected by environment dynamics but it provides effective traffic control even for low-SNR nodes. Contrarily, ALOHA nodes are divided into two extremes where one yields good performance while the other suffers from low PRR hence low goodput.

3.4.3 Energy Overhead

LMAC energy overhead is mainly attributed to CADs performed under *DIFS* and *BO* windows. We derive the percentage energy overhead of LMAC in comparison with a conventional ALOHA transmission.

We review the indoor experiment results based on 50 nodes with 10 different traffic demands in §3.4.1 and derive the average number of CADs a node needs to perform to send out a frame with the different network contentions, denoted by N_{CADs} . N_{CADs} accounts to average CADs performed during *DIFS* and *BO* windows across multiple SFs. From that, the average energy overhead per frame of LMAC, denoted by E_{LMAC} , can be computed as $E_{LMAC} = E_{CAD} \times N_{CADs}$, where E_{CAD} denotes the average energy consumption per CAD across all SFs. Therefore, the per-frame percentage energy overhead of LMAC is estimated as $\frac{E_{LMAC}}{E_{frame}} \times 100\%$ where E_{frame} denotes the transmission energy for a single LoRa frame averaged across all SFs. We estimate through energy measurements that E_{CAD} and E_{frame} correspond to 0.356 mJ and 0.31 J, respectively. We also find through measurements that N_{CADs} is similar across LMAC-2 and LMAC-3, which is also signified by the per

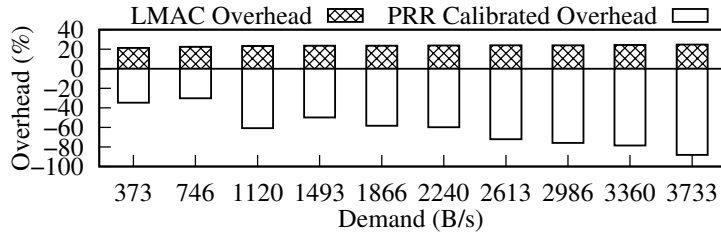


FIGURE 3.19: Percentage energy overhead of LMACs versus demand.

frame energy presented in Fig. 3.13c. Therefore, we compute the energy overhead of LMAC as a single entity for both LMAC-2 and LMAC-3. We then extend the percentage energy overheads of LMAC for varied network demands in Fig. 3.19. We see an energy overhead of about 20% to 25% which does not significantly grow with the increase of network demands (thus higher contentions).

Simply computing LMAC overhead in comparison with ALOHA frame energy E_{frame} does not fairly represent a real LPWAN network's performance that suffers from frame loss. We factor in the frame loss when considering the energy overhead of goodput, and derive the PRR calibrated energy overhead as expressed in Eq. 3.1,

$$\left[\frac{E_{LMAC} + Er_{frame(LMAC)}}{Er_{frame(ALOHA)}} - 1 \right] \times 100\% \quad (3.1)$$

where $Er_{frame(LMAC)}$ and $Er_{frame(ALOHA)}$ correspond to the PRR calibrated per frame energy, i.e., $\frac{E_{frame}}{PRR(LMAC)}$ and $\frac{E_{frame}}{PRR(ALOHA)}$, respectively.

The two quantities characterize the energy costs per successfully transmitted frame with LMAC and ALOHA. We present the PRR calibrated energy overhead of LMAC atop ALOHA in Fig. 3.19 as well. The results show negative overhead and attest that significant energy gains (40% to over 80% energy savings) are achieved with LMAC, especially under high network contentions where ALOHA is subject to much higher frame loss. Fig. 3.19 suggests that at a light energy cost in CADs, LMAC is able to greatly improve the PRR, which gains energy savings in achieving the same amount of goodput.

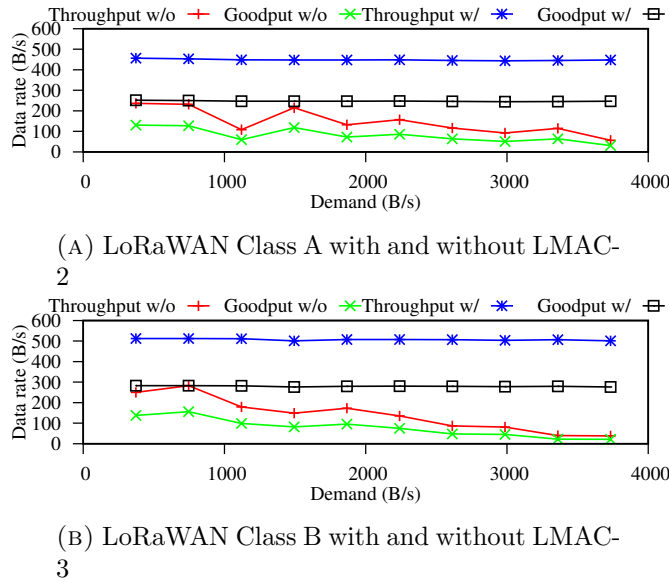


FIGURE 3.20: LoRaWAN performance.

3.5 LoRaWAN Implications

The testbed experiments in §3.4 have shown that LMACs improve the performance of LoRa networks. In this section, we apply LMAC to LoRaWAN which is the prevalent data link layer protocol primarily based on ALOHA. As LoRaWANs are constrained by the channel access time requirements (< 1% duty cycle ratio for each end node, etc.), it is difficult to experimentally show the full advantage of LMAC with limited number of devices. Instead, we conduct trace-driven simulations to exhibit the LMAC advantage for a scaled LoRaWAN network. We replace the ALOHA MAC in LoRaWAN Class A with LMAC-2 and LoRaWAN Class B with LMAC-3. LMAC-2 does not require information from the gateway, similar to the autonomy of LoRaWAN Class A; LMAC-3 requires gateway feedback which is provided by the beacon slot of LoRaWAN Class B.

3.5.1 Data Rates of LMAC-based LoRaWANs

The data traces used are collected from 30 experiments each spanning one minute for each of the three protocols. Thus, there is a 10-minute trace in total for each protocol. Trace frames are added with LoRaWAN headers and mandatory delays (e.g., guard time, RX slots, etc.). With the addition of LoRaWAN overheads, trace durations are recalculated. Once trace duration has been updated, frames received

and lost are replayed in the simulation as per trace records. The throughput and goodput of the replayed simulation are then recorded and presented in Fig. 3.20.

Despite the low data rate, LMAC could still bring $3.06\times$ and $5.93\times$ performance improvements on LoRaWAN Class A with LMAC-2 and LoRaWAN Class B with LMAC-3, respectively. The simulation results suggest the performance of LoRaWAN can be improved by utilizing LMAC as the default MAC. A noticeable difference from the results in §3.4.1 is the data rate of LoRaWAN decreases due to protocol overheads. As most of the overheads are due to the delays imposed for the two RX slots following a TX, the data rate achieved without the imposed delays will be much higher. However, our simulations still impose such delays to be consistent with the current specification of LoRaWAN.

Since LMAC does not alter any part of the existing LoRaWAN protocol except the MAC mechanism, the integration of LMAC to the LoRaWAN protocol stack could be readily achieved. Moreover, as LoRaWAN imposes channel access restrictions for fairness and LMAC can improve the channel access fairness by avoiding occupied or congested channels, the channel access restrictions can be relaxed or even removed from the LoRaWAN should LMAC be used.

3.5.2 Network Capacity

Understanding the maximum number of nodes that can be supported by the LMAC-based LoRaWAN is important. This section adopts a numerical analysis method to estimate the number of frames that the LMAC-based LoRaWAN can receive in a given period. Such number can be translated to the maximum number of supported end nodes once the per-node demand is given.

Using the results in previous experiments, the total number of chirps observed by the gateway in a channel (S_{CH}^{RX}) can be extracted within an observation duration (T_{obs}). With the data above, the observable chirps per second in the channel (S_{CH}) can be obtained through $S_{CH}^{RX} \div T_{obs}$. Having S_{CH} , an estimated number of frames a channel can receive (Frm_{CH}^{RX}) can be estimated by simulating different S_{CH}^{RX} values generated from varying frame parameters, i.e., payload size, time period, SF, code rate (CR), etc. With the simulated S_{CH}^{RX} , Frm_{CH}^{RX} is computed by $(S_{CH} \times T_{sim}) \div S_{CH}^{RX}$, where T_{sim} is the simulated time period.

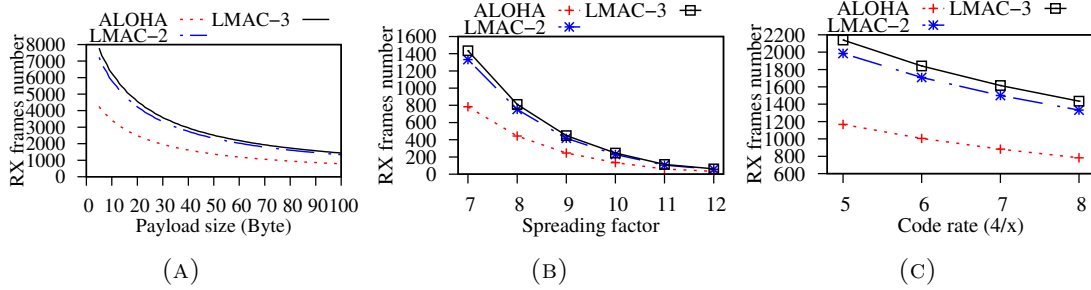


FIGURE 3.21: Number of successfully received frames in one minute vs. various parameters (a) varying payload size with SF7 and CR4/8; (b) varying SF with 16-byte payload and CR4/8; (c) varying CR with 16-bytes payload and SF7.

A network analysis using the above method to estimate the network capacity when three parameters (payload size, SF, and CR) vary are presented in Fig. 3.21. Varying payload size exhibit an exponential decay in the number of frames received shows that the payload size plays a vital role in network capacity. The network capacity declines exponentially as the payload size increases due to frame overhead. Frames with small payload size carry a larger overhead to payload ratio than frames with large payload size. Varying SF also exhibits similar decline as varying payload. Such decline is due to the non-linear increase in number of chirps per frame as SF increases. In contrast, varying CR decline is linear. This linearity reflects the linear increase in each CR setting from CR4/5 to CR4/8 where each increase in setting is an additional bit of redundancy added to every four bits of the frame. The results also show that LMAC-2 and LMAC-3 outperform ALOHA by 70% and 83% respectively, and the numbers of nodes that LMAC-2 and LMAC-3 could support would likely be similar.

Chapter 4

Technical Recommendations for Enabling CSMA for LoRaWAN

In Chapter-3, we designed a protocol which notably enhances LoRa communication in terms of network throughput, energy efficiency, and spectral utilization. Such advancements were substantially backed by rigorous experiments outlined within that chapter. Nevertheless, our proposed LMAC presented in Chapter-3, lacks the industrial perspective. For any wireless protocol to gain acceptance and integration within industry standards, a diverse set of facets need to be addressed. While our robust experiments on LMAC in Chapter-3 highlight its strong potential, making it a part of the industry standard requires more. It needs to fit well within worldwide wireless regulations and the needs of the industry. This means we need to look at it not just from an academic viewpoint, but also from a practical, industry-focused angle.

To bridge this gap and encourage the adoption of LMAC by broader industrial applications, we initiated engagement with the global regulatory authority of LoRaWAN, the LoRa Alliance. Our aim was to assimilate feedback and understand the needs and expectations from industry vanguards who are deeply rooted in the practicalities of the field. This not only involved interaction with the LoRaWAN Academia Workgroup and LoRaWAN Technical Committee, but also encompassed discussions with industry pioneers of LoRaWAN. A prime example is Semtech, the patent holder of LoRa technology, who, along with numerous other key stakeholders such as Actility, The Things Industries, GetWireless, and Comcast, were

instrumental in providing critical insights as to how to bridge this gap. They shared feedback on the modifications needed for worldwide adoption of LMAC, thus creating an example of industry-academia collaboration in evolving our academic contributions to meet the rigors of industry and worldwide regulations. The collective discussions pointed towards an overarching requirement — make LMAC a part of the global LoRaWAN standard as a Technical Recommendation (TR).

As we delve into the challenges of transforming LMAC into a globally applicable TR, the first challenge we confront is ensuring LMAC’s compliance with regions that mandate the use of Listen Before Talk (LBT). Our experimental evaluation indicates that while LBT may not be as effective in avoiding collisions, given its range limitations compared to LoRa devices, it is nonetheless mandatory for regulatory compliance in certain regions of the world. Such requirements transform into a unique research and an engineering hurdle— how do we design and specify key parameters to render LMAC compliant with such regulations? As such, we propose optimized strategies and modifications to enable compatibility with LBT based regulations. Another significant issue we address is the Federal Communications Commission (FCC) mandates in the USA requiring equal utilization of all channels, which could potentially conflict with LMAC’s innate tendency to always switch to the most optimal channel [52]. To resolve all regulatory dilemmas, we propose multiple modifications to LMAC, thereby ensuring full global regulatory compliance.

We further examine challenges that may arise in the course of LMAC’s adoption. We consider the implications of gradual adoption of LMAC across networks, and its subsequent interoperability with ALOHA. Acknowledging the time it takes for new upgrades to reflect as firmware in end devices, we seek to prevent any disruption to ongoing LoRaWAN networks. We conducted experiments to estimate the performance impacts of mixing both LMAC with ALOHA-based LoRa networks.

Lastly, a concern of industry for LPWANs lies in the reception from weak nodes, which produce weak frames at the LoRa gateway due to greater distance or obstructions en route. We conduct experiments to demonstrate that LMAC significantly improves this problem and we provide a technical explanation as to why.

Having identified and addressed these challenges, we turn our focus towards engineering LMAC. By integrating all the above factors, we formulate a variant of

LMAC-2 that aligns with the industrial LoRaWAN protocol. We present this variant through a state transition diagram, elaborating on all possible states and detailing the technical motivations behind the modifications. Further, we present a table of recommended parameters for the widely deployed SX1262 LoRa Radio to deploy CSMA for LoRaWAN, considering the nuances and constraints of this specific model. To complete our exploration, we highlight the energy overheads incurred while utilizing CSMA, once again using the SX1262 radio as a representative example.

This chapter addresses the task of transforming the experimental LMAC protocol into a globally accepted TR. We navigate the divide between research innovation and real-world applicability. Our goal is to enable LMAC's widespread use in industrial applications.

4.1 Aligning LMAC with Industrial Desires

In this section, we explore how LMAC, specifically LMAC-2, can be leveraged to address two challenges. We focus on enhancing the performance of 'weak nodes', tackling the 'last mile problem', and understanding the performance with the inevitable 'hidden terminals' in the network. The aim is not only to further demonstrate the potential applicability of LMAC in optimizing LPWAN performance, but also to show that LMAC facilitates smooth adoption under real-world settings.

4.1.1 Enhancing Weak Nodes

As we further our investigation into the capabilities of LMAC, particularly its variant LMAC-2, we now shift our focus onto an often overlooked but critical part of any network – the *weak nodes*. These weak nodes, characterized by their significant path loss and lower instantaneous signal strength, are often situated far from the gateway or obstructed. In standard LoRa deployments, these nodes have been a persistent challenge for network service providers to enhance, thus being referred to as *the last mile problem*.

The Last Mile Problem. Typically, to increase reliability, nodes furthest from the gateway are configured to use the slowest data rates (e.g., SF-12), allowing

SF	SF-7	SF-8	SF-9	SF-10	SF-11	SF-12
Required SNR	-6.5dB	-8.5dB	-11dB	-13.5dB	-18.5dB	-21dB

TABLE 4.1: Minimum SNR requirements of LoRa SFs for successful reception at the gateway [1, 2]. A negative SNR implies that LoRa frames can traverse under the noise floor.

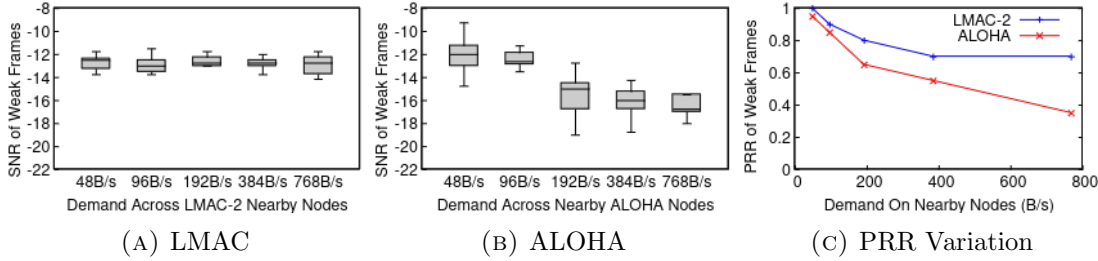


FIGURE 4.1: SNR variation of a weak LoRa frames while nodes perform LMAC-2 under schemes (a) LMAC and (b) ALOHA. PRR variation of weak frames for varying demands under LMAC-2 and ALOHA in (c)

their frames to travel farther. However, frames from these nodes, often facing high environmental obstructions or significant path loss, are much more vulnerable to arbitrary interference despite LoRa’s orthogonality principle. This issue stems from the fact that while nearby concurrent transmissions might be orthogonal, they still raise the noise floor during demodulation, impairing the reception of weak nodes.

Table-4.1 provides insight into this problem. It shows the minimum Signal-to-Noise Ratios (SNRs) needed for successful demodulation at the gateway across different Spreading Factors (SFs) in a LoRa network. Here, we can observe that SF-12 frames, used by weak nodes, offer an additional link budget of 14.5dB compared to SF-7, hence their resilience. Yet, even with this advantage, Semtech estimates that up to 18% of SF-12 frames can be affected by proximate SF-7 frames due to the increased noise floor [2].

Weak Node Performance. To explore the potential of LMAC in tackling the last mile problem, we set up an outdoor experiment with sixteen nearby nodes (SF-7) and one weak node (SF-12). The weak node was situated farther from the gateway (at a distance of 1000m), while the nearby nodes were within a 300m radius from the gateway. During the experiment, we measured the SNR and PRR of the weak node’s received frames under both ALOHA and LMAC-2. As seen in Fig.4.1, the SNR of weak frames under LMAC-2 experiences less fluctuation with increasing demands from nearby nodes compared to when ALOHA is in use. This enhanced SNR translates directly to increased PRR for LMAC-2 nodes.

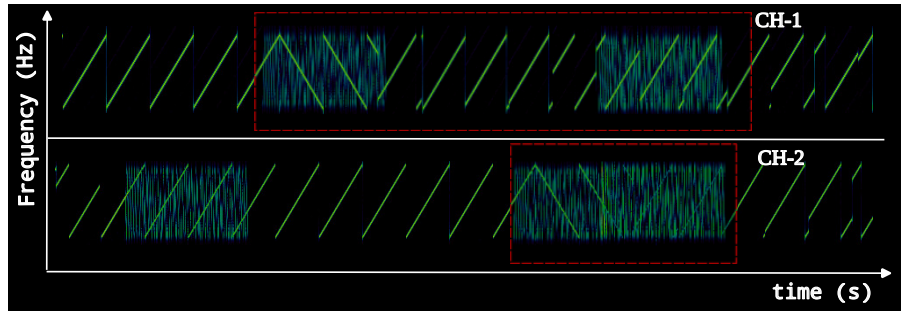


FIGURE 4.2: Interference to an SF-12 frame under two scenarios are showcased. (a) under LMAC-2, CH-1 experiences less instantaneous interference to the SF-12 frame as nearby SF-7 transmissions are less likely to collide with each other. (b) CH-2 shows a scenario under ALOHA where the absence of carrier sensing has caused two nearby SF-7 frames to collide resulting in higher instantaneous interference to the SF-12 frame.

The enhancements seen under LMAC-2 are due to its effective reduction of collisions across nearby transmissions. This decreases instantaneous interference to weak frames. Fig.4.2 further illustrates this phenomenon with a spectrogram that represents interference to a weak frame under ALOHA and LMAC-2. Notably, under LMAC-2, a weak SF-12 frame is less likely to be interfered with two or more simultaneous SF-7 frames. This results in less instantaneous interference on the weak SF-12 frame by nearby SF-7 frames.

These results illustrate the advantage of LMAC, especially LMAC-2, enhancing the performance of weak nodes in a network.

4.1.2 Hidden Terminals, Exposed Terminals and Interoperability

Another key aspect to consider while assessing network performance is the presence of *hidden terminals*. These nodes, due to their location or other factors, cannot detect each other's transmissions, yet their signals often reach the gateway. Consequently, simultaneous transmissions from these nodes can lead to collisions at the gateway, deteriorating the overall network performance. Notably, hidden terminals share a common trait with ALOHA nodes— their inability to perform effective carrier sense.

LMAC, being a CSMA protocol, isn't immune to the hidden terminal problem. Additionally, certain regions around the world do not regulate the ISM band to

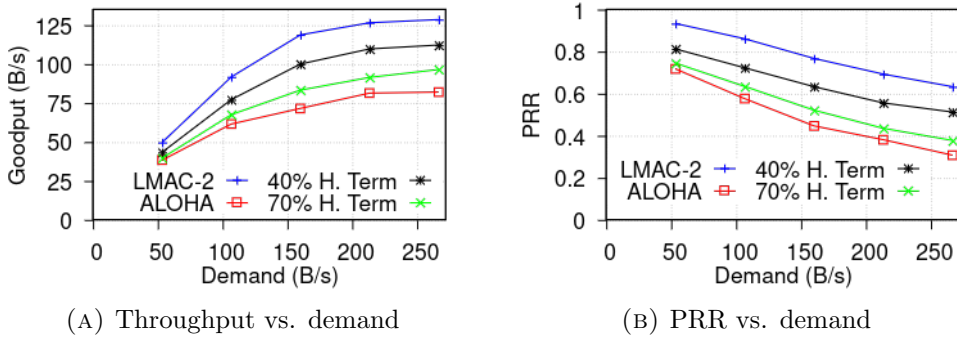


FIGURE 4.3: Throughput and PRR variations of LMAC-2 under varying hidden terminal loads. In this scenario, hidden terminals are ALOHA nodes. Therefore, the experiment also predicts the extent of interoperability of LMAC with ALOHA for varying combinations.

perform carrier sensing, leading to a mix of nodes that either perform or do not perform carrier sense. Even in regions that enforce strict LBT, they mandate the use of *RSS Based Sensing*, which is not an efficient carrier sense mechanism for LoRa [23, 52, 82]. Moreover, the adoption of LMAC is a gradual process, and transforming an entire network to utilize CSMA capabilities takes time. Therefore, it's inevitable that networks will contain a mix of ALOHA and LMAC nodes at any given time, forcing nodes that perform CSMA and do not perform CSMA to coexist.

LMAC performance with hidden terminals. To evaluate LMAC's resilience when coexisting with hidden terminals, we must control the quantity of hidden terminals, which is inherently challenging due to their nature. We emulated hidden terminals with ALOHA nodes, which do not perform any type of carrier sensing. This setup allowed us to evaluate the impact on an LMAC-2 network under different combinations of hidden terminals. The reason to doing so is because actual implementation of hidden terminal is challenging, specially given that these experiments require varying proportions of network to be hidden terminals at different times.

Fig.4.3 showcases the performance of LMAC-2 under various hidden terminal combinations. Even with 70% of hidden terminals, LMAC-2 still provides an additional 20% throughput gains and 26% PRR gains compared to a pure ALOHA network. Remarkably, with 40% hidden terminals, the throughput gains increase to 40%, and PRR gains rise to 71% compared to an ALOHA-only network.

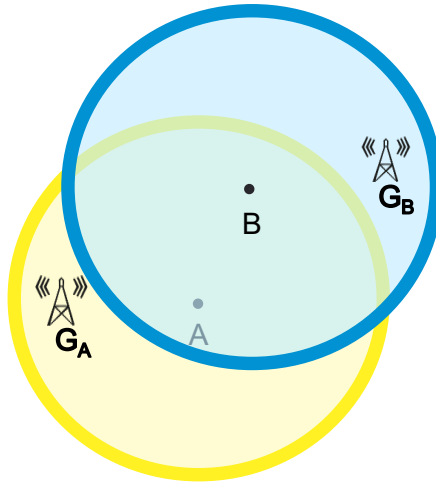


FIGURE 4.4: Conditions for the occurrence of an exposed terminal.

These results underline the robustness of LMAC-2 when dealing with hidden terminals, which were simulated as ALOHA nodes in this case. The results highlight LMAC's resilience and predicts the extent of interoperability of LMAC with ALOHA under different proportions of node types. Such findings further reinforce the potential of LMAC.

Impact by exposed terminals in LMAC. In addition to hidden terminals, *exposed terminals* represent another significant challenge in CSMA-based networks. Exposed terminals occur when a node unnecessarily defers its transmission because it senses the medium as busy due to a nearby transmission, even though its transmission would not have interfered with the on-going transmission. This scenario contrasts with hidden terminals, where nodes are unaware of each other's transmissions which leads to potential collisions at the gateway.

Exposed terminals are particularly relevant in LoRa networks due to the long-range nature of LoRa links. These situations arise when two nodes, say Node-A and Node-B, can detect each other's transmissions, but their respective transmissions are intended for different gateways that are out of range from each other. This leads to an inefficient use of the medium, as nodes might delay transmissions unnecessarily, reducing the overall network throughput. Exposed terminals occur upon fulfilling three mandatory conditions, as depicted in Fig. 4.4. Firstly, consider Node-A, which is located near Gateway-A but outside the range of Gateway-B. Conversely, Node-B is within Gateway-B's range but beyond Gateway-A's reach. Secondly, despite their separate locations relative to each other's gateways, Node-A and Node-B must be capable of sensing each other's transmissions. The third

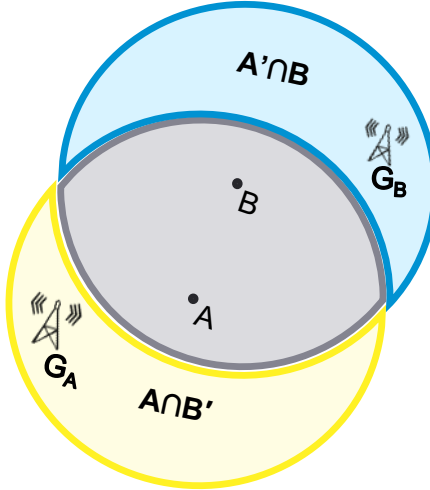


FIGURE 4.5: Approximating an exposed terminal

and crucial condition is that all these spatial and sensing criteria must be met simultaneously; if any of these conditions are not fulfilled, exposed terminals do not occur.

In the scenario depicted in Fig. 4.4, if Node-A begins its transmission slightly ahead of Node-B, Node-B, upon detecting a potential collision would decide to switch its transmission to a different channel. This adjustment by Node-B, though intended to avoid collision, is actually unnecessary. Node-A's transmission, due to its positioning, would not interfere with Gateway-B, highlighting an inefficiency characteristic of exposed terminals in the network.

Simulation Methodology for Exposed Terminals. To quantify the occurrence of exposed terminals in the network we opt for a simulation based approach, as depicted in Fig. 4.5. We fix Node-A at coordinates $(0,0)$, while Node-B's position varied across 10,000 iterations, ensuring mutual detection of transmissions between the nodes. We calculated the probability of an exposed terminal (P_{ET}) based on the exclusive coverage of each node by its respective gateway. The probability of Gateway-A exclusively covering Node-A ($P_{A\text{-exclusive}}$) was computed as $\frac{A \cap B'}{\pi \times r^2}$, and similarly, the probability of Gateway-B exclusively covering Node-B ($P_{B\text{-exclusive}}$) was $\frac{A' \cap B}{\pi \times r^2}$. Consequently, P_{ET} was derived as $\frac{(A \cap B') \times (A' \cap B)}{(\pi \times r^2)^2}$. We present our simulation results in Fig. 4.6.

Our simulation results indicated that exposed terminals were present in approximately 11% of the scenarios. Notably, the histogram depicting these outcomes

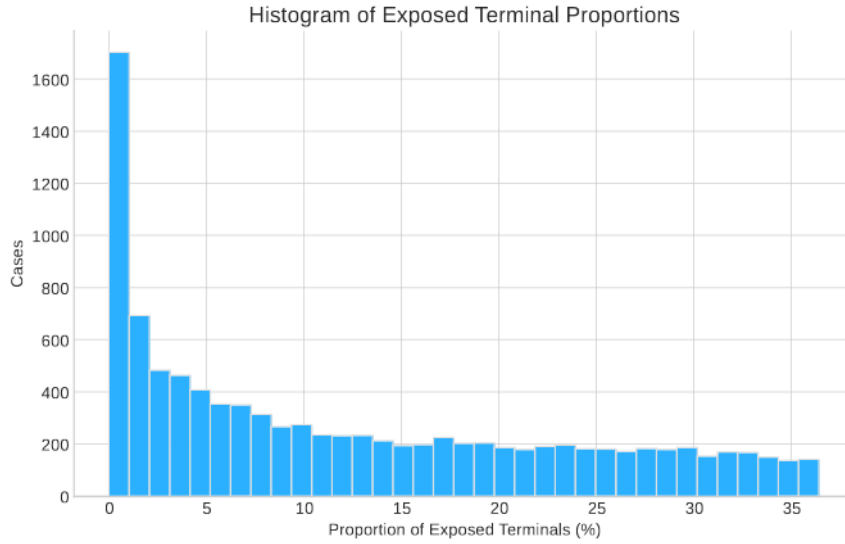


FIGURE 4.6: Histogram showing the distribution of exposed terminal scenarios in a simulated LoRa network.

showed no bars beyond the 36% mark, which we interpret as the maximum possible exposure limit within the network for exposed terminal. Notably, when an exposed terminal does occur, the primary consequence is an additional channel shift by the nodes. Such a shift is a low-energy process, ensuring that exposed terminal occurrences, while important to consider, have a minimal impact on overall network performance and individual node energy consumption.

4.2 Enabling Regulatory Compliance

In this section, we tackle regulatory compliance in LMAC implementation. We address the requirements for equal spectral utilization, in accordance with regional regulations, and propose necessary adaptations for LMAC protocols to meet these standards. Further, we analyze the use of the Received Signal Strength based Listen Before Talk (RSS-LBT) strategy relating to LoRa networks. Specifically, we examine its limitations within the scope of LoRa networks and propose modifications involving a CAD-based carrier sensing mechanism, aiming to improve the multiple access efficiency. The section provides essential insights into the integration of LMAC into LoRaWAN in compliance with regulatory standards.

4.2.1 Modifications for Equal Spectral Utilization

While striving to improve network performance through the choice of LMAC protocol, it is equally crucial to ensure regulatory compliance. This becomes even more significant in regions where equal use of channels for devices operating within the ISM spectrum is mandatory, as stipulated by bodies such as The Federal Communications Commission (FCC) [52].

The FCC requires technologies that use multiple physical channels, such as LoRaWAN, to utilize each channel equally. The LoRaWAN standard, under the ALOHA protocol, accomplishes this by making a pseudo-random choice for the transmission channel while consistently cross-verifying with local logs to prevent overutilization of any particular channel.

LMAC-1: Since LMAC-1 merely controls a node's behavior concerning time, its channel utilization is no different from the existing LoRaWAN practices. An LMAC-1 node senses the channel before transmitting and waits until the channel is free. Therefore, LMAC-1 can achieve FCC compliance by conforming to existing LoRaWAN practices of channel utilization. Protocols like LMAC-2 and LMAC-3, which are designed with a greater level of intelligence in the transmitter, make informed decisions for the transmission channel to minimize potential collisions. Hence, modifications to these protocols are necessary for full compliance, as detailed below:

LMAC-2: Unlike LMAC-1, LMAC-2 aims to select a less crowded channel, meaning the choice of channel is not pseudo-random. However, as described in Section 3.3.2, LMAC-2 still makes a random choice from a list of potentially free channels. For FCC compliance, a node must remember previous channel choices (akin to current practice) and exclude overutilized channels from future random selection. This approach ensures all channels are equally used on average by each transmitter in the long run.

LMAC-3: To ensure FCC compliance, LMAC-3 can adopt a similar strategy as proposed for LMAC-2.

In summary, regulatory compliance is a vital aspect to consider while choosing an LMAC protocol. While each protocol offers different benefits for network performance, modifications can and should be made to ensure they align with regional

and international regulatory standards. While adaptations for each protocol have been proposed, our primary focus for this chapter is on the modification of LMAC-2. This is because LMAC-2 requires no software modifications at the gateway.

4.2.2 Modifications for Regions with LBT

Received Signal Strength based Listen Before Talk (RSS-LBT) is a conventional strategy still in use in wireless technologies to reduce collisions. In essence, RSS-LBT minimizes collisions by monitoring the instantaneous signal strength (RSS_{det}) of a particular CH/BW combination. It subsequently holds transmissions when the detected instantaneous signal strength (RSS_{det}) exceeds a predetermined threshold set by the relevant authority. The endorsement for RSS-LBT within the ISM spectrum varies geographically, with it being optional in regions such as North America [52] and the EU [23], yet mandatory in Japan [82] and South Korea [83]. The threshold levels also differ across regions, for instance, Japan maintains a threshold of -80dBm , while South Korea has it set at -65dBm .

Our evaluation targets the sensing range of RSS-LBT to assess protection range it offers. This involved recording the RSS variation across different distances between two LoRa nodes, one transmitting at a power of 14dBm and the other consistently recording the RSS (RSS_{det}) with each incremental distance. The experiment was carried out under both indoor and outdoor conditions, with the outdoor one conducted under LoS conditions.

The RSS variation across these two nodes, compared against the RSS thresholds set by South Korea and Japan, is represented in Fig.4.7. The results revealed an approximate carrier sensing range of thirty meters for South Korea's threshold and a hundred meters for Japan's under outdoor conditions. These ranges shrink further under indoor conditions, potentially adequate for short-range communication protocols like Zigbee and WiFi but falling short for long-range ones like LoRa.

Despite RSS-LBT's proven performance with Zigbee and WiFi [34, 84], its effectiveness in carrier sensing is tightly coupled with close communication ranges [85]. Consequently, given LoRa's extensive range, the protection offered by RSS-LBT for LoRa nodes is somewhat limited, as illustrated in Fig.4.7. Comparing these

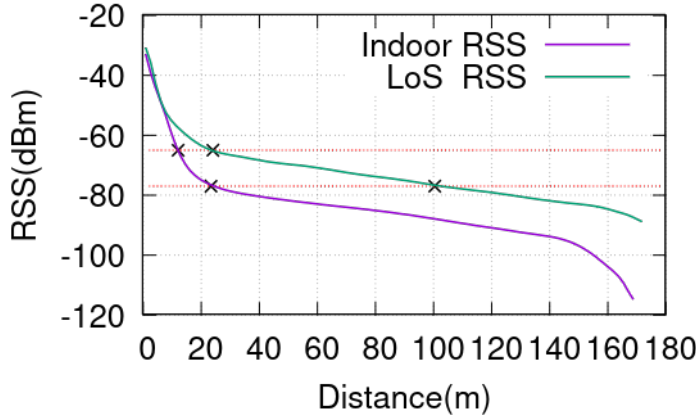


FIGURE 4.7: RSS variation under LoS and indoor environments.

ranges with CAD-based detection (Fig. 3.4), it's clear that CAD detection permits a significantly longer detection distance.

In addition, RSS-LBT faces the challenge of not being able to distinguish between concurrently transmitted orthogonal LoRa frames. This limitation leads to unnecessary transmission holds until all on-air transmissions cease, overlooking SF orthogonality—a significant loss to LoRa modulation. The fallout of this is a notable loss of transmission opportunities and unwarranted wait times, especially given that end-devices with multiple SFs could coexist. This consequently results in inefficient utilization of time, spectrum, and energy. One plausible resolution to this limitation is replacing this primitive RSS-LBT with a CAD-based carrier sensing mechanism, which naturally offers SF-selectivity.

For Regions with LBT. For regions mandate the use of LBT explicitly using RSSI prior to transmissions. Although we have shown that that LBT with RSSI thresholding may impair LoRa orthogonality and not improve LPWAN multiple access efficiency due to low SNRs of LoRa modulation, in the case where LBT is mandated, however, a decision based on the RSSI value should first be made in accordance with LoRaWAN Regional Parameter documentation [53] prior to proceeding with CAD based CSMA procedures. LoRaWAN Regional Parameter documentation can be used to identify such regions. Regional regulations are not listed in this section, but the reader may refer the corresponding specification so that most recent regulatory changes are reflected on the most recent version of LoRaWAN regional parameter documentation. In any case, the reader is expected to be up to date on all applicable local regulations and adhere them.

We have explored the potential LMAC offers to the LoRa communication, demonstrating the considerable advantages it offers. Particularly, LMAC not only promise significant improvements in terms of performance but also offer a feasible path towards their integration into existing networks, even when such integration has to occur gradually. Further, we have identified the necessary modifications to these LMAC protocols to ensure they are compliant with various spectral use regulations. We have also established that while RSS-LBT is currently the commonly accepted access mechanism in regions where LBT is mandated, it does not provide the best solution for LoRa networks. Instead, a more promising approach is to adopt LMAC which enables greater efficiency under LoRa. With these insights in mind, we can delve further into how LMAC can be integrated to LoRaWAN. The proposed CSMA protocol for LoRaWAN is based on LMAC-2 but incorporates modifications.

4.3 LMAC Based CSMA Protocol for LoRaWAN

In this section, we discuss the protocol modifications made to the original LMAC design in order to align it more closely with LoRaWAN’s requirements and constraints. The changes preserve the original performance benefits of LMAC while ensuring full compatibility with existing LoRaWAN network infrastructure. These modifications include adjustments to the protocol’s behavior in response to varying network conditions, regulatory requirements, and device priorities. The following subsections describe the details of these modifications, and the reasoning behind each alteration.

4.3.1 The Rationale of the Proposed Protocol

A LoRaWAN collision occurs when two or more devices chose the same CH/SF and transmit frames that overlap in time. Therefore, under a less congested environment, an end-device could likely estimate a clear channel *only* and proceed for transmission. This clear channel estimation is referred to as the DCF Inter-frame Space (DIFS) phase. The purpose of the DIFS phase is to ensure a clear channel. Once the CH and SF are configured, the DIFS phase comprises of performing two consecutive CADs, similar to description in Chapter-3. A successful

DIFS phase is attributed when both CADs report a clear channel. If either CADs fail, a failed DIFS window is attributed— indicating that the channel is not clear to send. In this case, the end-device should proceed to complete the DIFS phase after configuring the radio to a different CH while maintaining the same SF.

BO Phase. If the channels are known to be heavily contended, simply relying on the DIFS phase is not sufficient to ensure a good chance of collision avoidance. This is because as numbers of end-devices increase, the possibility that two or more devices starting and finishing the CSMA process at the same time also increases, thereby increasing the possibility of collisions. The addition of a random Backoff (BO) phase after the DIFS phase can aid in reducing such occurrences. Therefore, the CSMA protocol for the contended networks comprises of two parts—a DIFS phase followed by an optional BO phase. Apart from the DIFS phase, the BO phase further reduces collisions when networks are contended at the cost of few additional CADs. It does so by addressing the possibility where two or more frames collide should the end-devices start the DIFS processes at approximately the same time.

When BO phase is enabled, the end-device enters BO phase immediately after completing a successful DIFS phase. It first generates random a number between 1 and BO_MAX and assigns it to the variable NBO. NBO represents the number of BO slots the end-device should complete prior to transmission. During the BO phase, the end-device decrements NBO per each CAD reporting clear channel. When NBO reaches zero, the frame is immediately transmitted. Since the end-device continuously checks the availability of the channel during the BO phase, an occupied channel will reset the CSMA state of end-device back to DIFS phase, in which case, the end-device needs to complete a successful DIFS phase again to resume decrementing the remaining BO slots (NBO). Note that the initial number of BO slots (NBO) is neither reset nor regenerated until the said frame is transmitted. It should be noted that a busy channel during a CAD operation within DIFS or BO phase will render a failed DIFS or a BO slot respectively. In both cases, the end-device state is set back to DIFS, and should perform the next DIFS phase after configuring the radio to a different pseudo-random channel while maintaining the same SF.

However, some regulatory authorities mandate equal use of all channels [52]. I.e., a channel that was utilized for transmission once should not be utilized again until all other channels have been transmitted on. Therefore, when a CAD reports a busy

channel during either DIFS or BO phase, the available channels for the end-device is limited to the number of remaining unused channels (NUM_AVAIL_CHs) where AVAIL_CHs is the list of those channels. Suppose an end-device has eight available channels and only one of them has been used previously for a transmission. During the next transmission, the end-device should only attempt to transmit on either of seven remaining channels. During the unlikely case where all seven remaining channels were found to be busy, the end-device shall default to ALOHA and transmit the frame. However, the end-device may also restrict the number channel hops by setting the MAX-CHANGES parameter. In that case, upon finding a busy channel, end-device will only channel hop min (MAX-CHANGES, NUM_AVAIL_CHs) times before defaulting to ALOHA. The list AVAIL_CHs is reset when all channels have been transmitted on. The variable MAX-CHANGES is reset for each new frame. An example use of MAX-CHANGES, NUM_AVAIL_CHs is discussed later.

Device prioritization. Another application of adopting both BO phase and the DIFS phase is when some end-devices require prioritization. In a network where all end-devices use both BO phase and the DIFS phase, the end-device with lower BO_MAX value will receive an advantage in capturing the channel. The reason for the prioritization is as follows. After completing a successful DIFS phase, the random number of BO slots (NBO) assigned to the prioritized end-device will be lower than that assigned to a non-prioritized end-device due to the lower BO_MAX value. Therefore, devices with lower BO_MAX are more likely to capture the channel faster as opposed to others under the same CH/SF.

While the Back-off (BO) Phase is recommended in our methodology, it's not mandatory, as opposed to what was suggested in Chapter 3. This is primarily because there may be networks where service providers are aware of less congestion. In these situations, they may prefer to conserve the energy that would have been expended on BO operations. The energy saved, albeit small, is considered worthwhile despite the minor risk of collisions that could occur when end-devices choose to perform only DIFS. Therefore, the BO Phase can be disabled if desired, allowing the network service provider to make a decision based on the specific application type.

Fig. 4.8 illustrates the state transitions when an end-device follows CSMA.

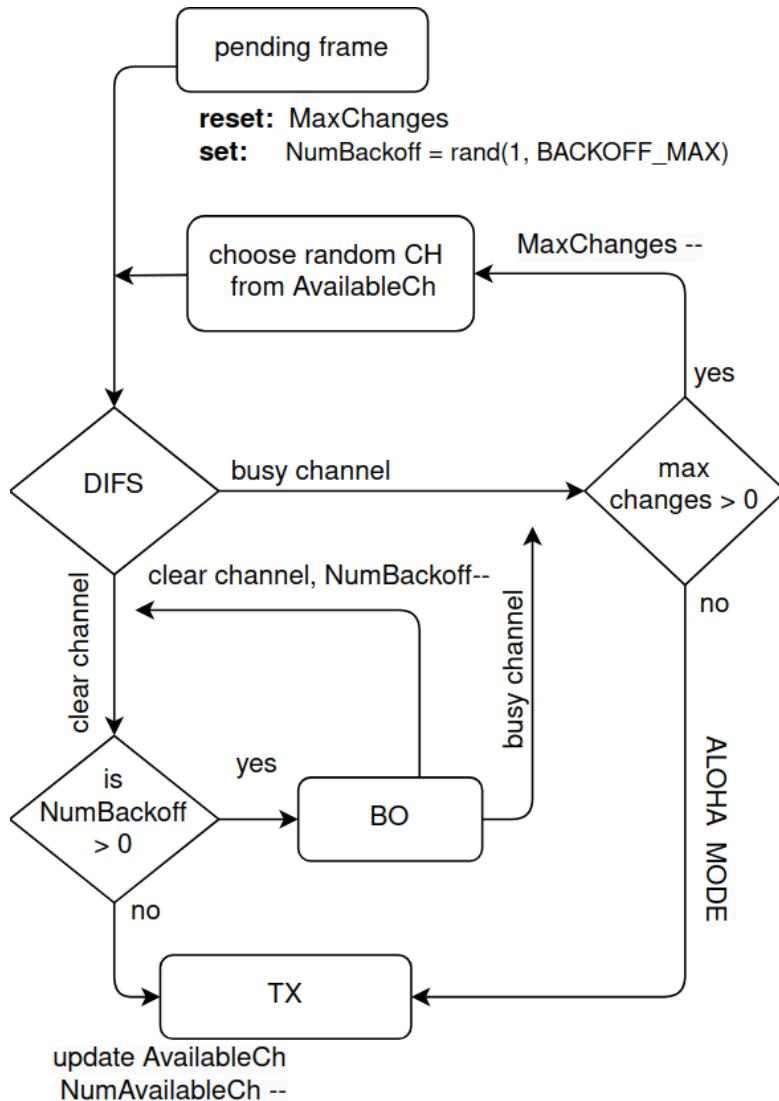


FIGURE 4.8: LoRaWAN Medium Access State Transition Diagram

4.3.2 State Transitions

This section delves into the dynamics of state transitions for end-devices operating under different configurations within a LoRaWAN network employing the LMAC. These state transitions are integral to understanding how devices handle potential collisions, and make channel choices. We will first consider the behavior of an end-device that opts for DIFS without the Backoff (BO) phase, typically suited for environments with low contention. Subsequently, we will discuss the more complex scenario where an end-device employs both DIFS and BO phases, the process that two devices undertake when contending for the same channel/spreading factor (CH/SF) combination. We further illustrate the process through an example use

case to provide a clearer understanding of the interactions and decision-making processes involved.

State transitions of an end-device adopting DIFS without BO. First, the state transitions for an end-device that follows DIFS phase only is explained. Such a device does not have the BO phase enabled and can typically be deployed under low contended environments. To disable BO phase, BO_MAX is simply set to 0.

The simplest scenario is where the selected CH/SF combination by the end-device is not contended by another. In this case, the end-device entering the DIFS state will complete two CADs conforming to a clear channel. This completes a successful DIFS phase. The end-device then transitions to transmission state when the frame is transmitted and decrements NUM_AVAIL_CHs by one. At the same time, the end-device marks the channel as used in the list of channels.

In case where the end-device identifies a busy channel during DIFS state, the end-device configures the radio to a different random channel from the list of available channels before starting a new DIFS phase. The key reason to hop to a different channel upon finding a busy channel is because repeatedly performing DIFS on a fixed channel that was just found busy is less likely to result a clear channel. Therefore, the end-device would have a better chance of finding a clear channel by hopping to a different one.

A key concern, however, is how many times the end-device should hop across channels in the unlikely case where many consecutive channels are found to be busy. At such times of high network demand, the end-device would spend too much time hopping across too many channels. This overhead can be high specially when the number of available channels is also high. Therefore, a stop condition is provided to control this behavior. The parameter MAX-CHANGES sets a limit on the number of times an end-device would hop to a different channel upon finding a busy channel. MAX-CHANGES is user configurable and is reset upon each transmission. Accordingly, prior to hopping to a random CH, the end-device checks if $\text{MAX-CHANGES} > 0$, i.e., to see if further channel changes are allowed. If so, the end-device can hop randomly to one of the AVAIL_CHs— one that has not been transmitted on yet. Each hop decrements MAX-CHANGES by one. When $\text{MAX-CHANGES}=0$ or when all AVAIL_CHs have been tried, no further CH changes

are allowed. In that case, the end-device shall simply transmit the frame under ALOHA.

As some regions require that an end-device uses all enabled channels once before being used again, in the unlikely case where all remaining channels are found to be busy, the end device may use any unused channel under ALOHA.

State transitions for an end-device adopting DIFS with BO. Fig. 3.10 also illustrates state transitions when an end-device adopts both DIFS and BO phases. The end-device enables BO phase in this case. To enable BO phase, BO MAX is set to a non zero value, e.g., 6.

Again, the simplest scenario is when the selected CH/SF combination by the end-device is not contended by another. The end-device first enters the DIFS state and completes a successful DIFS phase. After the successful DIFS phase, the end-device checks if existing NBO value is greater than 0. If $NBO > 0$, it means that the end-device previously met a busy channel during BO phase during this transmission effort, and the end-device is just returning from a subsequently successful DIFS phase to resume decrementing NBO. Since the BO phase is enabled, if the end-device exits the DIFS state with $NBO = 0$, it indicates that a value for NBO was never set and that end-device is transitioning to BO phase for the first time. Therefore, the end-device moves to the next state and generates a new random number that chooses the number of BO slots and assigns to NBO. The end-device then immediately moves to BO state and awaits until NBO is decremented to 0 per each CAD returning a clear channel. When $NBO = 0$, the end-device transitions to transmission state when the frame is transmitted. Upon transmission, the end-device updates AVAIL_CHs.

In case where the end-device identifies a busy channel during the DIFS state or BO state, the end-device shall immediately transition to the DIFS state. Following the channel hopping criteria explained later, the end-device then configures the radio to a different random channel from the list of AVAIL_CHs and transitions to DIFS phase again. Note that the generated NBO for a frame is neither reset nor regenerated until that frame is transmitted. The use of MAX-CHANGES, NUM_AVAIL_CHs parameters are described later.

For further clarity, Fig. 3.10 illustrates the use of back off under a typical use case where two end-devices, device A and device B, follow CSMA with both DIFS and

BO phases. The behavior of device A is described first. Device A first follows the DIFS phase. Device A completes a successful DIFS slot and then generates a random back-off (BO) value (NBO) and enters the BO phase immediately. An NBO of 2 is generated by device A. Device A then decrements NBO per each CAD reporting clear channel. When NBO reaches zero, the device transmits the frame.

Fig. 3.10 also reflects the process where two end-devices, device A and device B, contend for the same CH/SF. Note that, device A and device B starts the CSMA process approximately at the same time where both complete a successful DIFS phase. When device B performs DIFS, it detects a clear channel. Accordingly, device B then enters the BO state but with NBO=3. It starts decrementing NBO with each successful CAD and reports a failed CAD in its second BO window, while device A is transmitting, detecting a potential collision. As per the state transition diagram, device B decrements MAX-CHANGES by one, changes channel randomly to one of AVAIL_CHs and transitions again to the DIFS state. After completing a successful DIFS phase in the new channel, device B immediately transitions to BO phase and resumes decrementing NBO from two. When NBO reaches zero, device B transmits the frame. Upon transmission, the end-device updates avail_CH and num_avail_CH.

4.3.3 Recommended CSMA Parameters

Parameter	Recommended Value	Short Description
DIFS	2 CADs	CADs to assess a clear channel
BO_MAX	6	Integer for the maximum number of NBO. 0 to disable back off or n to back off n times
NBO	$rand(BO_MAX)$	Integer range for NBO
MAX-CHANGES	application specific, e.g., 6.	Limit of changing CH per frame
AVAIL_CHS	N/A	List of available channels that have not yet been transmitted on.
NUM_AVAIL_CHS	N/A	Number of channels available in AVAIL_CHS

TABLE 4.2: Table of Parameters

Table 4.2 provides a summary of recommended values for the key parameters involved. It should also be noted that the MAX-CHANGES and BO_MAX parameters are application specific. Once the MAX-CHANGES is reached the end-device will lock to the already set channel and transmit the frame using ALOHA. Also, the application can utilize different BO_MAX values for prioritization (lower BO_MAX means higher priority and vice versa).

4.3.4 Recommended CAD Configuration

Appropriate configuration of the CAD module is key to enabling accurate detection of potential collisions and improved energy efficiency during LoRaWAN CSMA. A single CAD operation comprises of two parts. First, the radio switches to the receive mode, gathers samples for a duration set number of symbols. Second, the radio briefly processes the received samples for the presence of LoRa symbols and informs the MCU whether a symbol is found. Recent versions of LoRa radios expose parameters such as received number of symbols, various thresholds that influence detection. However, CAD modules belonging to previous radio generations come preconfigured and further configuration is not allowed. Hence, CAD module of those can be used with the default configuration.

The rationale of configuring the CAD module is to achieve the highest energy efficiency per CAD whilst maintaining sufficient detection accuracy. For radios that allow CAD configuration, several parameters can be optimized. However, listing optimized configurations for each radio is not plausible due to the large portfolio of LoRa radios. As such, an example of optimal configuration for the SX1262 is summarized in Table-4.3. As CAD parameters of radios that allow for configuration is similar, the reader is requested to refer the respective datasheets to find radio specific values that offer optimal detection, e.g., cadSymbolMin, cadDetPeak, cadSymbolNum.

A noteworthy parameter for consideration is cadSymbolNum which configures the duration the radio tunes to receive mode to sample the channel. A cadSymbolNum=2 implies that each CAD requests the radio module to sample the channel for two symbol durations which varies based on the set SF. Accurately detection of the presence of an on-going transmission requires maintaining false positives to a minimum across a wide range of RSSI. In the case of SX1262, the application

note AN1200.48 [86] highlights CAD configuration parameters. These are highlighted in Table-4.4. The registers, `cadDetMin` , `cadDetPeak` , `cadSymbolNum` allow configuring the sensitivity of a single CAD operation.

SF	CAD Settings		
	cadDetMin	cadDetPeak	cadSymbolNum
SF7	10	22	2 symbols
SF8	10	22	2 symbols
SF9	10	24	2 symbols
SF10	10	25	2 symbols
SF11	10	26	2 symbols
SF12	10	30	2 symbols

TABLE 4.3: CAD Settings for different Spreading Factors

For radios that allow configurable CADs, consecutive CADs may be combined to form a single CAD to realize a slight energy gain. For example a DIFS phase consists of two CADs that together consume four symbols. These two consecutive CAD operations can be merged into a single CAD operation of four symbols. Optimized parameters for a four symbol CAD are different to those described in Table-4.2 and can be found from AN1200.48 [86].

4.3.5 CAD Energy Overhead

CSMA introduces an additional energy overhead for each transmission effort. In this section, a comparison between CSMA energy footprint against that required for average transmission is made for three different SFs under three different transmission power levels. The results indicate that the addition of CSMA adds an energy overhead of less than 1.5% for a 30-byte frame.

The CSMA energy footprint originates from two key phases: the DIFS phase and the BO phase. For the sake of simplicity, the overhead computation assumes that the end-device performs six CADs during both phases per frame – which is an approximate and may vary based on network contention and the type of CSMA used. In order to compute the energy overhead, key choices related to radio type, transmission power, SF and CAD configuration needs to be made. These choices are summarized below and in Table-4.4.

Frame size: 30 bytes (payload + LoRaWAN headers), LoRa Radio: SX1262, Band: 868/915 MHz. SX1262 CAD Configuration:

SF	CAD Setting			Energy(nAh)
	cadDetMin	cadDetPeak	cadSymbolNum	
SF7	10	22	2 symbols	2.84
SF9	10	23	2 symbols	11.7
SF12	10	28	2 symbols	64.59

TABLE 4.4: SX1262 CAD energy consumption (optimized for best detection)

Table-4.5 abstracts the transmission characteristic of the SX1262 radio under three different power levels where Table-4.6 summarizes the CAD energy overhead for those power levels for SF7, SF9 and SF12 from SX1261/2 [54].

SX1262 setting	Tx current (mA)
Tx Current @14 dBm	45 mA
Tx Current @17 dBm	58 mA
Tx Current @22 dBm	84 mA

TABLE 4.5: Transmission characteristics of SX1262 under (868/915 MHz) band

Approximately, performing CSMA for a 30-byte payload may impose an approximate overhead ranging from 0.8% - 2% of transmission energy. However, it should

SF	SF7	SF9	SF12
Airtime for 30 bytes	87.3 ms	287.7 ms	2138.1 ms
Tx energy @14dBm	1091.25 nAh	3596.25 nAh	26726.25 nAh
Tx energy @17dBm	1406.50 nAh	4635.16 nAh	34447.16 nAh
Tx energy @22dBm	2037.00 nAh	6713.00 nAh	49889.00 nAh
CSMA overhead @14dBm	1.56 %	1.95 %	1.45 %
CSMA overhead @17dBm	1.21 %	1.51 %	1.13 %
CSMA overhead @22dBm	0.84 %	1.04 %	0.78 %

TABLE 4.6: CSMA overhead for three different transmission power levels.

be noted that due to large number different configurations, values here are presented for illustration purposes only. Nonetheless, smaller values of overheads motivate the use of CSMA for LoRaWAN which encourage the efficient use of spectrum and eventually optimizes spectrum and battery life through collision avoidance.

Chapter 5

Efficient Spectral Utilization for LoRa

Chapter-5 builds on the advancements in media access control discussed in previous chapters and explores an innovative approach to further efficient use of spectral utilization in LoRa. Here, we introduce the 'Borderless' spectrum utilization method, a significant shift from traditional channelized transmissions for LoRa.

5.1 Motivation

In this section, we explore an alternative method for channel access in LoRa communication, moving away from the conventional channelized approach. We discuss various types of interference that can disrupt LoRa transmissions and how they can compromise the effectiveness of guard bands in a channelized scheme. We experimentally show that a channelless approach could lead to a more efficient use of spectrum compared to the conventional channelized approach. This leads us to consider questions about the potential benefits and challenges of implementing a channelless strategy in LoRa systems. Could removing guard bands increase the available spectrum for communication? Could we discard the use of channel plans and opt to transmit frames at arbitrary central frequencies? Could this strategy achieve better protection against interference and higher spectral efficiency?

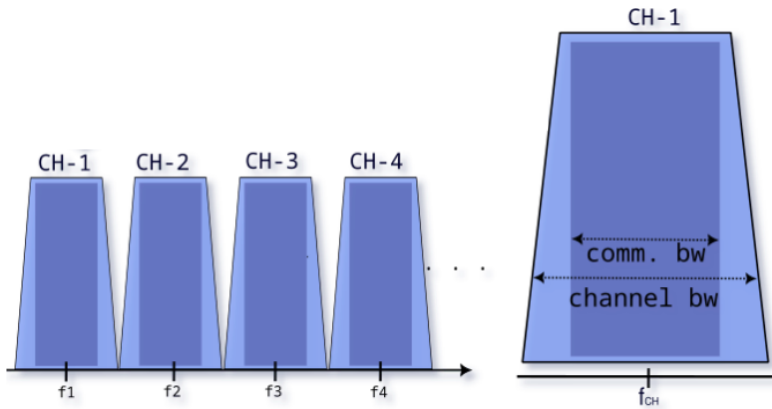


FIGURE 5.1: Organization of channels within a LoRaWAN/LoRa network. Each channel is composed of communication bandwidth and a guard band.

These questions are particularly relevant given the broader communication spectrum that becomes available at the absence of guard bands. However, implementing a channelless approach also presents significant challenges, such as accurately predicting the central frequency of a LoRa frame, which is key to successful demodulation. Without pre-configured channel plans, LoRa frames could be transmitted anywhere within the ISM spectrum, and the receiving gateway would not have any prior knowledge about where to look for these frames. In the following sections, we delve deeper into these challenges and propose a comprehensive solution to address them.

5.1.1 LoRa Channel Plans

Fig. 5.1 presents the conventional layout of the channel plan utilized in LoRa/LoRaWAN systems. As depicted, each channel is sequentially followed by the next and each channel is partitioned into two main sections—the communication band and the guard band. The communication band is utilized for actual data transmission and reception. The guard band serves as a buffer or a *protective band* to minimize inter-channel interference. This allocation to guard bands is significant. These 'silent' bands, despite not participating in data exchange, consume an 37% of the total spectrum across all channels. Borderless fundamentally questions the reason for existence and the effectiveness of guard bands for LoRa modulation.

5.1.2 Guard Band Efficacy vs. Interferences

LoRa networks, as with many wireless communication systems, encounter various types of interference that can negatively affect reception. Although the ISM spectrum, becoming increasingly crowded, needs effective strategies for managing these interferences, relying on these guard bands for protection often falls short of its original design goal in the face of various interference types.

Interferences to LoRa/LoRaWAN. Firstly, inter-channel interferences typically result from cross-network interactions. Suppose two LoRa networks, although sharing the same spectrum, have different channel plans - a situation often encountered with private LoRaWAN networks. As the ISM spectrum is open, channel plans of multiple private networks can be designed strategically to minimize interference without compliance to commonly utilized plans. When nodes from different networks, each with its own channel plan, transmit at closely spaced frequencies, their frames can overlap. This overlap demonstrates that guard bands may not effectively prevent interference when multiple networks share the same ISM band.

Secondly, there exists intra-channel interference, which usually originates within the same network. When two nodes from the same network transmit on the same CH using the same SF, the resulting interference can be the most disruptive due to 100% overlap of frames. Guard bands provide no protection against such interferences.

Lastly, there is interference from cross modulations. As different modulation types have distinct modulation properties and channel plans but share a common spectrum, they can potentially interfere with each other. Once again, guard bands do not offer any protection from this type of interference.

Despite their intention to protect, guard bands often fail to prevent these varied types of interference. This underlines that guard bands may not be as effective in providing the expected protections for LoRa.

Efficacy of Guard Bands. To investigate the efficacy of guard bands in safeguarding LoRa transmissions, we designed an experiment. The experiments were conducted under an outdoor environment and utilized two standard off-the-shelf SX1262 LoRa radios as nodes and two SX1301 LoRa gateways. Two nodes were placed equidistant from the gateways and the gateways were placed together. The

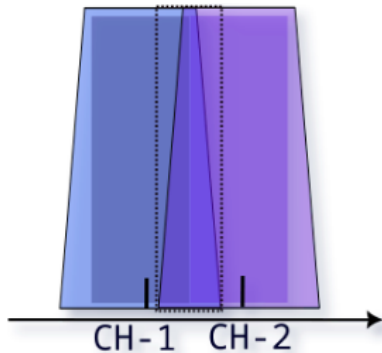


FIGURE 5.2: By adjusting the distance between CH-1 and CH-2 in the spectrum the % overlap between them can be adjusted.

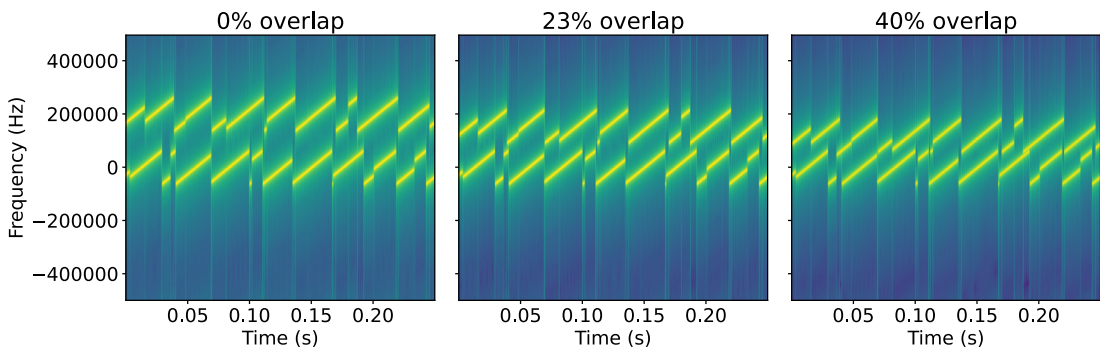


FIGURE 5.3: Spectrograms of frames overlapped at 0%, 23%, 40% overlaps on CH-1 and CH-2.

transmissions from nodes followed LOS paths to ensure a consistency across all configurations. A node/gateway pair was tuned to same channel. Only a single channel from one gateway was utilized while others were unused. Therefore, node-1 was set to transmit frames solely on CH-1, and similarly, node-2 used CH-2 exclusively. GW-1 listened exclusively to node-1 and vice versa.

The core of this experiment was to incrementally decrease the distance between the two channels while estimating the impact of interference. Bringing the channels together, first shrinks guard bands and after 23% overlap between two, CH-1 and CH-2 start to encroach on each others' communication band as indicated in Fig. 5.2. I.e., the special overlap of 23% indicates 0% guard band utilization between two. We utilized overlaps of 23%, 40%, 60%, 70%, 80%. For each overlap, we logged the average PRR and the average SNR of frames received at both gateways. To ensure thoroughness in our experiment, we replicated the entire process for all SFs and several power levels as well.

We collate the results in Fig .5.4. Due to the significant number of variations (six SFs, five power levels, and two gateways) we collate the averaged PRR and SNR of all variations on a per SF basis. In the SNR plots, the y-range is different for each SF and represents the maximum SNR capability of the LoRa gateway [87]. At an overview, it can be seen that the impact of bringing both channels together does not introduce a significantly destructive effect to reception at either gateways. To be more precise, it can be seen that while there is a decrease in the PRR, the magnitude of this reduction is large — only a $\tilde{0.38}$ dB reduction in SNR until 40% overlap and $\tilde{2}$ dB at most challenging 80% overlap. The PRR plots do not significantly reflect the effect of colliding channels for all collision levels.

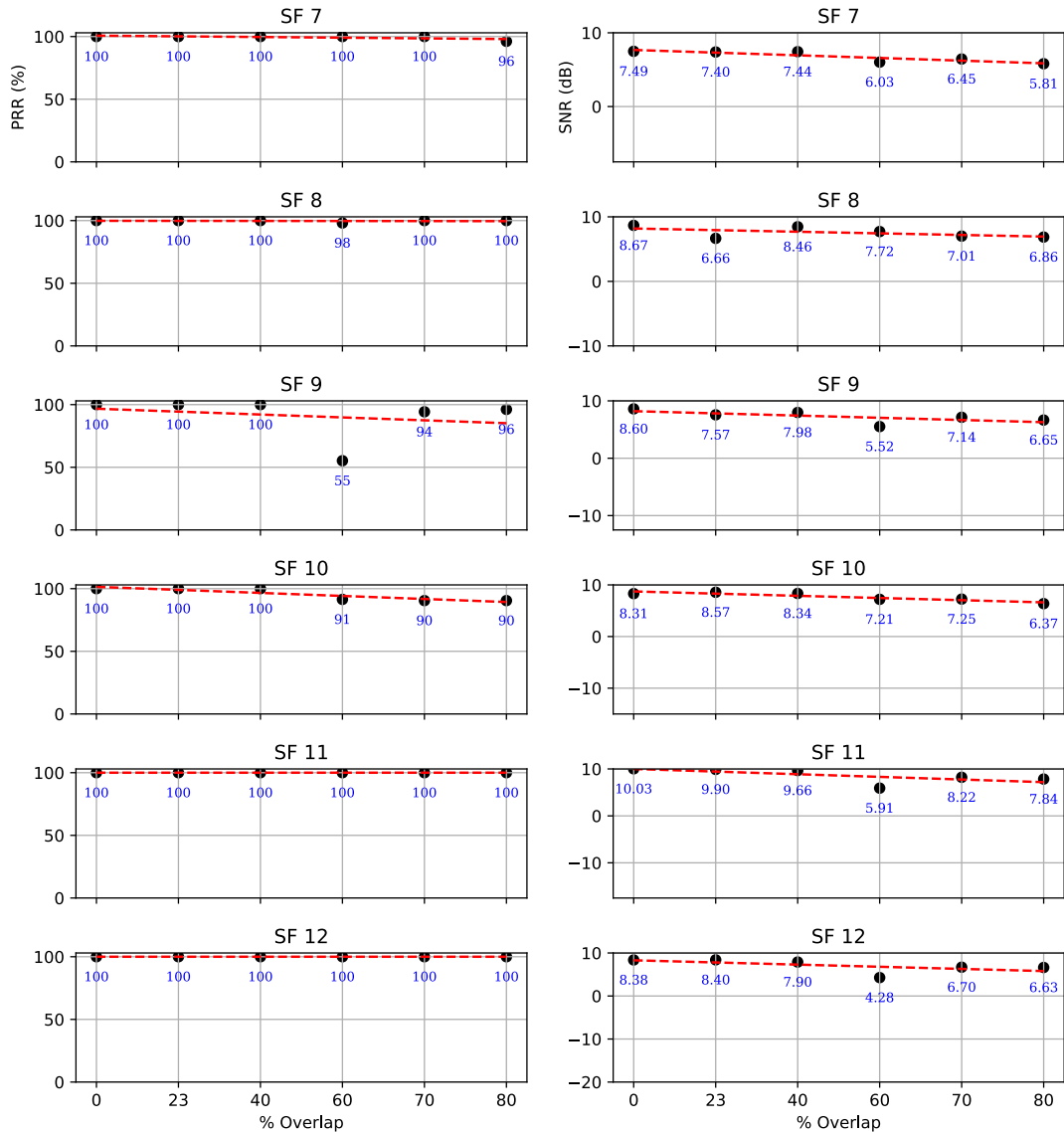


FIGURE 5.4: PRR vs % Overlap for different SF and dB values

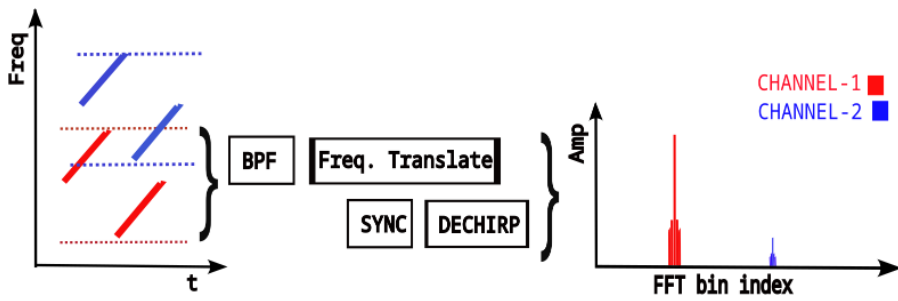


FIGURE 5.5: A partially colliding chirp segment from CH-2 falls in-band with CH-1. After standard demodulation process, the overlapping segment of the chirp translates to a weak amplitude peak during demodulation of CH-1.

This observation of minimal disruption due to overlapping collisions, to our knowledge, has not been extensively discussed for LoRa and the result in Fig .5.4 is counter intuitive. To make sense of this, it is necessary to delve deeper into demodulation process to understand what occurs when there are partially overlapping frames. Fig .5.5 provides a simplified illustration of how two frames could collide with a certain percentage overlap still be perfectly received. Suppose the frame in CH-1 is of interest. When the corresponding gateway, GW-1, is in operation, it applies BPF on the selected channel, in this case, on CH-1. This significantly minimizes the out of band interference to CH-1. As a result, LoRa chirp segments from CH-2 that fall out of band (out of CH-1) are suppressed while chirps present within CH-1 experience no power reduction. Consequently, during the dechirping process, FFT peaks for full chirps within CH-1 result in a higher amplitude than of those belonging to partially interfering chirp segments. This explanation paves way to identify the fundamental reason for the result in Fig .5.5.

In summary, guard bands are not effective in safeguarding LoRa frames from interference. Additionally, results in Fig .5.4 suggest that when two LoRa channels are brought together, communication still persists with minimal impact for both overlapped channels. Considering these two facts, Borderless poses an intriguing question; Could we increase the available spectrum for communication by removing guard bands? Could we, therefore, discard the use of channel plans and opt to transmit frames at arbitrary central frequencies? Could be attain better protections and spectral efficiency by doing so? These thoughts become compelling given the broader communication spectrum that becomes available at the absence of guard bands. Nevertheless, this approach is not without challenges. Accurately predicting the central frequency of a LoRa frame is key to demodulation. But,

with the absence of pre-configured channel plans, LoRa frames could be placed anywhere within the ISM spectrum and the gateway would not know which channels need to be continuously scanned for the presence of LoRa frames. Specifically, the receiving gateway lacks any prior knowledge of the potentially infinite possibilities of central frequencies a node could choose to transmit LoRa frames to use a Borderless approach towards spectrum utilization. This is explored next. Note that all signal processing is applied to complex data, i.e., I/Q data from an SDR.

5.2 Methodology

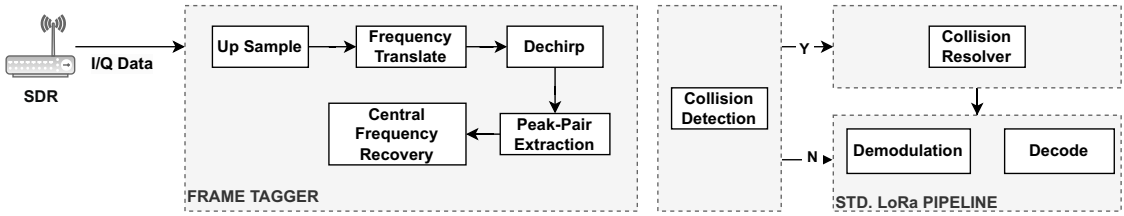


FIGURE 5.6: System overview of Borderless design

An overview of Borderless is presented in Fig .5.6. Borderless accurately predicts the central frequencies of multiple LoRa frames that are arbitrarily placed within the Borderless BW, in this work, 1MHz worth of ISM spectrum. Such a BW can accommodate five standard LoRa channels, i.e., 1MHz / 200KHz. The prediction is performed by the core component of Borderless called the *Frame Tagger*.

5.2.1 Frame Tagger

Frame Tagger is responsible for processing I/Q samples from an SDR, spanning across the Borderless BW. Its primary role is to identify and tag LoRa frames within this full bandwidth, which considerably exceeds the typical channel bandwidth of LoRa. The tagging process involves determining the central frequency and the start time of each LoRa frame. Once a frame is tagged, the Frame Tagger shifts the frame's I/Q data to baseband and forwards it to the subsequent processing blocks such as the demodulator.

Challenges. Detecting LoRa frames across the full Borderless BW poses significant challenges. Existing detection techniques, like correlation, can confirm the

presence of a LoRa frame but fall short of providing sufficient information for tagging. To *tag* a frame effectively, we need to accurately estimate both its central frequency and start time, which becomes complicated when dealing with a bandwidth several times larger than the standard LoRa BW. Moreover, the possible presence of multiple simultaneous frames within the Borderless BW adds another layer of complexity to the process. To navigate these challenges, Frame Tagger employs a unique and efficient approach, discussed in detail below.

Unique Approach. Frame Tagger’s solution is to generate a distinct signature for each frame, which is then used to determine the frame’s central frequency and start time. This signature, as shown in Fig. 5.7E, is generated from a dechirp operation executed across the entire Borderless BW, with precautions taken to avoid aliasing.

Recall from Section-2.2 that a chirp sampled at the LoRa BW, when dechirped, results in a single bin due to aliasing. The same operation, when expanded to the entire Borderless BW, could still lead to aliasing. If not mitigated, aliasing can cause confusion when interpreting signature properties to calculate the central frequency and start time of frames. To circumvent this, we implement precautions during the dechirping process. This careful approach results in a unique signature for any frame positioned within the Borderless BW, as shown. This signature generation process requires a few preprocessing steps to eliminate ambiguity. The derived signatures are then used in the Frame Tagger to detect the presence, estimate the start time, and determine the central frequency of each LoRa frame. What follows is a detailed discussion on this implementation to prevent aliasing, an essential factor in generating unique and clear signatures.

Signature Generation. For clarity, we’ll focus on the generation of a signature for a single LoRa frame, arbitrarily located within the Borderless BW, as depicted in Fig.5.7A. The spectrogram of the received I/Q buffer reveals the presence of a LoRa frame within the Borderless BW, information not initially available to the Frame Tagger. It is essential that the dechirp operation between the downchirps and potential LoRa frames in the Borderless buffer yields no ambiguous outcomes. Therefore, the dechirp operation must generate a result free of aliased information. We achieve this through two signal preprocessing steps before dechirping the received samples.

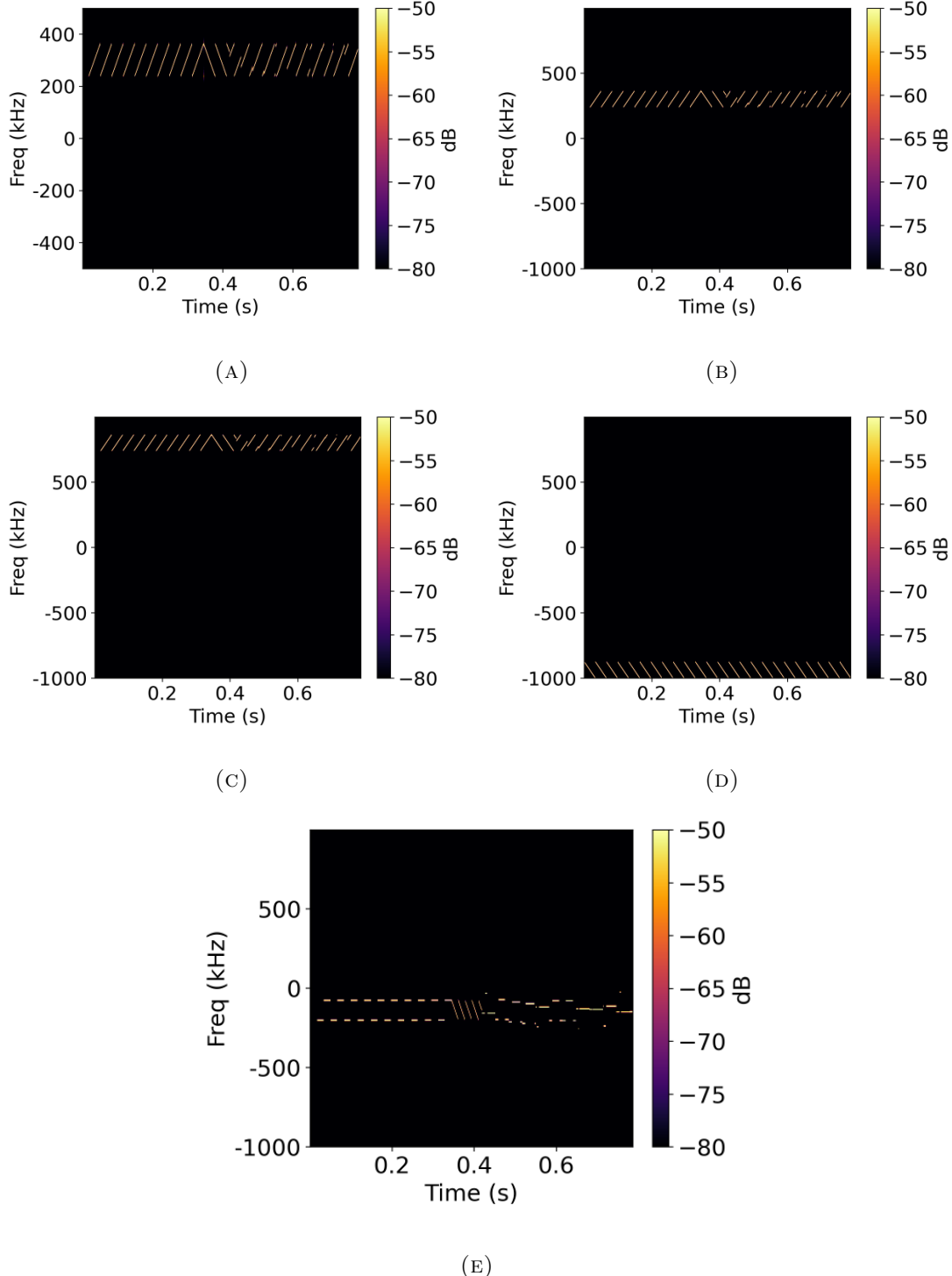


FIGURE 5.7: Fig. 5.7A-E highlights the pre-processing steps in Borderless. (A) Shows initial samples from the SDR at Borderless BW *happens to* contain a LoRa frame. (B) The Borderless BW buffer is upsampled 2X. (C) The upsampled buffer is given a positive frequency translation of half the value of Borderless BW, e.g., 500khz. (D) A series of downchirps, locally synthesized to match the exact length of Borderless buffer. (E) The spectrogram of the product of frequency translated signal in (C) with the series of downchirps in (D).

First, the received Borderless sample buffer (of Borderless BW) is upsampled to twice its original rate, as shown in Fig. 5.7B. This upsampled data then undergoes a positive frequency translation of $\frac{\text{Borderless BW}}{2}$, as seen in Fig. 5.7C. Lastly, we generate a local signal comprising a series of downchirps, each starting at a frequency (f_{start}) of $-\text{Borderless BW} + \text{LoRaBW}$, ending precisely at $-\text{Borderless BW}$, and repeating for the exact duration of the Borderless sample buffer, as seen in Fig. 5.7D. These steps, upsampling and frequency translation, ensure that the system's complex sampling rate can accommodate the multiplicative results for all possible frames across the Borderless BW and the local downchirps.

As mentioned in Section-2.2, a LoRa frame contains a preamble, which consists of a series of contiguous chirps spanning across the LoRa BW, contrasting with data chirps that show abrupt frequency shifts. This continuous chirp structure in the preamble helps in creating a distinct signature when multiplied by the series of downchirps, as displayed in Fig. 5.7E. The resulting signature comprises two alternating single tones for each LoRa frame, with each tone exactly 125kHz apart. From this signature, we can deduce:

- The preamble of the LoRa frame generates a signature comprising exactly two tones, 125kHz apart.
- These two tones alternate throughout the duration of the preamble.

The following sections will delve deeper into detection and estimation processes based on this signature.

Peak-Pair Detection. The Peak-Pair detector uses signatures to reliably detect the presence of LoRa frames within the Borderless BW. This is achieved by performing the FFT on samples potentially containing signatures (Fig. 5.8) and identifying peak-pairs that are 125kHz apart. A peak-pair suggests the possible existence of a LoRa preamble. It's important to note, however, that the presence of a peak-pair doesn't definitively confirm the existence of a LoRa preamble. This scenario arises because bins resulting from individual data chirps may also create peak-pairs fulfilling the above criterion. Nonetheless, the absence of a peak-pair in Fig. 5.8 *does guarantee* the absence of a LoRa preamble within the sample buffer depicted in Fig. 5.7A. As a result, the peak-pair detection process is followed by

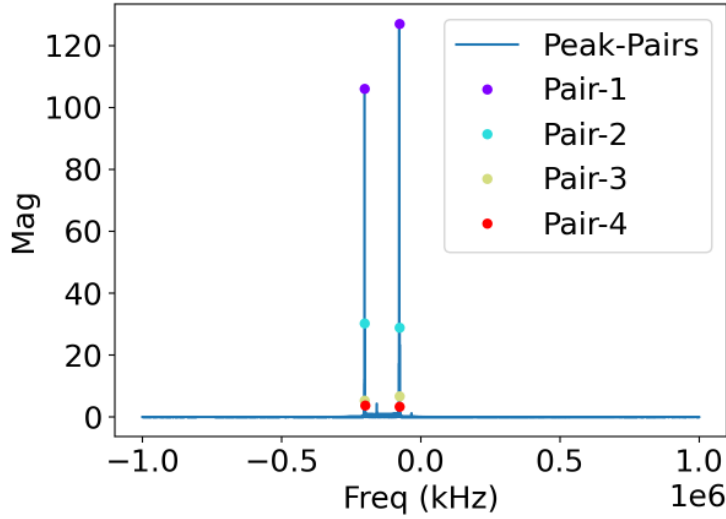


FIGURE 5.8: FFT of Fig. 5.7E. The detected peak-pairs are marked. Pair-1 is a result of the LoRa frame preamble in Fig. 5.7A. Additional peak pairs are normal and a result of dechirped data chirps and the scalloping loss after the standard FFT.

a second step, which involves further processing of the buffer from Fig. 5.7E to extract more detailed information about the LoRa frame. This two-step approach is designed to enhance the computational efficiency of Borderless by allowing early discarding of I/Q data when no LoRa frames are detected at the earliest stage. As shown in Fig. 5.8, Peak Pair-1 consists of two distinct peaks. The presence of additional peak pairs is normal and can result from dechirped data chirps and the scalloping loss following the standard FFT. Peak-pairs not associated with a LoRa frame pose no issues for Borderless, as they are easily filtered out during the subsequent step.

Central Frequency Estimation. To comprehend how the central frequency is calculated from the signature, we first consider a straightforward case where only one signature is present, resulting from one LoRa preamble. The signature presented in Fig. 5.9 closely resembles the one observed in Fig. 5.7E. To facilitate our explanation, we have superimposed the LoRa preamble and downchirps onto the same figure, although these elements do not exist in the IQ data of the signature. The two alternating tones, tone-0 and tone-1 in Fig. 5.9, produce the previously observed peak-pair-1 in Fig. 5.8.

The initial step in computing the central frequency involves performing an STFT

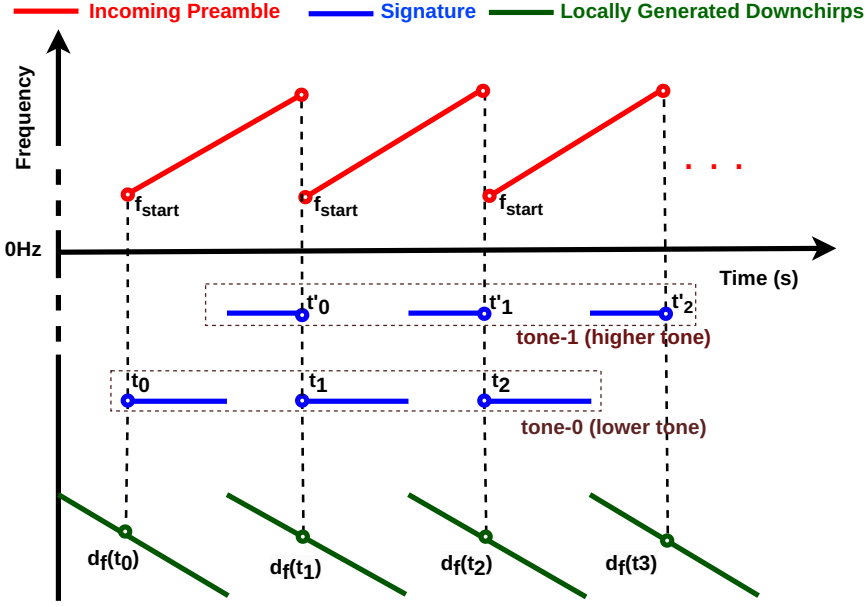


FIGURE 5.9: Illustration of the central frequency estimation process: a demonstration of the interplay between received preamble chirps, locally generated downchirps and the generated signature.

on the dechirped result (Fig. 5.7E) if any peak-pairs have been identified during the peak-pair detection step. We prioritize time accuracy in the STFT because we already have precise frequency accuracy for both tones from the peak-pair detection stage.

To verify the validity of peak-pairs parsed from the peak-pair detection step, we check if both tones within a peak-pair alternate for the duration of a preamble in the STFT. This allows elimination of tone-pairs that are falsely picked up due to data chirps, given that only a preamble would generate a signature with two alternating tones 125KHz apart for the duration of a preamble.

Upon identifying valid tone pairs, we move forward with estimating the start times for all lower tones and the end times for all higher tones within each pair. Lower tone and the higher tone is marked in Fig.5.9. It's important to note that the number of time samples per tone equates to the number of chirps in the preamble, less one. For instance, in a LoRa frame with 10 preamble chirps, we are able to estimate 18 time samples. Each time sample provides the same estimation of the central frequency of the LoRa frame. Given the abundance of time samples, to take best advantage of this redundancy, our strategy involves disregarding central

frequencies that deviate by several standard deviations and averaging the remaining to compute the most accurate central frequency of the LoRa frame.

Operating in the complex domain, Borderless takes advantage of the characteristic that the multiplication of two frequencies results in a single outcome, which is the sum of the two frequencies. This property allows the calculation of start frequency, f_{start} , for all time samples. For samples derived from tone-0, we compute f_{start} as $f_{start} = f_{tone-0} - d_f(t_i)$, and for those from tone-1, as $f_{start} = f_{tone-1} - d_f(t'_i)$, where i represents the tone segment index, and $d_f(t_i)$ and $d_f(t'_i)$ denote the instantaneous frequency of the downchirp at time t_i or t'_i , respectively. Here, f_{tone-0} and f_{tone-1} refer to the lower and higher tones, as highlighted in Fig. 5.9.

It's important to note that calculating $d_f(t_i)$ and $d_f(t'_i)$ for each time sample allows for the elimination of potentially erroneous time samples. For instance, although t'_{i-1} equals t_i , these time samples should be extracted from the STFT as distinct samples to maximize the use of all chirps from the LoRa preamble.

After the averaged f_{start} is calculated, the final step involves reversing the frequency translation of $\frac{\text{Borderless BW}}{2}$ and adding $\frac{\text{LoRa BW}}{2}$ to compute the central frequency of the LoRa frame. This can be represented by the formula $f_{c,f} = f_{start} - \frac{\text{Borderless BW}}{2} + \frac{\text{LoRa BW}}{2}$.

Start Time Estimation The start time estimation is crucial as I/Q data needs to be sliced prior to parsing into the demodulator. We define the start time as an approximate time when the signature begins. From this point, we slice the IQ data to include the maximum LoRa payload of 255 bytes, ensuring we capture the maximum possible LoRa frame, regardless of its actual payload length. This approach doesn't require any prior knowledge about the payload length of the LoRa frame. Having estimated the start time and central frequency, we have the key parameters needed to parse the correct segment of IQ data to the demodulator. This information allows for successful demodulation and decoding of the LoRa frame.

5.2.2 Collision Avoidance.

While it is evident that deep overlaps lead to some reduction in SNR, we can significantly mitigate this loss by employing a simple MAC protocol. Like all PHY

protocols, Borderless too can gain from a MAC layer. In our case, we chose the use of LMAC as the MAC layer for Borderless.

It's worth noting that in standard channelized LoRaWAN, the presence of hidden terminals and the absence of CSMA can lead to 100% collisions. This is innately minimized in Borderless because nodes are unaware of each other's exact channel plans—as they don't exist. This is precisely the advantage Borderless offers. By allowing nodes to select their own channels, we optimize the probability of avoiding the most damaging types of collisions in LoRaWAN. The use of LMAC further enhances this advantage.

Nonetheless, no MAC protocol is perfect, and there will still be instances of highly overlapping collisions for various reasons, e.g. hidden terminals. Borderless plans to incorporate CIC [68] to resolve such collisions.

5.3 Evaluation

This section delves into a series of experiments assessing the Borderless under different scenarios. Each experiment outlines the setup, procedure, and results, providing insights into Borderless' performance. The section explores two main experiments. In the first experiment, the Borderless system's capability to handle multiple concurrent LoRa frames was assessed. The second experiment evaluated Borderless's performance when dealing with overlapping LoRa frames, checking its frequency estimation and decoding ability under various degrees of frame overlap.

5.3.1 Performance Under Concurrent Frames

The Borderless methodology, by design, is equipped to handle multiple simultaneous LoRa frames. This is due to the unique feature of the signature—consisting separate but identifiable tone-pairs that are always separated by a consistent 125kHz and alternate in a specific pattern making it possible to distinguish between distinct LoRa frames. We tested this by placing seven LoRa frames across the borderless bandwidth in a way that fully utilized it. Conventionally, seven LoRa frames would require 1.4MHz of bandwidth. However, we fit them into just 1MHz of Borderless bandwidth, saving approximately 30% BW.

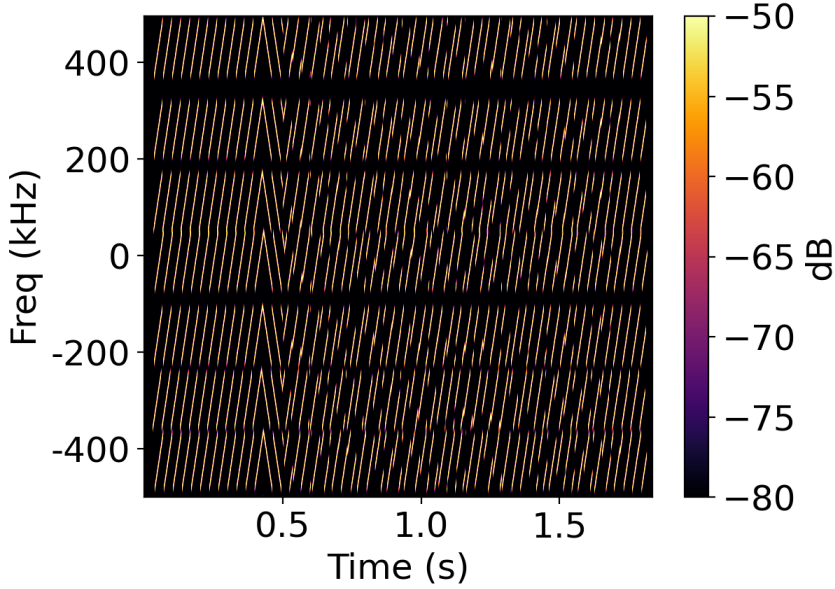


FIGURE 5.10: Seven LoRa frames occupying the Borderless BW.

The following step involved tagging these frames using the Borderless method, and then forwarding the tagged frames' I/Q data through a Python-implemented standard demodulator and a decoder. Notably, this process did not employ any specific methods to resolve collisions. The outcome demonstrated that detection of all seven frames, in addition to demodulation and decoding, was feasible without encountering any issues. This result underscores the potential of the Borderless approach for practical application in scenarios where multiple concurrent LoRa frames are encountered.

Ground Truth C.F(Hz)	Estimated Freq (Hz)	Absolute Err(Hz)
-427500	-427378.34	121.66
-300500	-300530.75	30.75
-167500	-163415.09	4084.91
-12500	-12483.22	16.78
110500	110407.51	92.49
260500	260546.37	46.37
430500	430545.81	45.81

TABLE 5.1: Comparison of Ground Truth and Estimated Frequencies Through Borderless Approach

The performance of Borderless in terms of frequency estimation is evaluated and summarized in Table 5.1. This table provides a comparison between the ground

truth frequencies used for transmission and the frequencies estimated by Borderless after passing through the Borderless system. The third column details the absolute error in central frequency estimation, which represents the absolute difference between the ground truth and central frequency determined by Borderless.

As seen from the table, the Borderless system exhibits commendable performance in frequency estimation. The errors are in the order of tens of Hertz, which is a relatively minor deviation considering the operating frequencies in the hundreds of kilohertz range. Notably, the maximum error observed is around 4.08 kHz, which, while being the maximum, is still a small fraction of the actual frequency value and did not cause any problem for the standard non-collision resolving demodulator to handle.

These results underscore the effectiveness of Borderless in accurately estimating frequencies, even when dealing with multiple simultaneous LoRa frames. This not only validates the robustness of the Borderless system in a multi-frame scenario but also signifies its potential for efficient utilization of the available bandwidth in practical applications.

5.3.2 Performance Under Overlapping Frames.

In this experiment, we evaluate the performance of Borderless when two LoRa frames overlap to varying degrees, ranging from 10% to 80%. It should be clarified here that we enforce overlapping for the communication BW, i.e., the experiment does not utilize guard bands as a part of overlapping. This makes overlaps more significant in comparison to varying overlaps of two standard LoRa channels we showed in Fig. 5.2. Therefore, this challenging test case assesses how well the algorithm handles frequency estimation under the presence of critically overlapped circumstances, a situation that could be encountered in real-world LoRa deployments. Several overlapping scenarios are illustrated in Fig. 5.11. The results of this experiment provide insights into the robustness and accuracy of Borderless under different degrees of overlaps.

The results of our experiment are presented in Table 5.2. This table illustrates the frequency estimation of Borderless for different degrees of overlaps. The Ground Truth CF (Hz) column lists the true central frequencies of the overlapping frames,

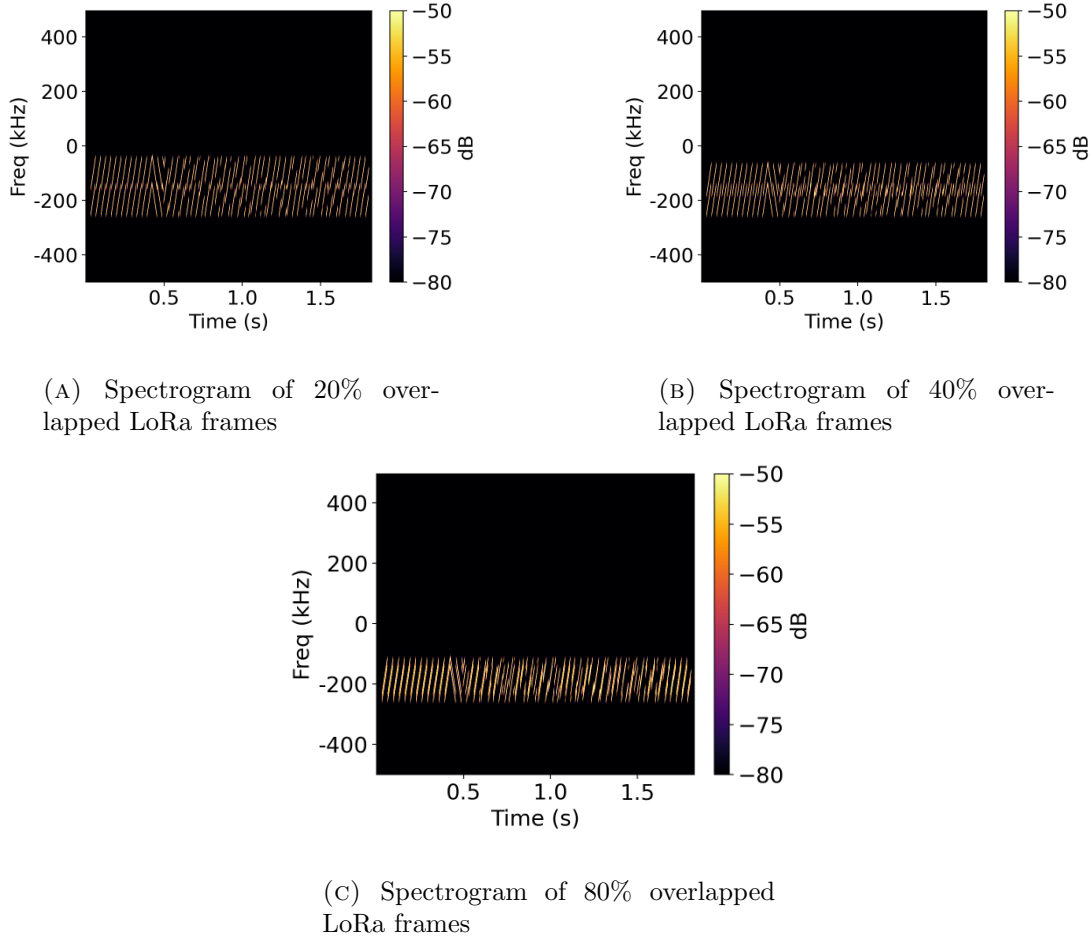


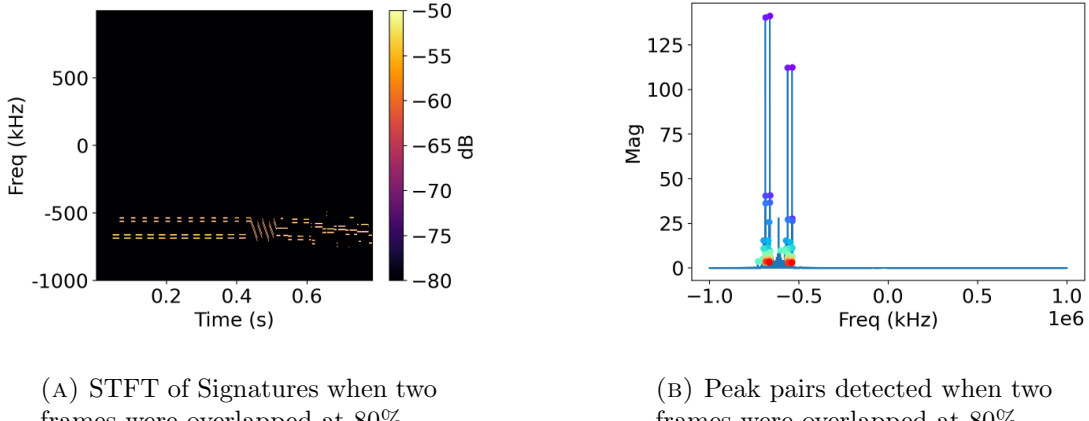
FIGURE 5.11: Spectrograms of overlapped LoRa frames at different overlap percentages

while the Estimated Freq (Hz) column presents the frequencies estimated by Borderless. The Absolute Error (Hz) column shows the absolute difference between these two frequencies, giving a quantitative measure of the algorithm's accuracy. The Overlap column indicates the degree of overlap between the two frames. From the results, it is evident that Borderless provides accurate frequency estimations even when there is substantial overlap between frames. Lastly, our python based demodulator demodulated and decoded all overlapping collisions without the application of special collision resolving mechanisms. This demonstrates the robustness of the algorithm in complex scenarios, further validating its potential.

We further explore the case of an 80% overlap between two LoRa frames. Selected interim results are presented in Fig. 5.12. Despite the high degree of overlap, it can be seen that each frame continues to generate a unique signature, as shown in Fig. 5.12a. The Short-Time Fourier Transform (STFT) of these signatures clearly

Ground Truth CF (Hz)	Estimated Freq (Hz)	Absolute Error (Hz)	Overlap
-200000	-200014.75	14.75	80%
-175000	-175015.77	15.77	80%
-200000	-200030.64	30.64	40%
-125000	-125015.26	15.26	40%
-200000	-200030.64	30.64	20%
-100000	-100030.26	30.26	20%
-200000	-200014.75	14.75	10%
-87500	-87576.55	76.55	10%

TABLE 5.2: Comparison of Ground Truth and Estimated Frequencies by Borderless Approach under Various Overlapping Scenarios Per Each Frame.



(A) STFT of Signatures when two frames were overlapped at 80%

(B) Peak pairs detected when two frames were overlapped at 80%

FIGURE 5.12: Signatures and peak pairs of LoRa frames at 80% overlap. It can be clearly seen that even at 80% overlap, there exist two clear signatures for both frames overlapped at 80%. Similarly, two peak-pairs are observed detected peak pairs.

reveals two distinct signatures corresponding to the two overlapping frames. This emphasizes the robustness of the signature-based approach in distinguishing between overlapping frames. Similarly, the analysis of peak pairs, shown in Fig. 5.12b, also exhibits two clear sets of peak pairs corresponding to the two frames. This further substantiates claims about the effectiveness of the peak pair detection method even in scenarios with a high degree of overlap. Thus, the combination of these two methods enables reliable frame detection and decoding in densely populated spectra.

5.4 Discussion

Borderless introduces a unique methodology to utilize the ISM spectrum for LoRa communication. By assigning distinct signatures to each LoRa frame and allowing nodes to select their channels within the whole available ISM spectrum, Borderless maximizes the uses of available communication bandwidth. It excels in challenging scenarios involving multiple concurrent frames and substantial frame overlaps, maintaining reliable detection, decoding, and central frequency estimation.

While Borderless has demonstrated effective detection and decoding capabilities without specific collision resolution methods, it is worth exploring potential benefits of employing collision resolving schemes. By doing so, Borderless can achieve improved spectral efficiency and reliability, further enhancing its performance. It is important to note that the collision avoidance provided by the MAC layer in Borderless significantly reduces the chances of severe overlapping frames. However, the application of collision resolvers may be more beneficial in scenarios with very high frame overlap caused by hidden terminals or under dense deployments. Furthermore, Borderless can be applied to scenarios where multiple LoRa networks coexist, each operating on different channel plans. Its ability to differentiate frames using signatures allows for improved coexistence with other networks.

Borderless is a positive step towards mitigating the real-world challenge of the overcrowded ISM spectrum. Its effectiveness in complex scenarios, coupled with the flexibility it offers, makes it a promising prospect for future LoRa communication.

Chapter 6

Conclusion and Future Work

Chapter-6 reflects on the journey thus far but also outlines future directions for research in LPWAN technologies, emphasizing the need for continuous evolution of LoRa and its applications in the IoT ecosystem.

6.1 Discussion

This dissertation explored the advancement of LoRa networks by presenting three works that address specific challenges and improve the performance of these systems. Each work presents a methodology with practical implications, demonstrating the potential for further enhancement of LoRa communications.

The first work, LMAC, reveals how the Channel Activity Detection (CAD) feature of LoRa radios can be used for efficient carrier sense. Based on CAD, LMAC designs three versions of LMAC that respectively implements CSMA for LoRa networks, and balances the loads of the channels defined by frequencies and spreading factors by using the end nodes' local information only and then additionally the gateway's global information. Testbed experiments showed that, compared with ALOHA, LMAC brings significant performance improvements in terms of PRR and goodput, as well as radio energy saving per successful frame delivery.

In our second work, we proposed an adapted version of LMAC-2, specifically designed to cater to the nuances and practical needs of industrial LoRaWAN deployments. This variant, built to align with global industry standards, was carefully

designed while paying consideration to numerous practical aspects and regulatory guidelines. This work was officially acknowledged by the LoRa Alliance, and consequently, it has been published as a LoRaWAN Technical Recommendation TR13-1.0.0. This work involved a comprehensive exploration of LMAC’s potential from an industry-focused view. We did not merely aim at optimizing network performance, but went further to address challenges related to achieving regulatory compliance and compatibility with existing infrastructure. We navigated the requirements for equal spectral utilization and devised strategies to resolve limitations imposed by LBT regulations. Anticipating the inevitable gradual adoption of LMAC across networks, we deliberated on its potential interoperability with ALOHA. We conducted a series of experiments to understand the performance implications of this transition and to ensure that the introduction of LMAC does not impair existing LoRaWAN networks. Another significant aspect we considered was the performance of weak nodes in the network, often associated with the ‘last mile problem’. Through our experimentation, we were able to demonstrate how our LMAC-2 variant can significantly enhance the performance of LoRaWAN. Overall, our work signifies a milestone towards bridging the gap between academic research and industry collaboration.

The third work, Borderless, fundamentally rethinks the use of LoRa’s modulation scheme to significantly improve the efficiency of LoRa networks. By breaking away from the traditional channelized approach, Borderless enables a unique method to access the available spectrum. Our implementation of Borderless on an SDR demonstrates its practical feasibility. Our experiments show that Borderless can handle concurrent LoRa transmissions and can accurately detect and decode overlapping LoRa frames with a high degree of accuracy.

6.2 Future Directions

While this dissertation has contributed advancements to the field of LoRa networks, it also opens up several new avenues for future research.

A key question that emerges from our work on LMAC is how to further optimize network and energy efficiency. Enhancing CAD functionality could be a promising approach. Current CAD operations are limited to individual channels. A potential

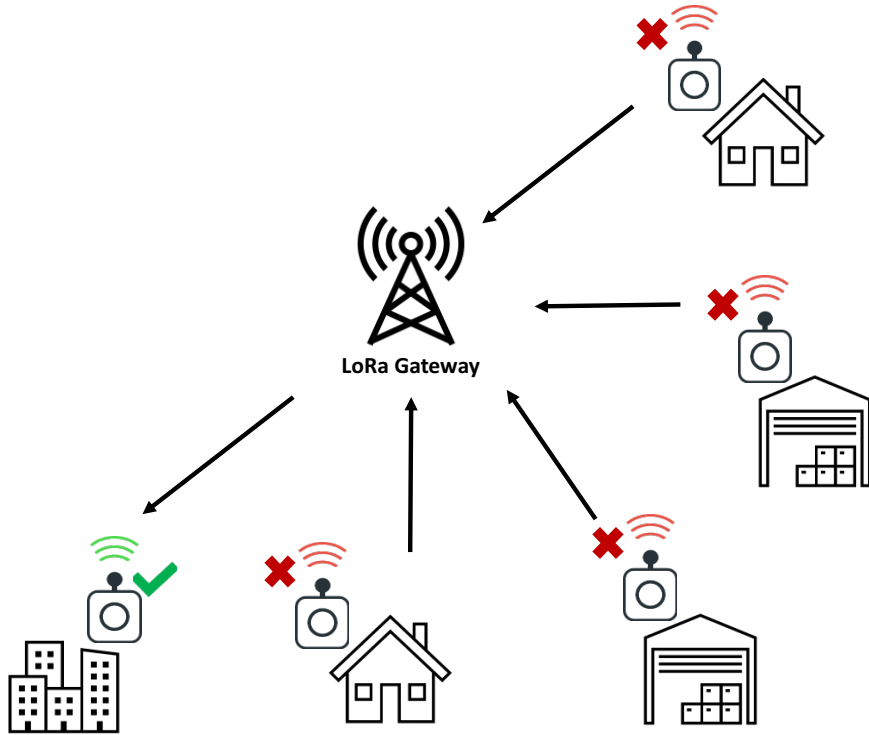


FIGURE 6.1: Illustration of the Downlink-Uplink Communication Conflict in LoRaWAN Networks: This figure demonstrates the issue where uplink communications are failed due to ongoing downlink transmissions from the gateway, highlighting the challenge of non-full duplex operation in LoRa gateways.

improvement would be to expand CAD across a wider bandwidths, allowing power efficient detection of larger BW availability in a single operation. This approach could significantly reduce energy and time costs and improve network efficiency by shifting to unused parts of spectrum and unnecessary channel shifts. Addressing challenges posed by hidden and exposed terminals, which complicate accurate in-air sensing, could also bring about substantial improvements to LMAC.

The Borderless approach, while currently designed for LoRa, has potential applications beyond. At its core, Borderless contains a detection algorithm that can operate across a wide bandwidth, in contrast to traditional detection algorithms that are limited to a single "channel" or a "BW". This makes Borderless applicable to a wide array of fields. Since radar systems also utilize chirps, Borderless could enable unique detection capabilities for radar systems across larger bandwidths. In security, the ability to accurately detect the presence of a chirp across a wide bandwidth can make a difference in applications such as targeted real-time jamming. Moreover, the core idea of Borderless— efficient and accurate detection across a

wide bandwidth could potentially be applied to other modulation schemes. With additional research and development, this could bring significant improvements to the way we utilize the spectrum.

One critical area for future exploration is the enhancement of downlink communication in LoRaWAN. Currently, LoRa gateways are not full duplex, leading to the loss of uplink communication capabilities during downlink transmissions. This limitation is significant as LPWANs are expected to support both sensing and actuation functionalities. Developing a method to enable downlink communication without compromising uplink communication is essential. This advancement will transform LoRa-based LPWANs into more versatile networks capable of extensive sensing and actuation at scale.

Overall, while this dissertation has made contributions to the field of LoRa networks, improvements are possible with further research. Continued works could further improve the performance and efficiency of spectrum utilized by LPWAN networks, paving the way for new applications and technologies.

List of Author's Awards, Patents, and Publications¹

Industry Standards

- **A. Gamage**, G. de Guillebon, M. Luis, M. Li, O. Seller, "Technical Recommendations for Enabling CSMA for LoRaWAN, TR13-1.0.0," by the *LoRa Alliance*, 2023.

Journal Articles

- **Amalinda Gamage**, Jansen Christian Liando, Chaojie Gu, Rui Tan, Mo Li, and Olivier Seller, "Efficient Carrier-Sense Multiple Access for LoRa," in *ACM Transactions on Sensor Networks*, Vol. 19, No. 2, Article 44, 2023.
- Jansen Christian Liando, **Amalinda Gamage**, Agustinus W. Tengourtius, Mo Li, "Known and Unknown Facts of LoRa: Experiences from a Large Scale Measurement Study," in *ACM Transactions on Sensor Networks*, Vol. 15, No. 2, Article 16, 2019.

Conference Proceedings

- **Amalinda Gamage**, Jansen Christian Liando, Chaojie Gu, Rui Tan, and Mo Li, "LMAC: Efficient Carrier-Sense Multiple Access for LoRa," in *MobiCom 2020 The 26th Annual International Conference on Mobile Computing and Networking*, 2020.

¹The superscript * indicates joint first authors

- Malitha Wijesundara, Cristiano Tapparello, **Amalinda Gamage**, Yadhavan Gokulan, Logan Gittelson, Thomas Howard, and Wendi Heinzelman, "JumboNet: Design of a Kinetic Energy Harvester for Elephant Mounted Wireless Sensor Nodes," in *2016 IEEE Global Communications Conference (GLOBECOM)*, 2016.

Bibliography

- [1] Ningning Hou, Xianjin Xia, and Yuanqing Zheng. Don't miss weak packets: Boosting lora reception with antenna diversities. *ACM Trans. Sen. Netw.*, aug 2022. doi: 10.1145/3563698. Just Accepted. [xxi](#), [48](#)
- [2] Olivier Seller. Predicting lorawan™ capacity. Technical report, Semtech Corporation, 2020. [xxi](#), [48](#)
- [3] LoRa Alliance Technical Committee. Lorawan™1.1 specification. Technical report, LoRa Alliance, October 2017. [1](#), [5](#)
- [4] Olivier Bernard, André Seller, and Nicolas Sornin. Low power long range transmitter. U.S. Patent 9,252,834, 2016. [1](#)
- [5] Lora modulation basics. <https://www.semtech.com/uploads/documents/an1200.22.pdf>, 2015. [1](#)
- [6] Eyuel D Ayele, Chiel Hakkenberg, Jan Pieter Meijers, Kyle Zhang, Nirvana Meratnia, and Paul JM Havinga. Performance analysis of lora radio for an indoor iot applications. In *Proceedings of the IEEE International Conference on Internet of Things for the Global Community (IoTGC'17)*, 2017. [1](#)
- [7] Norbert Blenn and Fernando Kuipers. Lorawan in the wild: Measurements from the things network. *arXiv preprint arXiv:1706.03086*, 2017.
- [8] Aloÿs Augustin, Jiazi Yi, Thomas Clausen, and William Mark Townsley. A study of lora: Long-range and low-power networks for the internet of things. *Sensors*, 16(9):1466, 2016.
- [9] Ferran Adelantado, Xavier Vilajosana, Pere Tuset-Peiro, Borja Martinez, Joan Melia-Segui, and Thomas Watteyne. Understanding the limits of lorawan. *IEEE Communications Magazine*, 55(9):34–40, 2017.
- [10] Rashad Eletreby, Diana Zhang, Swarun Kumar, and Osman Yağan. Empowering low-power wide-area networks in urban settings. In *Proceedings of the Conference of the ACM Special Interest Group on Data Communication*, pages 309–321. ACM, 2017.
- [11] Taoufik Bouguera, Jean-François Diouris, Jean-Jacques Chaillout, Randa Jaouadi, and Guillaume Andrieux. Energy consumption model for sensor nodes based on lora and lorawan. *Sensors*, 18(7), 2018.

- [12] Jonathan de Carvalho Silva, Joel JPC Rodrigues, Antonio M Alberti, Petar Solic, and Andre LL Aquino. Lorawan-a low-power wan protocol for internet of things: A review and opportunities. In *Proceedings of the 2nd International Multidisciplinary Conference on Computer and Energy Science (SpliTech'17)*, pages 1–6. IEEE, 2017.
- [13] Rúben Oliveira, Lucas Guardalben, and Susana Sargent. Long range communications in urban and rural environments. In *Proceedings of the IEEE Symposium on Computers and Communications (ISCC'17)*, pages 810–817. IEEE, 2017. [1](#)
- [14] Juha Petäjäjärvi, Konstantin Mikhaylov, Marko Pettissalo, Janne Janhunen, and Jari Iinatti. Performance of a low-power wide-area network based on lora technology: Doppler robustness, scalability, and coverage. *Int. J. Distrib. Sensor Netw.*, 13(3):1550147717699412, 2017. [2](#)
- [15] Juha Petäjäjärvi, Konstantin Mikhaylov, Antti Roivainen, Tuomo Hanninen, and Marko Pettissalo. On the coverage of lpwans: Range evaluation and channel attenuation model for lora technology. In *Proceedings of the 14th International Conference on ITS Telecommunications (ITST'15)*, pages 55–59. IEEE, 2015.
- [16] Jetmir Haxhibeqiri, Abdulkadir Karaagac, Floris Van den Abeele, Wout Joseph, Ingrid Moerman, and Jeroen Hoebeke. Lora indoor coverage and performance in an industrial environment: Case study. In *Proceedings of the 22nd IEEE International Conference on Emerging Technologies and Factory Automation (ETFA'17)*, pages 1–8. IEEE, 2017.
- [17] Jetmir Haxhibeqiri, Floris Van den Abeele, Ingrid Moerman, and Jeroen Hoebeke. Lora scalability: A simulation model based on interference measurements. *Sensors*, 17(6):1193, 2017.
- [18] Oratile Khutsoane, Bassey Isong, and Adnan M Abu-Mahfouz. IoT devices and applications based on lora/lorawan. In *Proceedings of the 43rd Annual Conference of the IEEE Industrial Electronics Society (IECON'17)*, pages 6107–6112. IEEE, 2017.
- [19] Alexandru Lavric and Valentin Popa. A lorawan: Long-range wide-area networks study. In *Proceedings of the International Conference on Electromechanical and Power Systems (SIELMEN'17)*, pages 417–420. IEEE, 2017. [2](#)
- [20] Knight Mathew and Seeber Balint. Decoding lora: Realizing a modern lpwan with sdr. In *Proceedings of the GNU Radio Conference*, 2016. [2](#), [16](#)
- [21] Pieter Robyns, Peter Quax, Wim Lamotte, and William Thenaers. gr-lora: An efficient lora decoder for gnu radio, 2017.
- [22] Zhenqiang Xu, Pengjin Xie, and Jiliang Wang. Pyramid: Real-time lora collision decoding with peak tracking. In *Proceedings of IEEE INFOCOM*, 2021. [2](#), [13](#), [18](#)

- [23] ETSI. Short range devices (srD) operating in the frequency range 25 mhz to 1 000 mhz; part 2: Harmonised standard for access to radio spectrum for non specific radio equipment. Standard, STSI, Valbonne, FR, April 2018. [2](#), [50](#), [55](#)
- [24] Branden Ghena, Joshua Adkins, Longfei Shangguan, Kyle Jamieson, Philip Levis, and Prabal Dutta. Challenge: Unlicensed lpwans are not yet the path to ubiquitous connectivity. In *Proceedings of the International Conference on Mobile Computing and Networking (MobiCom '19)*. ACM, 2019. [2](#), [14](#)
- [25] Jothi Prasanna Shanmuga Sundaram, Wan Du, and Zhiwei Zhao. A survey on lora networking: Research problems, current solutions and open issues. *IEEE Communications Surveys & Tutorials*, 2019.
- [26] Xianjin Xia, Yuanqing Zheng, and Tao Gu. Ftrack: parallel decoding for lora transmissions. In *Proceedings of the Embedded Networked Sensor Systems (SENSYS '19)*. ACM, 2019. [17](#)
- [27] Aloës Augustin, Jiazi Yi, Thomas Clausen, and William Mark Townsley. A study of lora: Long range & low power networks for the internet of things. *Sensors*, 16(9), 2016.
- [28] Ferran Adelantado, Xavier Vilajosana, Pere Tuset-Peiro, Borja Martinez, Joan Melia-Segui, and Thomas Watteyne. Understanding the limits of lorawan. *IEEE Communications magazine*, 55(9), 2017.
- [29] Pierre Neumann, Julien Montavont, and Thomas Noël. Indoor deployment of low-power wide-area networks (lpwan): A lorawan case study. In *Proceedings of the IEEE 12th International Conference on Wireless and Mobile Computing, Networking and Communications (WiMob'16)*, pages 1–8. IEEE, 2016.
- [30] Konstantin Mikhaylov, Juha Petaejaejaervi, and Tuomo Haenninen. Analysis of capacity and scalability of the lora low power wide area network technology. In *Proceedings of the European Wireless Conference (EW '16)*. VDE, 2016.
- [31] Cui Zhao, Zhenjiang Li, Ting Liu, Han Ding, Jinsong Han, Wei Xi, and Ruowei Gui. Rf-mehndi: A fingertip profiled rf identifier. In *Proceedings of the International Conference on Computer Communications (INFOCOMM '19)*. IEEE, 2019.
- [32] Martin C Bor, Utz Roedig, Thiem Voigt, and Juan M Alonso. Do lora low-power wide-area networks scale? In *Proceedings of the International Conference on Modeling, Analysis and Simulation of Wireless and Mobile Systems (MSWIM '16)*. ACM, 2016.
- [33] Konstantin Mikhaylov, Juha Petäjäjärvi, and Janne Janhunen. On lorawan scalability: Empirical evaluation of susceptibility to inter-network interference. In *Proceedings of the European Conference on Networks and Communications (EuCNC '17)*. IEEE, 2017. [2](#)

- [34] Ieee standard for information technology - telecommunications and information exchange between systems - local and metropolitan area networks - specific requirements - part 11: Wireless lan medium access control (mac) and physical layer (phy) specifications. *IEEE Std 802.11-2007 (Revision of IEEE Std 802.11-1999)*, 2007. [3](#), [18](#), [55](#)
- [35] Ieee standard for information technology- local and metropolitan area networks- specific requirements- part 15.1a: Wireless medium access control (mac) and physical layer (phy) specifications for wireless personal area networks (wpan). *IEEE Std 802.15.1-2005 (Revision of IEEE Std 802.15.1-2002)*, 2005. [3](#)
- [36] LMAC Integrated LoRaWAN. arduino-lmic-csma, 2020. URL <https://wands.sg/lmac>. [4](#)
- [37] Lora alliance®. <https://lora-alliance.org/>. Accessed: 2023-07-07. [5](#)
- [38] Member directory, 2023. URL <https://lora-alliance.org/member-directory/>. [5](#)
- [39] Amalinda Gamage, Jansen Christian Liando, Chaojie Gu, Rui Tan, and Mo Li. Lmac: Efficient carrier-sense multiple access for lora. In *Proceedings of the 26th Annual International Conference on Mobile Computing and Networking*, page 43. Association for Computing Machinery, 2020. doi: 10.1145/3372224.3419200. [6](#)
- [40] Amalinda Gamage, Jansen Liando, Chaojie Gu, Rui Tan, Mo Li, and Olivier Seller. Lmac: Efficient carrier-sense multiple access for lora. *ACM Transactions on Sensor Networks*, 19(2):44, 2023. URL <https://doi.org/10.1145/3564530>. [6](#), [15](#)
- [41] Semtech. Lora gateway project, 2020. URL https://github.com/Lora-net/lora_gateway. [12](#)
- [42] Jansen C. Liando, Amalinda Gamage, Agustinus W. Tengourtius, and Mo Li. Known and unknown facts of lora: Experiences from a large-scale measurement study. *ACM Transactions on Sensor Networks (TOSN)*, 15(2), 2019. [13](#), [15](#), [29](#)
- [43] Pei Tian, Fengxu Yang, Xiaoyuan Ma, Carlo Alberto Boano, Xin Tian, Ye Liu, and Jianming Wei. Environmental impact on the long-term connectivity and link quality of an outdoor lora network. In *19th ACM Conference on Embedded Networked Sensor Systems*, pages 565–568, 2021. [13](#)
- [44] Weitao Xu, Jun Young Kim, Walter Huang, Salil S. Kanhere, Sanjay K. Jha, and Wen Hu. Measurement, characterization, and modeling of lora technology in multifloor buildings. *IEEE Internet of Things Journal*, 7(1):298–310, 2019. [13](#)

- [45] Roman Trüb and Lothar Thiele. Increasing throughput and efficiency of lorawan class a. In *Proceedings of the International Conference on Mobile Ubiquitous Computing, Systems, Services and Technologies (UBICOMM '18)*. IARIA, 2018. [14](#)
- [46] Rajeev Piyare, Amy L. Murphy, Michele Magno, and Luca Benini. On-demand lora: Asynchronous tdma for energy efficient and low latency communication in iot. *Sensors*, 18(11), 2018.
- [47] Chaojie Gu, Rui Tan, and Xin Lou. One-hop out-of-band control planes for multi-hop wireless sensor networks. *ACM Transactions on Sensor Networks (TOSN)*, 15(4), 2019. [14](#)
- [48] Luca Beltramelli, Aamir Mahmood, Patrik Österberg, and Mikael Gidlund. Lora beyond aloha: An investigation of alternative random access protocols. *arXiv preprint arXiv:2002.10732*, 2020. [14](#)
- [49] Justin Chan, Anran Wang, Arvind Krishnamurthy, and Shyamnath Gollakota. Deepsense: Enabling carrier sense in low-power wide area networks using deep learning. *arXiv preprint arXiv:1904.10607*, 2019. [14](#)
- [50] Congduc Pham. Robust csma for long-range lora transmissions with image sensing devices. In *Proceedings of Wireless Days (WD '18)*. IEEE, 2018. [14](#)
- [51] R. Subbaraman, Y. Guntupalli, S. Jain, R. Kumar, K. Chintalapudi, and D. Bharadia. Bsma: Scalable lora networks using full duplex gateways. In *Proceedings of the 28th Annual International Conference on Mobile Computing And Networking*, pages 676–689. Association for Computing Machinery, 2022. doi: 10.1145/3495243.3560544. [14](#)
- [52] Federal communications commission 47 cfr part 15. 2022. [15](#), [46](#), [50](#), [54](#), [55](#), [58](#)
- [53] A. Yegin, O. Seller, D. Kjendal, et al. Lorawan® regional parameters. Technical report, LoRa Alliance Technical Committee Regional Parameters Workgroup, 2023. [15](#), [56](#)
- [54] Semtech Corporation. *SX1262 Long Range, Low Power, sub-GHz RF Transceiver*, December 2022. URL <https://www.semtech.com/products/wireless-rf/lora-connect/sx1262>. Data Sheet Rev. 2.1. [15](#), [66](#)
- [55] Pieter Robyns, Peter Quax, Wim Lamotte, and William Thenaers. A multi-channel software decoder for the lora modulation scheme. In *Proceedings of the International Conference on Internet of Things, Big Data and Security (IoTBDS)*. SciTePress, 2018. [16](#), [21](#)
- [56] Z. Xu, S. Tong, P. Xie, and J. Wang. From demodulation to decoding: Toward complete lora phy understanding and implementation. *ACM Trans. Sen. Netw.*, 18(4):64, 2023. doi: 10.1145/3546869. URL <https://doi.org/10.1145/3546869>. [16](#)

- [57] Daibo Liu, Zhichao Cao, Mengshu Hou, Huigui Rong, and Hongbo Jiang. Pushing the limits of transmission concurrency for low power wireless networks. *ACM Transactions on Sensor Networks*, 16(4):1–29, 2020. [16](#)
- [58] Rashad Eletreby, Diana Zhang, Swarun Kumar, and Osman Yaundefinedan. Empowering low-power wide area networks in urban settings. In *Proceedings of Special Interest Group on Data Communication (SIGCOMM ’17)*. ACM, 2017. [16](#)
- [59] Mehrdad Hessar, Ali Najafi, and Shyamnath Gollakota. Netscatter: Enabling large-scale backscatter networks. In *Proceedings of the Symposium on Networked Systems Design and Implementation (NSDI ’19)*. USENIX Association, 2019. [17](#)
- [60] Adwait Dongare, Revathy Narayanan, Akshay Gadre, Anh Luong, Artur Balanuta, Swarun Kumar, Bob Iannucci, and Anthony Rowe. Charm: exploiting geographical diversity through coherent combining in low-power wide-area networks. In *Proceedings of the International Conference on Information Processing in Sensor Networks (IPSN ’18)*. IEEE, 2018. [17](#), [18](#)
- [61] Akshay Gadre, Revathy Narayanan, Anh Luong, Anthony Rowe, Bob Iannucci, and Swarun Kumar. Frequency configuration for low-power wide-area networks in a heartbeat. In *Proceedings of the Symposium on Networked Systems Design and Implementation (NSDI ’20)*. USENIX Association, 2020. [17](#)
- [62] Thiemo Voigt, Martin Bor, Utz Roedig, and Juan Alonso. Mitigating inter-network interference in lora networks. In *Proceedings of the 2017 International Conference on Embedded Wireless Systems and Networks (EWSN ’17)*. Junction Publishing, 2017. [17](#)
- [63] Xianjin Xia, Ningning Hou, Yuanqing Zheng, and Tao Gu. Pcube: Scaling lora concurrent transmissions with reception diversities. In *27th Annual International Conference on Mobile Computing and Networking*, pages 670–683, 2021. [17](#)
- [64] Huai Tong, Zhenqiang Xu, and Jiliang Wang. Colora: Enabling multi-packet reception in lora. In *IEEE INFOCOM 2020-IEEE Conference on Computer Communications*, pages 2303–2311. IEEE, 2020. [17](#), [18](#)
- [65] Shuai Tong, Jiliang Wang, and Yunhao Liu. Combating packet collisions using non-stationary signal scaling in lpwans. In *18th International Conference on Mobile Systems, Applications, and Services*, pages 234–246, 2020. [18](#)
- [66] Xiong Wang, Linghe Kong, Liang He, and Guihai Chen. Mlora: A multi-packet reception protocol in lora networks. In *2019 IEEE 27th International Conference on Network Protocols (ICNP)*, pages 1–11. IEEE, 2019. [18](#)
- [67] Mohamed Amine Ben Temim, Guillaume Ferré, Baptiste Laporte-Fauret, Dominique Dallet, Bryce Minger, and Loïc Fuché. An enhanced receiver to decode

- superposed lora-like signals. *IEEE Internet Things J.*, 7(8):7419–7431, 2020. [18](#)
- [68] Muhammad Osama Shahid, Millan Philipose, Krishna Chintalapudi, Suman Banerjee, and Bhuvana Krishnaswamy. Concurrent interference cancellation: Decoding multi-packet collisions in lora. In *ACM SIGCOMM Conference*, pages 503–515. ACM, 2021. [18](#), [82](#)
- [69] Runesh Mishra, Vivek Shrivastava, Suman Banerjee, and William Arbaugh. Partially overlapped channels not considered harmful. In *Proceedings of the Joint International Conference on Measurement and Modeling of Computer Systems*, pages 63–74, 2006. [18](#)
- [70] Paramvir Bahl, Ranveer Chandra, Thomas Moscibroda, Rohan Murty, and Matt Welsh. White space networking with wi-fi like connectivity. *ACM SIGCOMM Computer Communication Review*, 39(4):27–38, 2009. [19](#)
- [71] E. Li, K. Tan, H. Viswanathan, Y. Xu, and Y. R. Yang. Retransmission repeat: Simple retransmission permutation can resolve overlapping channel collisions. In *Proceedings of the ACM Mobicom*. ACM, 2010. [19](#)
- [72] Lu Wang, Xiaoke Qi, Ruifeng Huang, Kaishun Wu, and Qian Zhang. Exploring partially overlapping channels for low-power wide area networks. *ACM Trans. Sen. Netw.*, 18(4), 2023. doi: 10.1145/3546075. [19](#)
- [73] Feng Li, Jun Luo, Gaotao Shi, and Ying He. Art: Adaptive frequency-temporal co-existing of zigbee and wifi. *IEEE Transactions on Mobile Computing*, 16(3):662–674, 2016. [19](#)
- [74] Feng Li, Jun Luo, Gaotao Shi, and Ying He. Favor: Frequency allocation for versatile occupancy of spectrum in wireless sensor networks. In *Proceedings of the ACM International Symposium on Mobile Ad Hoc Networking and Computing (MobiHoc)*. ACM, 2023. [19](#)
- [75] Silvia Demetri, Marco Zúñiga, Gian Pietro Picco, Fernando Kuipers, Lorenzo Bruzzone, and Thomas Telkamp. Automated estimation of link quality for lora: a remote sensing approach. In *Proceedings of the International Conference on Information Processing in Sensor Networks (IPSN ’19)*. IEEE, 2019. [21](#)
- [76] Shuai Tong, Jiliang Wang, and Yunhao Liu. Combating packet collisions using non-stationary signal scaling in lpwans. In *Proceedings of the International Conference on Mobile Systems, Applications, and Services (MobiSys ’20)*. ACM, 2020. [21](#)
- [77] Reading channel rssи during a cad. Technical report, Semtech Corporation, October 2014. AN1200.21. [21](#)

- [78] Monsoon Solutions. High voltage power monitor, 2020. URL <https://www.msoon.com/online-store/High-Voltage-Power-Monitor-Part-Number-AAA10F-p90002590>. [24](#)
- [79] Sandeep Mistry. Arduino-lora, 2020. URL <https://github.com/sandeepmistry/arduino-LoRa>. [26](#)
- [80] Jason A. Donenfeld. Wireguard: Next generation kernel network tunnel. 2017. [26](#)
- [81] Sx1272/3/6/7/8: Lora modem. Technical report, Semtech Corporation, July 2013. AN1200.13. [33](#)
- [82] Association of Radio Industries and Businesses. Arib std-t108: 920mhz-band telemeter, telecontrol and data transmission radio equipment. Standard, ARIB, Tokyo, JP, February 2012. [50](#), [55](#)
- [83] LoRa Alliance Inc. Lorawan regional parameters 1.0.3. Standard, LoRa Alliance Inc., Fremont, CA, February 2021. [55](#)
- [84] 802.15 WG Wireless Specialty Networks (WSN) Working Group. Ieee 802.15.4-2020: Ieee standard for low-rate wireless networks. 2020. [55](#)
- [85] Salim Jibrin Danbatta and Asaf Varol. Comparison of zigbee, z-wave, wi-fi, and bluetooth wireless technologies used in home automation. In *2019 7th International Symposium on Digital Forensics and Security (ISDFS)*, pages 1–5. IEEE, 2019. [55](#)
- [86] Semtech Corporation. Sx126x: Application note. Technical Report AN1200.48, Semtech Corporation, November 2019. URL <https://www.semtech.com>. AN1200.48, Rev 2.1. [65](#)
- [87] Semtech Corporation. Lora sx1301 digital baseband chip, 2020. URL <https://www.semtech.com/products/wireless-rf/lora-gateways/sx1301>. [73](#)